

***In planta* studies on the biosynthesis
of pyrrolizidine alkaloids and the
involvement of copper-containing
amine oxidases**

by Thomas Stegemann

Dissertation in fulfillment of requirements of the Doctoral Degree

Doctor rerum naturalium

of the Faculty of Mathematics and Natural Sciences at

Christian-Albrechts Universität zu Kiel

Kiel, 2020

Erster Gutacher: Prof. Dr. Dietrich Ober
Zweite Gutachterin: Prof. Dr. Birgit Classen
Tag der mündlichen Prüfung: 16.06.2020

I. Abstract

Many plants especially from the families of Asteraceae, Boraginaceae, Heliotropiaceae, Fabaceae and Orchidaceae produce pyrrolizidine alkaloids (PAs) that are often toxic to fend off herbivores. Till this work only the first step of PA biosynthesis was elucidated. The entry-step of the PA biosynthesis is performed by an enzyme called homospermidinesynthase (HSS) which transfers an aminobutyl moiety of spermidine onto putrescine and creates the symmetric triamine, homospermidine. This enzyme, resulting from a duplication of the gene encoding the enzyme deoxyhypusine synthase (DHS) was shown to have developed several times independently.

Using common comfrey (*Symphytum officinale*, Boraginaceae) as a model, different aspects of PA biosynthesis have been studied. It was shown that PA biosynthesis, though constitutive, is dynamic with respect to its regulation. A second site of PA biosynthesis was identified *in planta* within leaves subtending the reproductive parts (inflorescence) of the plants.

Furthermore the work showed that this variability is also found on the intraspecific and intraindividual level by analyzing PA distribution and amounts in common comfrey. This result was validated also in another model system the Indian heliotrope (*Heliotropium indicum*, Heliotropiaceae) in respect to the variability of PA levels. This variability of PA levels was mirrored by the expression levels of HSS, an observation that was also valid for a copper-containing amine oxidase (CuAO). This CuAO was regarded as a candidate for a further step in PA biosynthesis, i.e. the oxidation of homospermidine.

The sequence of the CuAO candidate was used to design virus-induced gene silencing (VIGS) experiments to knock down the candidate CuAO. Successful knock-downs showed reduced PA levels confirming the hypothesis of this CuAO is involved in PA biosynthesis. Chemical elucidation of the homospermidine transformation by the candidate CuAO resulted in the identification of a double oxidized and already double cyclized PA precursor. This result was further validated by tracer-feeding experiments to further support the involvement of the candidate CuAO, now named homospermidine oxidase in PA biosynthesis.

II. Zusammenfassung

Viele Pflanzen vor allem aus den Familien der Asteraceae, Boraginaceae, Heliotropiaceae, Fabaceae und Orchidaceae produzieren oft giftige Pyrrolizidinalkaloide (PAs), um sich vor Fraßfeinden zu schützen. Bis zu dieser Arbeit war nur der erste Schritt der PA-Biosynthese aufgeklärt. Dieser wird von dem Enzym Homospermidinsynthase (HSS) katalysiert, das eine Aminobutyl-Einheit von Spermidin auf Putrescin transferiert und dadurch das symmetrische Triamin Homospermidin produziert. Dieses Enzym, welches aus einer Genduplikation des Primärstoffwechsellenzym Desoxyhypusinsynthase entstanden ist, entwickelte sich mehrfach unabhängig.

Anhand des Arzneibeinwells (*Symphytum officinale*, Boraginaceae) als Modellpflanze wurden verschiedene Aspekte der PA-Biosynthese untersucht. Es zeigte sich, dass die PA-Biosynthese, obwohl sie konstitutiv ist, einen dynamischen Aspekt der Regulation besitzt. Ein zweiter Ort der PA-Biosynthese wurde *in planta* in jenen Blättern identifiziert, welche sich unterhalb den reproduktiven Organen (Blütenstand) der Pflanze befinden.

Desweiteren macht die Arbeit deutlich, dass die PAs auch eine deutliche intraspezifische und intraindividuelle Variabilität ihrer Mengen ihrer Verteilung zeigen. Diese Beobachtung konnte in einer weiteren Modellpflanze, der Indischen Sonnenwende (*Heliotropium indicum*, Heliotropiaceae), in Bezug auf die Menge der PAs bestätigt werden. In dieser Pflanze wurde zudem beobachtet, dass sich die Variabilität der PA-Level in der Transkriptmenge der HSS widerspiegeln. Gleiches wurde für eine kupferhaltige Aminoxydase (CuAO) beobachtet, von der vermutet wurde, dass sie an der PA-Biosynthese, der Oxidation des Homospermidins, beteiligt sein könnte. Der Hinweis auf eine mögliche Koregulation von HSS und der CuAO wurde genutzt, um virus-induced gene silencing (VIGS) Experimente durchzuführen. Infolge einer erfolgreichen Reduktion der CuAO-Transkriptmengen wurden auch reduzierte Mengen an PAs beobachtet, was die Hypothese einer Beteiligung der CuAO an der PA-Biosynthese unterstützt. Die biochemische Charakterisierung der CuAO zeigte zudem, dass dieses Enzym in der Lage ist, aus Homospermidin die Bildung eines Pyrrolizidingrundkörpers zu katalysieren. Dass dieser ein mögliches Intermediat der

Biosynthese sein kann, wurde durch Fütterungsexperimente mit markierten Vorstufen belegt..

Index:

I. Abstract.....	I
II. Zusammenfassung.....	III
1. Introduction.....	1
1.1 Secondary/Specialized metabolites.....	1
1.2 Biosynthesis of different alkaloids.....	5
1.3 Pyrrolizidine alkaloids.....	8
1.4 Biosynthesis of pyrrolizidine alkaloids.....	10
1.5 Objectives and outline of this work.....	12
2. Identification of a Second Site of Pyrrolizidine Alkaloid Biosynthesis in Comfrey to Boost Plant Defense in Floral Stage.....	15
2.1 Abstract.....	16
2.2 Introduction.....	16
2.2 Results.....	19
2.2.1 Levels of hss Transcript and Protein Expression Are Dependent on Leaf Position in Relation to the Inflorescence.....	19
2.2.2 Immunolocalization of HSS in Leaves of Comfrey.....	20
2.2.3 Capacity of Comfrey Leaves to Synthesize PAs.....	23
2.2.4 Leaves Boost PA Levels in Inflorescences.....	25
2.3 Discussion.....	29
2.4 Materials and Methods.....	31
2.4.1 Plant Material.....	31
2.4.2 RNA Isolation and Quantification of Transcripts.....	31
2.4.3 Protein-Blot Analysis of Comfrey Leaves.....	33
2.4.4 Immunohistochemical Staining of HSS in Leaf Cross Sections.....	33
2.4.5 Radioactive Tracer Feeding Experiments and Product Analysis.....	34
2.4.6 Quantification of Total PAs in Inflorescences.....	36
2.4.7 Accession Numbers.....	36
2.5 Acknowledgments.....	36
3. Radioactive Tracer Feeding Experiments and Product Analysis to Determine the Biosynthetic Capability of Comfrey (<i>Symphytum officinale</i>) leaves for Pyrrolizidine Alkaloids ...	37
3.1 Abstract.....	38
3.2 Background.....	38
3.3 Materials and Reagents.....	38
3.4 Equipment.....	40
3.5 Software.....	40
3.6 Procedure.....	41

5.6.1 Radioactive tracer feeding experiments	41
3.6.2 Product analysis	48
3.6.3 Data analysis	51
3.6.4 Notes	52
3.7 Recipes.....	53
3.8 Acknowledgments	53
4. Specific Distribution of Pyrrolizidine Alkaloids in Floral Parts of Comfrey (<i>Symphytum officinale</i>) and its Implications for Flower Ecology	54
4.1 Abstract	55
4.2 Introduction.....	55
4.3 Methods and Material	59
4.3.1 Plant Material	59
4.3.2 Plant Dissection and Pollen Harvest.....	59
4.3.3 Alkaloid Extraction and Solid Phase Extraction	62
4.3.4 Sample Preparation for the Identification of PAs	62
4.3.5 Quantification of PAs.....	63
4.3.6 GC-MS Analysis.....	63
4.3.7 LC-MS Analysis.....	64
4.4 Results	64
4.4.1 Total PA Levels in Various Flower and Fruit Tissues of <i>S. officinale</i>	64
4.5 Discussion	67
4.6 Supplemental Table.....	71
5. Variance of Pyrrolizidine alkaloid-content and gene transcription in <i>Heliotropium indicum</i> .	72
5.1 Abstract	73
5.2 Introduction.....	73
5.3.1 Intraspecific variation of PA concentration in leaves of <i>H.indicum</i>	75
5.3.2 Intraspecific variation of hss-transcripts in leaves of <i>H.indicum</i>	76
5.3.3 Intraspecific variation of possible candidate gene-transcription in leaves of <i>H.indicum</i>	77
5.3.4 Possible correlation of hss and CuAO	78
5.4 Experimental	80
5.4.1 Plant material	80
5.4.2 Quantification of PAs.....	80
5.4.3 Quantification of transcript levels.....	80
5.4.4 Primers	80
6. Double oxidation of homospermidine by a copper-containing amine oxidase results in a pyrrolizidine backbone	81

6.1 Abstract	81
6.2 Introduction.....	82
6.3 Results	85
6.3.1 Identification of a putative homospermidine oxidase	85
6.3.2 Substrate specificity and kinetic properties of HSO	87
6.3.3 HSO is involved in PA biosynthesis.....	90
6.3.4 HSO is sufficient for the formation of the methyl-pyrrolizidine backbone	92
6.3.5 Carboxypyrrolizidine is an intermediate of PA biosynthesis.....	95
6.4 Discussion	95
6.4.1 HSO has all characteristics of a typical CuAO	96
6.4.2 HSO catalyzes the oxidation of both primary amino groups of homospermidine	97
6.4.3 HSO is involved in PA biosynthesis and shows substrate preference for homospermidine	99
6.4.4 Evolution of HSO.....	100
6.5 Materials and Methods	102
6.5.1 Plant Material and Growth Conditions.	102
6.5.2 Relative transcript quantification.....	102
6.5.3 Identification of complete open reading frame of HSO and CuAO2 and transient protein expression in <i>N. benthamiana</i>	102
6.5.4 Protein extraction and purification.	103
6.5.5 Protein Gel Blot Analysis.....	104
6.5.6 Microsequencing of HSO.	104
6.5.7 Photometrical assay for CuAO.	104
6.5.8 Site directed mutagenesis.	105
6.5.9 Preparation of homospermidine and [¹⁵ N]homospermidine	105
6.5.10 Virus-induced gene silencing in <i>Heliotropium indicum</i>	106
6.5.11 Enzymatic reaction for identification of the product 1-carboxypyrrolizidine	106
6.5.12 NMR Analyses	107
6.5.13 DIP-EI-HRAMS	107
6.5.14 Tracer feeding experiments.....	107
6.6 Acknowledgments	108
6.7 Supplementary Table.....	109
6.8 Supplemental Figures:.....	111
7. Conclusions and General Perspective	119
7.1 HSO oxidation follows the blueprint of alkaloid biosynthesis.....	119
7.2 Biosynthesis of the necine base moiety	120
7.3 Unique features of the double oxidation via HSO.....	121

7.4 Impact of this study for further research on PA biosynthesis.....	122
Contributions.....	126
Acknowledgements.....	127
References	128
Lebenslauf:	149
Erklärung	150

1. Introduction

1.1 Secondary/Specialized metabolites

Across the whole plant kingdom several strategies are observed to counteract dangers from herbivores. Due to their sessile nature plants are unable to adopt a fight-or-flight strategy like most animals and therefore needed to develop a broad variety of mechanisms to deter possible dangers to their existence (Gong & Zhang, 2014). This broad variety comprises different strategies which are not all unique to the plant kingdom, like mimicry, an increased protective shielding or even the attraction of herbivore predators (Gong & Zhang, 2014). Thus, many of those specialized traits are not solely developed to pursue plant defense. The balance between attracting pollinators or herbivore predators and defending against herbivores has been shaped and refined over the course of evolution. This formed a complex network of attraction, deterrence and communication in host-plant relationships within their specialized habitats (Wink, 2010).

Compounds produced by plants for these complex ecological interactions are often classified as secondary or specialized metabolites. These compounds are not vital for central processes of the living cell like energy metabolism (e.g. photosynthesis, respiration) or essential metabolic pathways, but for the survival of the plant in its environment (Hartmann, 2007). During the course of evolution, a vast variety of secondary metabolites arose, and biosynthetic processes were established. Recent advances studying such processes result in a better understanding that those chemical defense compounds are non-“waste” products that were optimized in their biological activities during evolution. Due to the assumed “degrading classification” as “secondary” the new term of specialized metabolites came up during the last years. Throughout this thesis the term “secondary metabolites” will be used to avoid confusion.

At present many more than 50 000 different structures of secondary metabolites have been elucidated (Wink, 2010). Secondary metabolites are further classified into different groups, for example according to their biosynthetic origin.

One example is the large group of the terpenoids, that comprises all secondary metabolites with a common C5-precursor, *i.e.*, isopentenylidiphosphate (IPP) and its isomeric dimethylallyldiphosphate (DMAP). This large group is further subclassified by the number of precursors necessary for their build. While monoterpenes (C10-skeleton) require two C5-precursors, sesquiterpenes (C15-skeleton) require three C5-precursor molecules. Diterpene (20C-skeleton), triterpenes (30C-skeleton) and tetraterpenes (40C-skeleton) follow the same logic. This variety is often present in a single plant species as they produce various compounds of the different classes of terpenes, for example European spruce, *Picea abies* contains at least 14 different monoterpenes (Bufler et al., 1990) besides various sesquiterpenes, and diterpenes (Cheng et al., 2007).

The most important group of secondary metabolites for this work is the group of alkaloids. The alkaloid group is defined to encompass nitrogen-containing compounds that are derived from amino acids (Habermehl et al., 2008). They comprise a vast variety of about 21 000 different structures (Fig 1) (Wink, 2010).

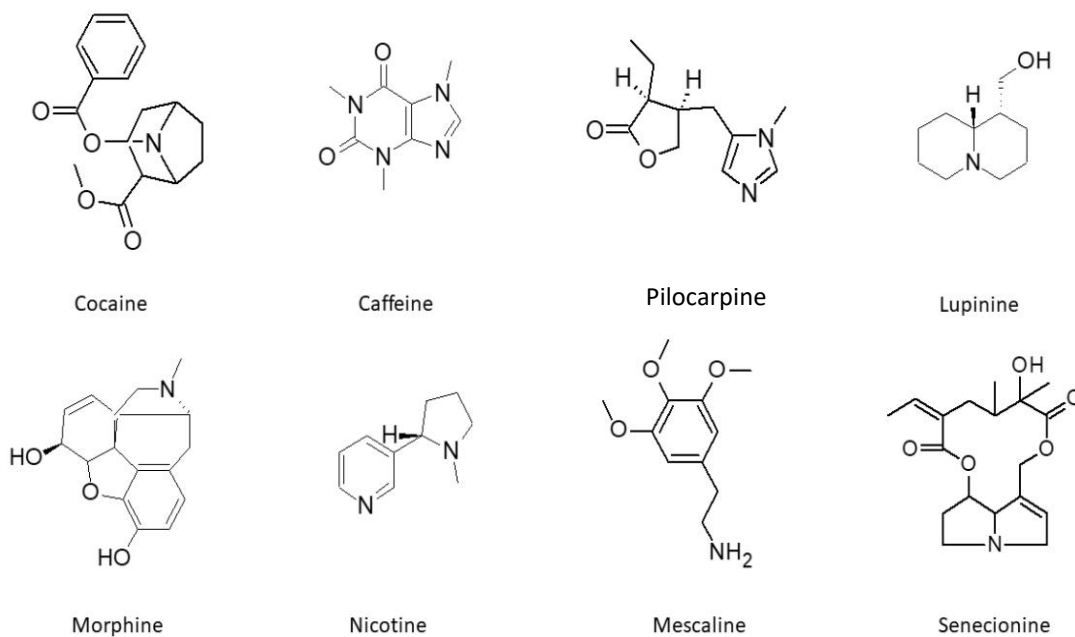


Figure 1: Selected examples of the vast structural variety of alkaloids

Unique to the group of alkaloids is the fact that they neither possess a common precursor nor do they show structural similarities. In fact, the term alkaloid must be understood as a supra-group containing secondary metabolites which derive from more than one group of precursors of primary metabolism, *i.e.*, the various amino acids. Therefore, for the alkaloids many different subclassification systems are in use that are based on the type of amino acid precursor, on their occurrence in certain plant lineages, or on certain characteristic features of their chemical structure.

subclassification system	example groups	examples group members
precursor-system	lysine alkaloids	lupinine, piperine, matrine, anabasine
	glycine alkaloids	caffeine, theobromine, theophylline
	histidine alkaloids	pilocarpine
	tyrosine alkaloids	morphine, colchicine, codeine, berberine
	ornithine alkaloids agmatine alkaloids	cocaine, nicotine senecionine
occurrence based system	opiates	morphine, papaverine, codeine, noscapine, thebaine
	curare alkaloids	toxiferine, alcuronium
	senecionine alkaloids	senecionine, sencyphylline
	lupine alkaloids	lupanine, sparteine, matrine
	ergot alkaloids	ergotamine, ergometrine
chemical system	pyridine alkaloids	nicotine, anabasine
	tropane alkaloids	cocaine, hyoscamine
	isoquinoline alkaloids	morphine, codeine, papaverine
	purine alkaloids	caffeine, theophyllin, theobromine
	indole alkaloids	ergotamine, strychnine, reserpine
	acyclic alkaloids	mescaline
	pyrrolizidine alkaloids	senecioine, lycopsamine, heliotrine, indicine

Figure 2: Examples of different subclassification systems for alkaloids

Alkaloid-containing plants (Macht, 1915) and later the isolated alkaloids (Sertürner, 1805) are in medical use since antique times. The World Health Organization even classified four alkaloids (morphine, codeine, atropine and quinine) as essential drugs for human health (World Health Organization, 2017). The strong activity of different alkaloids is also cause for their common misuse by humans a fact that is well documented and prevails to this day, with the most prominent example being nicotine-usage in terms of cigarette- and cigar-smoking. Other prevalent examples would be the abuse of cocaine, codeine, morphine and their derivatives in an illegal way or as legally prescribed drugs.

1.2 Biosynthesis of different alkaloids

In order to understand the source of the huge variety of alkaloids the different biosynthetic routes have to be considered. In contrast to terpenoids that possess a common biosynthetic start with the formation of IPP the alkaloid groups lack this kind of common origin. Instead they start on different kind of ubiquitous degradation products from amino acid, the so called polyamines pool, or directly from amino acids (Habermehl et al., 2008). Since there are multiple biosynthetic pathways the details of each would exceed the introduction of this work, but similarities can be found in comparing different pathways. The biosynthetic pathway of nicotine-type pyrimidine alkaloids and tropane alkaloids start at the same polyamine putrescine and are a good example for alkaloid formation in plants since the biosynthesis of alkaloid core structure have been elucidated in the case of nicotine and tropane alkaloids.(Fig 3). Even producing vastly different alkaloids many pathways rely at first on the modification of the amino acid/polyamine precursor and then oxidation of the resulting intermediate results after cyclization processes into a heterocyclic compound. The oxidizing enzyme, which is often named after its substrate, is in the case of tropane alkaloids and in the case of nicotine-type alkaloids a copper-containing amine oxidase (CuAO) (Hashimoto et al., 1990; Mizusaki et al., 1972). The copper-containing amine oxidase (CuAO) is an enzyme described to be involved in primary metabolism of the plant that is present in multiple copies in the genome of most plants. This oxidation process is followed by spontaneous cyclisation due to the nature of the resulting

aminoaldehyde (Mestrom et al., 2017) and the resulting core structure of the alkaloidal base is then further derivatized to result in the bouquet of individual structures later observed in the plants.

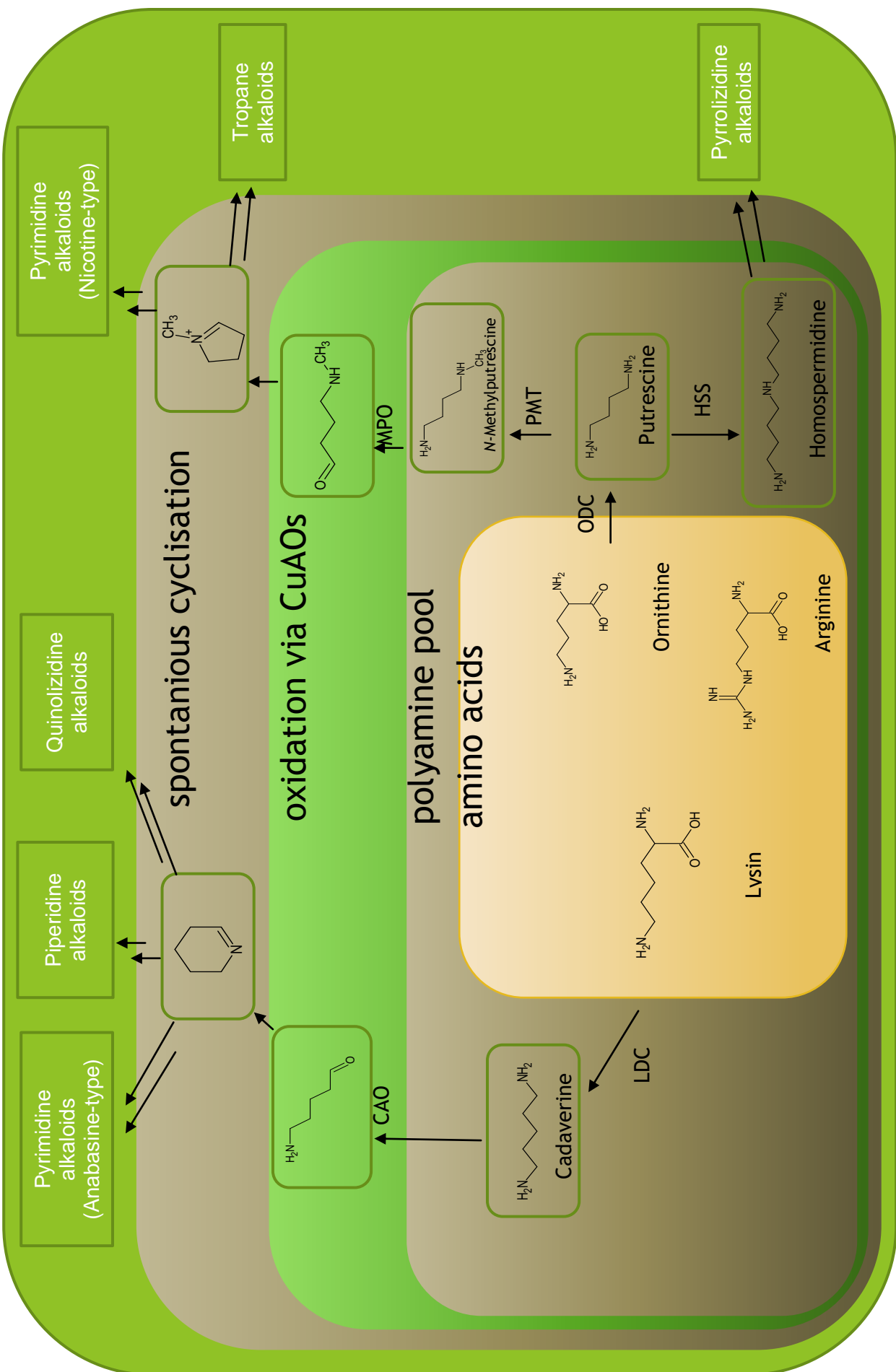


Figure 3: Biosynthetic scheme of different alkaloid biosynthesis. Multiple arrows indicate a not yet fully elucidated pathway. The color scheme represents the different types of enzymatic or chemical processes. The individual enzymes are labelled with following abbreviations: ODC = ornithine decarboxylase, LDC = lysine decarboxylase, PMT = N-putrescine methyltransferase, HSS = homospermidine synthase, MPO= N-methylputrescine oxidase, CAO = cadaverine oxidase.

1.3 Pyrrolizidine alkaloids

Pyrrolizidine alkaloids (PAs) are a typical class of plant derived alkaloids. PAs comprise of two different subunits: a necine base moiety that is esterified with a one or more necic acids. The necine base is a nitrogen containing heterocycle, the pyrrolizidine, which gives the group its characteristic name. Up to this day more than 600 different PAs have been identified (Fu et al., 2004). While the necine base is found only to vary by a limited number of functional groups and double bonds within the ring system, the necic acids can provide an almost limitless diversity and therefore creating a huge variety of PAs.

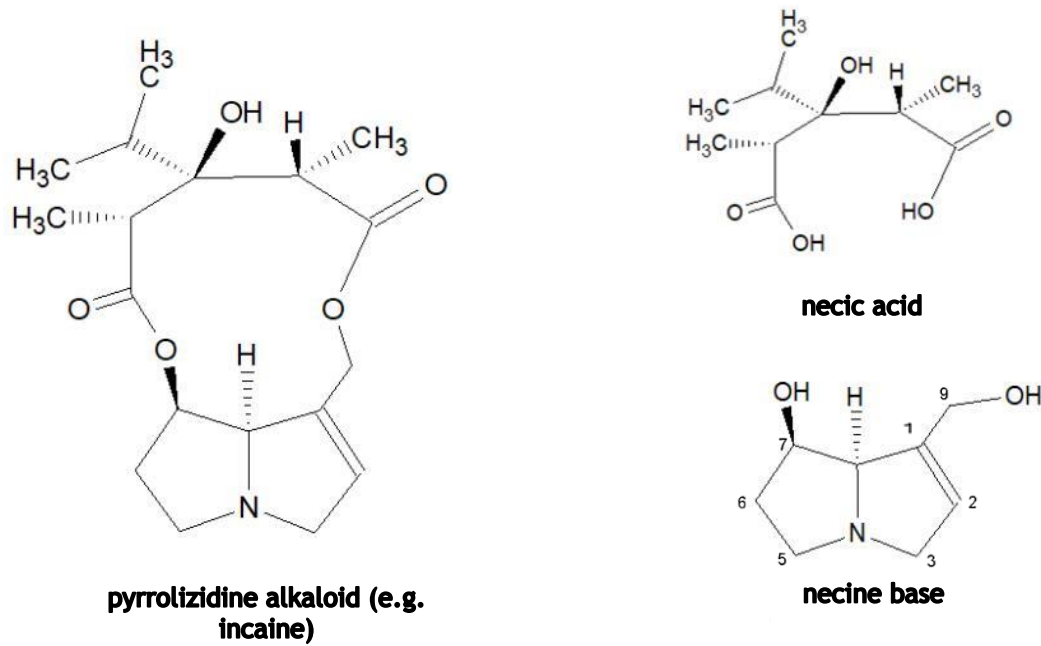


Figure 4: Structural properties of PAs

The presence of PAs is not limited to a single family in the plant kingdom. Up to this day PAs have been found for example in members of the families of the Orchidaceae, Poaceae, Asteraceae, Fabaceae, Convolvulaceae, Heliotropiaceae and Boraginaceae (Hartmann & Witte, 1995; Jenett-Siems et al., 1993; Koulman et al., 2008; Langel et al., 2011; Smith & Culvenor, 1981). This work focuses on the PA-containing model plant species common comfrey (*Symphytum officinale*, Boraginaceae) and Indian heliotrope (*Heliotropium indicum*, Heliotropiaceae).

While the ecological function of PAs have not been studied extensively they are assumed to be selected as defensive compounds against herbivores (Hartmann, 1999). There has been done testing concerning the medical potential of different PAs. Heliotrine, a PA present in *Heliotropium europaeum*, showed *in vitro* antiviral activities, but due to its toxicity they have been assessed as not suitable for medical use (Singh et al., 2002). The toxicity of PAs is also responsible for their bad public reputation since their hepatotoxic properties are known for a long time (Mattocks, 1968) and even mass intoxication have been reported due to contamination of food with PA-containing plants (Kakar et al., 2010). PAs also possess pneumotoxic properties after high dosage intake (Huxtable, 1990) and are commonly used to induce pulmonary hypertension in rodents for medicinal research

purposes (Gomez-Arroyo et al., 2011). Not all PAs are toxic by nature since a few chemocharacteristics are required for the hepatotoxic and pneumotoxic properties, which are esterification at the C9 atom, hydroxylation at the C7 atom and a double bond in the 1-2-position of the necine base (Mattocks, 1970; Mattocks & White, 1971a, 1971b).

1.4 Biosynthesis of pyrrolizidine alkaloids

The biosynthesis of PAs is considered to be a constitutive mechanism, which is not influenced by typical elicitors like jasmonic acid (Hartmann, 1999; Sievert et al., 2015). Today, only the first step of PA biosynthesis is well characterized, *i.e.* the formation of homospermidine by homospermidine synthase (HSS). Homospermidine is a symmetric triamine that was shown to be the first specific intermediate (Khan & Robins, 1985; Ober & Hartmann, 1999) in the biosynthesis of the necine base moiety (Fig 5). The HSS has been shown to be evolved from a duplication event of the gene encoding deoxyhypusine synthase (DHS). Obviously this gene duplication occurred several times independently in various angiosperm lineages resulting in a polyphyletic origin (Kaltenegger et al., 2013; Reimann et al., 2004).

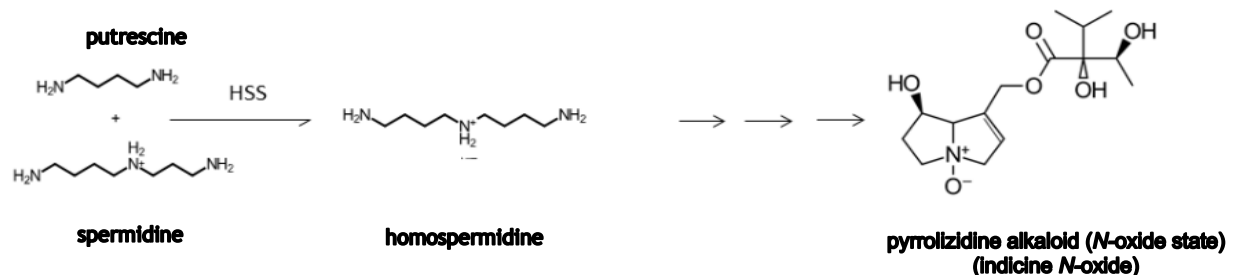


Figure 5: Formation of homospermidine, the first specific intermediate of the necine base moiety of PAs (e.g. indicine *N*-oxide)

Biosynthesis of PAs was shown to be restricted to specific plant tissues. While common comfrey (*S. officinale*) has been shown to produce PAs in the root, the indian heliotrope (*H. indicum*) was shown to produce PAs in the leaves and stem (Frölich et al., 2007). The HSS expression was localized to specific cells in these tissues (Niemüller et al., 2012). While the cells of the lower epidermis and of the stem were identified as expression HSS in *H. indicum*, *S. officinale* showed expression of HSS in the root endodermis. Surprisingly, protein blot analyses in

Niemüller et al (2012) gave hints that there might also be a second site of HSS expression in *S. officinale*, i.e. in young leaves subtending the inflorescences, but immunolocalization or tests on PA biosynthesis were performed.

The function of HSS enzyme in the biosynthesis of PAs is to modify the polyamine pool to create a unique precursor for PAs: homospermidine. It is similar to the pattern of biosynthesis of tropane and pyrimidine alkaloids (nicotine-type), where the natural polyamine pool is also derivatized to create a single precursor (*N*-methylputrescine) for alkaloidal biosynthesis (Figure 3). To study if the second step after creating the precursor is also similar to the biosynthesis of other alkaloids a copper-containing amine oxidase (CuAO) from *Pisum sativum* was used for a biomimetic experiment and incubated with homospermidine for a week. After further reduction by dehydrogenases or chemically with NaBH₄ the necine base of hydroxymethyl-pyrrolizidine (trachelanthamidine) was detected (Robins, 1995).

Based on this information a general inhibitor of CuAOs, hydroxyethylhydrazine (HEH), was given to PA-producing root cultures of *Senecio vulgaris* (Asteraceae) together with labeled putrescine. Indeed, inhibition with HEH prevented putrescine to be incorporated into PAs while homospermidine accumulated. This observation supported the hypothesis of an involvement of a CuAOs in the biosynthesis of PAs (Böttcher et al., 1993).

Recent investigations combined the knowledge of the biosynthetic localization of HSS with the hypothesis that a CuAO might be involved in PA biosynthesis. The transcriptome of the upper epidermal tissue of *H. indicum* was subtracted from the lower epidermal tissue to enrich sequences putatively involved in PA biosynthesis and to create a set of candidate genes. In a further approach the transcriptome of non-PA producing leaves of *S. officinale* was subtracted from the transcriptome of PA producing roots of *S. officinale*. With two sets of candidate genes even further false positive candidate genes could be excluded that didn't have a homologue in the other candidate gene set. In both cases a CuAO-encoding sequence came up as a possible candidate for PA biosynthesis (Kruse, 2017; Sievert et al., 2015).

1.5 Objectives and outline of this work

Objective of this work was to further elucidate the step after formation of homospermidine in PA biosynthesis. This would be an important step for the overall aim to understand the complete PA pathway: Since the origin of the HSS has been shown to be polyphyletic, i.e. it evolved independently several times in different plant lineages, also the evolution of PA biosynthesis might be polyphyletic. Therefore, a characterization of further steps of PA biosynthesis will allow in the future to understand in more detail the evolutionary mechanisms that shaped this ecological trait in the different plant lineages. Are the specific genes of PA biosynthesis the product of independent gene duplication events as it was shown for the evolution of HSS (Kaltenegger et al., 2013) or have sequences of enzymatic steps been recruited *en bloc* from other parts of plant metabolism?

Speculating that the high spatiotemporal specificity in expression of HSS is also valid for the other enzymatic steps of PA biosynthesis, the two plant species *H. indicum* and *S. officinale* have been selected as model systems for this study. Both model systems have been studied in detail on the phytochemical level (Frölich et al., 2007) and also with respect to HSS-localization by immunolocalization experiments (Niemüller et al., 2012).

Within *S. officinale*, Niemüller et al (2012) identified the root endodermis as the predominant tissue of HSS expression but had also hints that HSS might also be expressed in a specific type of leaves. Assuming that all genes of the core pathway of PAs are coexpressed with HSS, such a specific expression in only a certain developmental stage could be used for identification of candidate genes for PA biosynthesis by comparing to a similar, but non-PA-producing phase. Therefore, the preliminary observation of HSS expression in specific leaves of *S. officinale* warrants further studies.

In **Chapter 2** of this thesis the studies are presented that resulted in the identification of a second site of PA biosynthesis in *S. officinale*. By immunolocalization experiments, young leaves subtending the inflorescences

have been identified, in addition to the roots, as the site of HSS expression. Using tracer-feeding experiments it was shown that not only HSS is expressed in this stage of plant development, but the whole PA pathway. This observation adds another facet of diversity in plant secondary metabolism covering not only structural diversity but also diversity in the field of spatiotemporal regulation. This research was published in *Plant Physiology* in 2017. The detailed method for the tracer-feeding experiment used to confirm the second site of PA biosynthesis described in **Chapter 3** was published separately in *Bio-Protocols* in 2018.

The results of Chapter 2 indicated that PAs synthesized in the young leaves subtending the inflorescences of *S. officinale* are used to boost PA levels in the reproductive parts of the plant. The analyses presented in **Chapter 4** provide a closer look into the distribution and variability of PA-levels in the different parts of the inflorescences of *S. officinale*. One central observation was a surprising variability in terms of amounts and distribution of alkaloids within different parts of the flower. This research was published in *Journal of Chemical Ecology* in 2019.

The strong variability reported in Chapter 4 within the different tissue of one plant individual might mask coexpression patterns of candidate genes with HSS in further studies. Therefore, we tested in a more detailed analysis if the intraindividual variation of PA levels and HSS expression is also observed in other species. In **Chapter 5** the data is presented that resulted from analyses of PA levels in individual leaves of a single individual of *H. indicum*. Indeed also in this species a variability of PA levels and HSS transcript levels was confirmed. In addition for a first candidate, a gene encoding a CuAO, a coexpression with HSS was shown.

Based on the results from the projects described in chapter 2 to 5 a tool was available to compensate intraindividual variation by using HSS transcript levels as reference. This should allow the confirmation of candidate genes even in a highly

variable background. In **Chapter 6** research is described that used this strategy and resulted in the identification and characterization of a homospermidine oxidase (HSO), a CuAO catalyzing the second step of PA biosynthesis, i.e. the oxidation of homospermidine. An unexpected result was the observation that one enzyme is sufficient to oxidize both primary amino groups of homospermidine in a single reaction resulting in the formation of a pyrrolizidine moiety, a characteristic of the necine base moiety of PAs.

In Chapter 7 the overall implications of the research presented in this thesis are discussed in relation to the most recent literature.

2. Identification of a Second Site of Pyrrolizidine Alkaloid Biosynthesis in Comfrey to Boost Plant Defense in Floral Stage

Lars H. Kruse, Thomas Stegemann, Christian Sievert, Dietrich Ober

Detailed author contributions are listed at the end of the thesis.

2.1 Abstract

Pyrrolizidine alkaloids (PAs) are toxic secondary metabolites that are found in several distantly related families of the angiosperms. The first specific step in PA biosynthesis is catalyzed by homospermidine synthase (HSS), which has been recruited several times independently by duplication of the gene encoding deoxyhypusine synthase, an enzyme involved in the posttranslational activation of the eukaryotic initiation factor 5A. HSS shows highly diverse spatiotemporal gene expression in various PA-producing species. In comfrey (*Symphytum officinale*; Boraginaceae), PAs are reported to be synthesized in the roots, with HSS being localized in cells of the root endodermis. Here, we show that comfrey plants activate a second site of HSS expression when inflorescences start to develop. HSS has been localized in the bundle sheath cells of specific leaves. Tracer feeding experiments have confirmed that these young leaves express not only HSS but the whole PA biosynthetic route. This second site of PA biosynthesis results in drastically increased PA levels within the inflorescences. The boost of PA biosynthesis is proposed to guarantee optimal protection especially of the reproductive structures.

2.2 Introduction

Plant secondary metabolism is highly diverse on the chemical and regulatory levels (Cordell, 2013; Grotewold, 2005; Pichersky et al., 2006; Weng et al., 2012). It is often characterized by a complex interplay of various cell types and enzymes (Facchini & St-Pierre, 2005; Ziegler & Facchini, 2008). Well-characterized examples of the involvement of various cell types in the biosynthesis of alkaloids can be found in the benzyloquinoline alkaloid biosynthesis of opium poppy (*Papaver somniferum*; (Bird et al., 2003)), in the tropane alkaloid biosynthesis of *Hyoscyamus niger* and *Atropa belladonna* (Nakajima et al., 1999; Suzuki et al., 1999), and in the monoterpenoid indole alkaloid biosynthesis of *Catharanthus roseus* (Burlat et al., 2004; St-Pierre et al., 1999). Moreover, the transport from the site of synthesis to the site of accumulation requires various cell types as described for nicotine in tobacco (*Nicotiana tabacum* (Morita et al., 2009; Neumann, 1985)) or pyrrolizidine alkaloids (PAs) in *Senecio* spp. (Sander & Hartmann, 1989).

PAs are toxic compounds for the chemical defense of plants and show a scattered occurrence in many distantly related angiosperms but have in common homospermidine synthase (HSS), which is the first pathway-specific enzyme of PA biosynthesis in all these lineages. HSS uses spermidine and putrescine as substrates to catalyze the formation of homospermidine, an intermediate that has been shown to be incorporated exclusively into the necine base moiety, the characteristic bicyclic ring system of PAs (Böttcher et al., 1993, 1994). HSS has evolved by gene duplication of deoxyhypusine synthase (DHS), an enzyme involved in the posttranslational activation of the eukaryotic initiation factor 5A (D. Ober & Hartmann, 1999; Dietrich Ober & Hartmann, 1999).

Recent studies have shown that this duplication occurred several times independently during angiosperm evolution in lineages that are able to produce PAs (Anke et al., 2008; Irmer et al., 2015; Kaltenecker et al., 2013; Reimann et al., 2004). This observation suggests that the whole pathway of PA biosynthesis also evolved several times, requiring repeated integration into the metabolism of the plant. Expression analyses of HSS in PA-producing plants of various lineages show that this integration resulted in the different cellular organization of PA biosynthesis in different species. In the Asteraceae family, for example, in which independent duplications have been described in two lineages, HSS expression has been detected in *Senecio* spp. (ragwort; tribe Senecioneae) only in cells of the endodermis and adjacent root parenchyma, cells that lie opposite to the phloem, whereas in *Eupatorium cannabinum* (hemp agrimony; tribe Eupatorieae), HSS expression has been found in all cells of the root cortex but not in the endodermis. In orchids (*Phalaenopsis* spp.), HSS has been localized in meristematic cells of the root apical meristem and in young flower buds (Anke et al., 2008).

Within Boraginales, a single duplication event resulted in the evolution of HSS. However, in this lineage, the expression pattern of HSS has been shown to be multifaceted, suggesting independent scenarios of optimization and integration of the gene duplicate into the metabolism of the plant. Within the Heliotropiaceae (Indian heliotrope (*Heliotropium indicum*)), HSS expression is found in the lower leaf epidermis, whereas in *Cynoglossum officinale* (houndstongue; Boraginaceae), the endodermis and pericycle of the root express HSS (Niemüller et al., 2012). In

comfrey (*Symphytum officinale*; Boraginaceae), HSS has been localized exclusively in cells of the endodermis (Niemüller et al., 2012), supporting previous studies by (Frölich et al., 2007), who identified the roots of comfrey as the site of PA biosynthesis by tracer experiments with radiolabeled putrescine. Studies by (Niemüller et al., 2012) using protein-blot analyses suggested that HSS expression occurs also during a restricted window of leaf development in comfrey, an observation that warrants a closer look at the PA biosynthetic capacity of leaves of this plant species.

In this study, we show that comfrey synthesizes PAs not only in the roots but also in young leaves subtending an inflorescence with unopened flower buds. We further show that HSS is expressed in specific cells of the leaf during certain stages of inflorescence development coinciding with PA production in the leaf. This second auxiliary site of PA biosynthesis during flower development is discussed in comparison with a similar mechanism observed previously in the orchid *Phalaenopsis amabilis*, in which young flower buds produce PAs to boost PA levels in the mature flower in order to guarantee an efficient supply of deterrent PAs for the developing reproductive structures (Anke et al., 2008).

2.2 Results

2.2.1 Levels of *hss* Transcript and Protein Expression Are Dependent on Leaf Position in Relation to the Inflorescence

Analyzing three species of Boraginales, (Niemüller et al., 2012) showed that HSS expression is species specific. In comfrey, in which the whole PA biosynthesis is localized in the roots, that study indicated that HSS also is expressed in leaves of a specific developmental stage (i.e. leaves that are directly beyond a terminal inflorescence with closed flower buds).

In order to correlate leaf position with *hss* expression in comfrey, we harvested leaves from various positions in the shoot system of a plant just opening its first flower buds (Fig. 7A). Analyses with reverse transcription (RT)-PCR and quantitative reverse transcription (qRT)-PCR showed that the highest levels of *hss* transcript were detectable in young leaves directly next to inflorescences with buds and flowers that had just opened (Fig. 7B; Supplemental Fig. S2). The *hss* transcript level differed between the youngest and the oldest leaf by almost a factor of 30 (Supplemental Fig. S2). To test whether *hss* transcript levels were correlated with the expression of HSS protein, protein extracts of leaves from various positions of the shoot system from another individual plant were analyzed by protein gel blot with an antibody specific for HSS of comfrey (Niemüller et al., 2012). Like the *hss* transcript level, *hss* protein expression is strongest in young leaves directly subtending an inflorescence (leaves 1 and 2) and fades away with increasing distance of the leaves from the flower (Fig. 7C). Of note, in leaves that have no axillary branch developing in their axils, HSS protein is not detectable (leaves 9 and 10; blue in Fig. 7A), whereas leaves that possess axillary branches show distinct HSS expression (leaves 3, 4, 6, and 8; red in Fig. 7A). Congenital fusions of an axillary branch with the main axis are common for comfrey (Kotelnikova et al., 2011) and result in a lateral bud on the axis distant from its subtending leaf (e.g. leaves 5 and 7; purple in Fig. 7A).

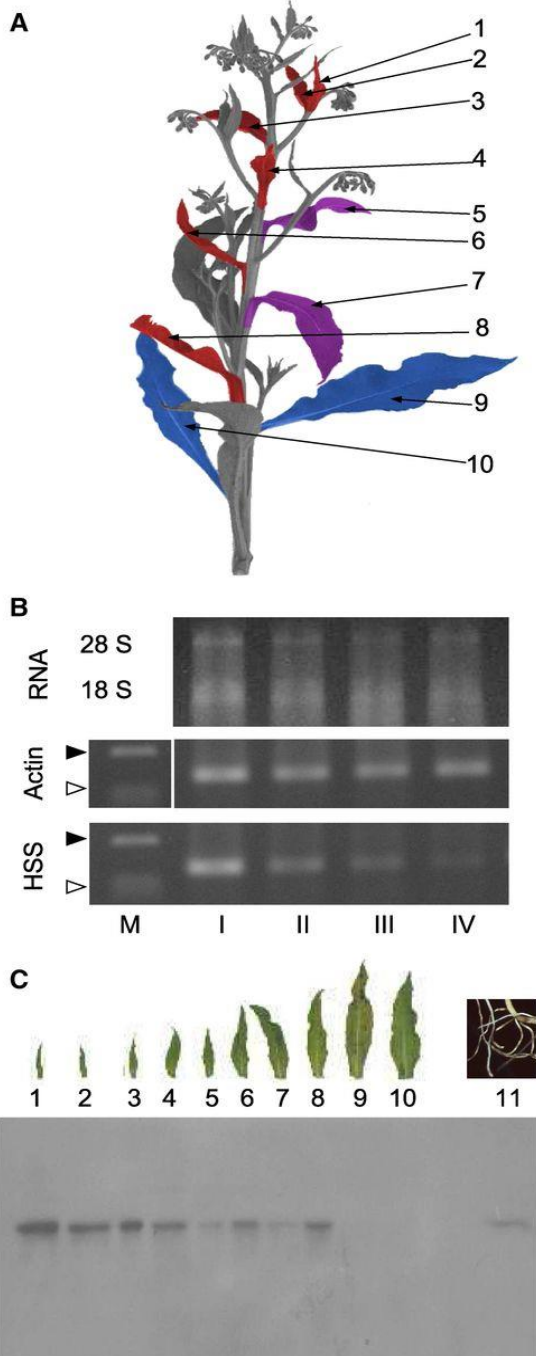


Figure 6: Transcript and protein-blot analyses of leaves at various developmental stages. **A**, Habitus of a comfrey shoot. Numbers indicate leaves that were analyzed by protein-blot analysis. The color code indicates the level of HSS expression according to the protein-blot analysis given in C (red, high expression; purple, medium expression; blue, no expression). **B**, Semiquantitative RT-PCR shows the highest expression of HSS transcripts in leaf type I. Leaf types I to IV comply with leaves 1, 4, 8, and 10 in A, respectively, but were harvested from another individual plant as independent proof. RNA integrity was confirmed by the detection of two distinct bands of 28 S and 18 S rRNA. Actin served as the reference gene. Black arrowheads show marker bands (M) at 150 bp, and white arrowheads indicate marker bands at 100 bp. **C**, Protein-blot analysis of protein extracts from leaves numbered according to A. Crude protein extracts (10 μ g of protein per lane) were separated via SDS-PAGE and blotted onto a polyvinylidene difluoride (PVDF) membrane. Affinity-purified HSS-specific antibody was used for detection in combination with a secondary goat anti-rabbit antibody conjugated with

horseradish peroxidase. A protein extract of a root of comfrey served as a positive control (sample 11).

2.2.2 Immunolocalization of HSS in Leaves of Comfrey

Leaves that tested positive for HSS expression were used to identify, by immunolocalization, the cells expressing HSS. HSS expression was found to be

restricted to bundle sheath cells that formed a layer of compactly arranged parenchyma around the vascular bundle (Fig. 7, C and D). The labeled layer had a thickness of one to two cells and was separated from the epidermis by at least a single row of unlabeled mesophyll cells. The specificity of the label was tested by preincubation of the antibody with soluble, heterologously expressed HSS, DHS, or BSA before labeling. Only preincubation with HSS resulted in a decrease of signal, whereas preincubation with DHS or BSA had no effect.

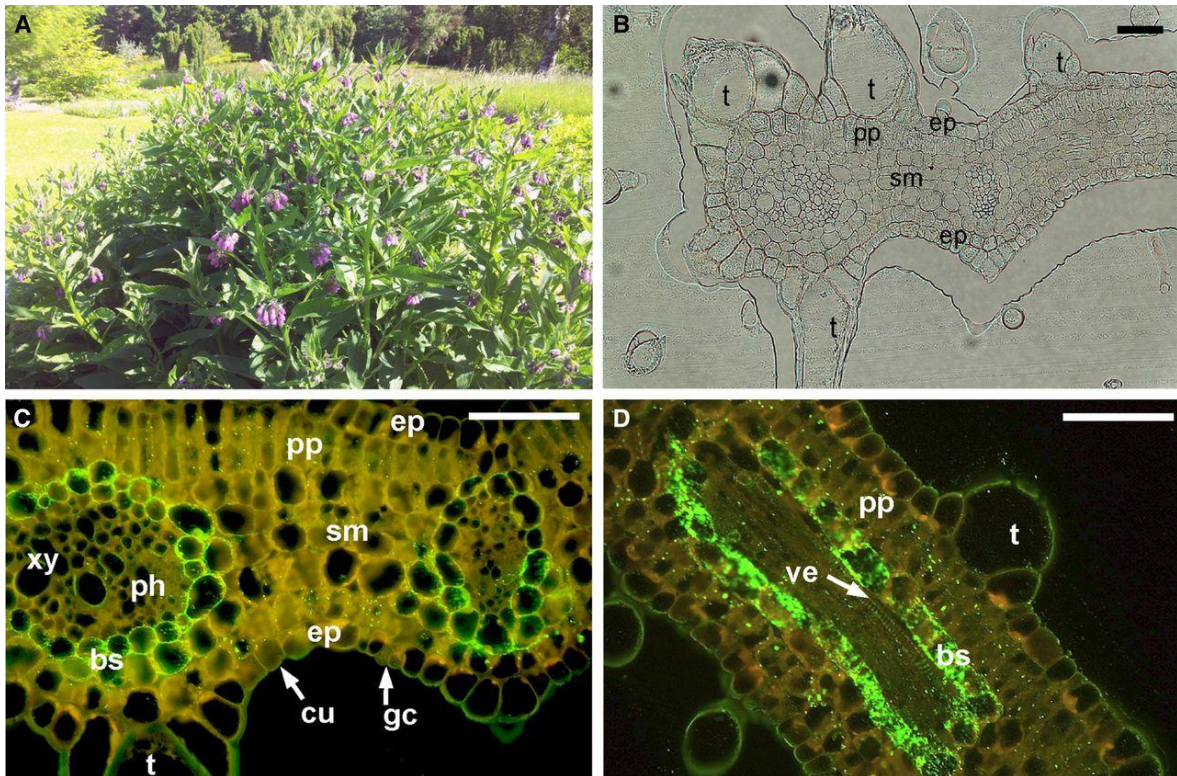


Figure 7: **Immunolabeling of HSS in cross sections of a young leaf subtending an inflorescence with unopened flower buds of comfrey.** A, Plant habitus. B, Bright-field microscopy of a leaf cross section. C, Detail of B. D, Leaf cross section with a vascular bundle cut longitudinally. In C and D, HSS was immunolabeled by incubation with an affinity-purified HSS-specific antibody and visualized with a secondary antibody conjugated with AlexaFluor488 under UV light. bs, Bundle sheath cells; cu, cuticle; ep, epidermis; gc, guard cell; ph, phloem; pp, palisade parenchyma; sm, spongy mesophyll; t, trichome; ve, vessel element; xy, xylem. Bars = 10 μ m.

The close vicinity of HSS expression and the vascular bundle also is observed in the roots of comfrey, in which HSS is only detectable in the endodermis that encloses the root central cylinder with the vascular tissue (Niemüller et al., 2012). Both of these tissues, namely the endodermis and the bundle sheath cells, play a key role in controlling fluxes to and from the vascular bundle and are important for maintaining the transport of nutrients and water in the plant (Geldner, 2013; Leegood, 2008; Steudle & Peterson, 1998).

Of note, nucleotide sequences encoding HSS amplified from the leaves proved to be identical to those amplified from the roots, suggesting that a single *hss* gene is responsible for the expression of HSS in the endodermis of the root and the bundle sheath of specific leaves.

2.2.3 Capacity of Comfrey Leaves to Synthesize PAs

By applying ^{14}C -labeled putrescine to young detached leaves expressing HSS, we tested whether leaves expressed only HSS or the complete biosynthetic machinery to produce PAs. After incubation for 4 d, the tracer was completely taken up by the leaves, of which 16% of the applied radioactivity was detectable in the alkaloid-containing sulfuric acid crude extract. After reduction to convert all PA *N*-oxides to their tertiary form, PAs were enriched by solid-phase extraction. This alkaloid-enriched fraction containing 8% of the applied radioactivity was split into two fractions that were treated differentially to confirm the identity of the labeled compounds as PAs (Table I). One fraction was analyzed directly by HPLC to detect radioactively labeled PAs; several peaks of putative PAs were found (Fig. 9A). To establish that the detected radioactive peaks were PAs that resulted from the incorporation of the tracer putrescine, the second fraction was hydrolyzed to reduce all potential PAs to their backbone, the necine base. Comfrey produces a PA bouquet of intermedine derivatives, including O^9 -monoesters, O^7, O^9 -diesters, and 3'-acetyl derivatives such as 7-acetylintermedine, 7-acetyllycopsamine, 7-seneciylintermedine (echiupinine), or 7-tigloylintermedine (myoscorpine; (Frölich et al., 2007; Hartmann & Witte, 1995)). The necine base of these PAs, all belonging to the so-called lycopsamine type, is retronecine (Hartmann & Witte, 1995). If the radioactive peaks represent PAs, hydrolyzation should result in a single peak that

comigrates with a retronecine standard. In contrast to the several peaks detectable in the nonhydrolyzed extracts (Fig. 9A), the hydrolyzed extract (Fig. 9B) showed only one prominent peak that had the same retention time as retronecine (Fig. 9C). Spiking the hydrolyzed sample with retronecine resulted only in an intensification of the signal, indicating that the same substance was being analyzed (Fig. 9D). As an additional proof of identity, the feeding experiment was repeated as described, but with unlabeled putrescine. The alkaloid-containing fraction was hydrolyzed and separated by thin-layer chromatography (TLC) parallel to the hydrolyzed sample resulting from the tracer feeding experiment. After the localization of radioactivity, the corresponding area in the lane of the nonradioactive samples was scraped off the plate, and the compounds were eluted and analyzed by gas chromatography-mass spectrometry (GC-MS). In this spot, retronecine was detected as the major compound, giving support to the interpretation that retronecine was the radioactive compound detected after hydrolysis of the extract after tracer feeding (Supplemental Fig. S4).

Tracer feeding experiment: recovery of applied radioactivity

Parameter	Radioactivity	Percentage of Recovered Radioactivity
	<i>kBq</i>	
Total radioactivity applied	169	100
Crude extract (sulfuric acid)	25	16
Crude extract after reduction	27	16
Extract purified via SCX-SPE (PA enrichment)	15	8

Figure 8: Tracer feeding experiment: recovery of applied radioactivity

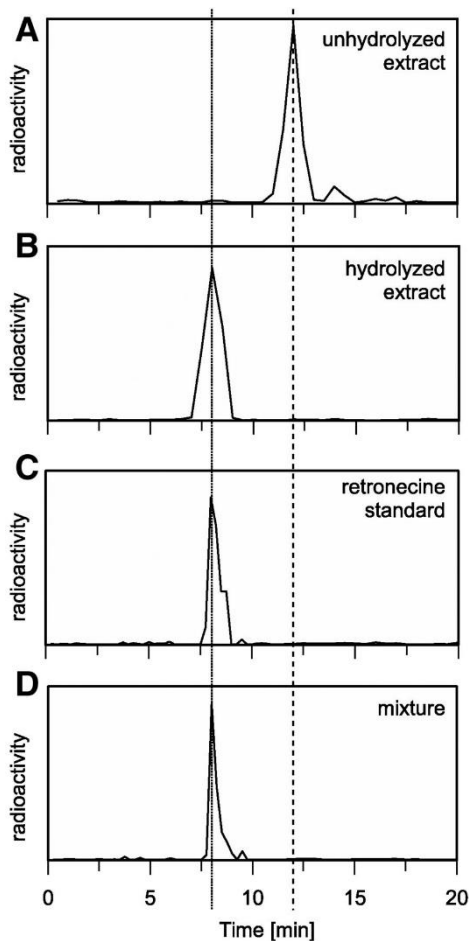


Figure 9: HPLC elution profiles of alkaloid extracts of leaves after tracer feeding. Young leaves subtending an inflorescence with unopened flower buds were fed with $[^{14}\text{C}]$ putrescine as a tracer. Extracts were enriched for PAs by solid phase extraction (SPE) purification before separation. **A**, Nonhydrolyzed leaf extract. **B**, Hydrolyzed leaf extract. **C**, Radiolabeled leaf extract, **D**, Mixture of hydrolyzed extract and retronecine standard

2.2.4 Leaves Boost PA Levels in Inflorescences

To test the consequences of the capacity of leaves to produce PAs, we analyzed the transcript and protein levels of HSS and the total PA content in leaves subtending an inflorescence and in their associated inflorescences during development. Seven different inflorescence developmental stages were defined with respect to size and flowering state (Fig. 10A). Stage I was characterized by its small size (~1 cm in diameter), whereas stage II was much larger but had flower buds that were still closed. Size increased until stage V. At stage IV, the flower bud tips became purple. At stage V, the first buds started flowering but most of the buds remained closed, whereas by stage VI, all the flowers had opened, and those that had opened first were beginning to darken. At stage VII, the flowers withered and fruits began to develop. We observed that HSS transcript and protein in leaves were detectable from stage I onward and that HSS expression levels reached their maximum at stages II and III, after which they decreased to a low level and

remained constant to the last stage (Fig. 10B and Supplemental Fig. S6). PAs were not detectable in leaves of stage I. PA levels increased from stage II to stage IV to a concentration of about $20 \mu\text{g g}^{-1}$ dry weight, and at stage VII they reached concentrations of about $180 \mu\text{g g}^{-1}$ dry weight (Fig. 10C), similar to that described for leaves of comfrey (Couet et al., 1996; Lindigkeit et al., 1997; Mattocks, 1980). As in the leaves, no PAs were detectable in inflorescences at stage I. Inflorescences at stages II to V showed PA concentrations of ~ 300 to $400 \mu\text{g g}^{-1}$ dry weight, increasing at stage VI to $3,344 \mu\text{g g}^{-1}$ dry weight (Fig. 10C), with a total PA content of $700 \mu\text{g}$ per inflorescence (Fig. 10D). These high concentrations correspond to PA levels described for flowers of other PA-producing plant species (Couet et al., 1996; Frölich et al., 2006, 2007; Mutterlein & Arnold, 1993). In the last analyzed stage, stage VII, the concentration dropped to $\sim 500 \mu\text{g g}^{-1}$ dry weight. The comparatively low PA concentrations in leaves compared with inflorescences suggest that PAs are efficiently translocated from the leaves to the inflorescences. Thus, PA biosynthesis in the young leaf subtending the inflorescence ensures a sufficient supply of PAs (1) to keep alkaloid levels constant as long as the inflorescences enlarge and (2) to enable high PA levels to accumulate when the flowers open.

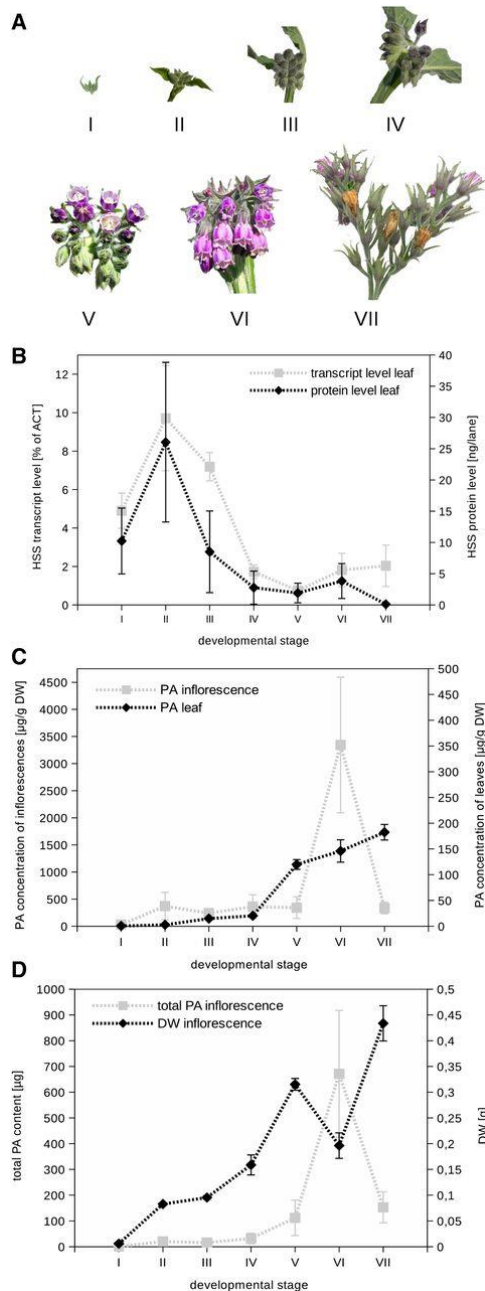


Figure 10: PA content and HSS expression in leaves and inflorescences of various developmental stages. **A**, Inflorescences at various developmental stages. **B**, Protein and transcript levels of HSS in leaves subtending inflorescences. **C**, PA concentrations in the inflorescences and in the subtending leaves at the respective developmental stages. **D**, Total PA content and dry weight (DW) of the inflorescence. Inflorescences and corresponding subtending leaves were harvested, and inflorescences at the developmental stages I to VII were weighed. PAs from inflorescences and leaves were extracted and analyzed according to the sum parameter method (C and D). For relative transcript quantification, qRT-PCR was used with actin (ACT) as the reference gene (B). For relative protein quantification, total protein was extracted and separated via SDS-PAGE before being transferred to a PVDF membrane. Affinity-purified HSS-specific antibody was used for detection in combination with a secondary goat anti-rabbit antibody conjugated with horseradish peroxidase. Protein level was calculated in relation to 25 ng of recombinant HSS that was used as a standard (B).

Error bars indicate se of three independent biological replicates for each developmental stage. Error bars of PA concentration in leaves of stages II and III are missing in C because of insufficient sample material

To test whether the inflorescence itself contributes to the high PA concentrations, we analyzed HSS expression in inflorescences of various developmental stages (Supplemental Fig. S7). Only very low levels of HSS protein were detectable at any stage of inflorescence development. This observation is in accordance with (Niemüller et al., 2012), who found low levels of HSS transcript but no protein in inflorescences. In contrast to the inflorescences, roots showed a high HSS level of ~40 to 50 ng per 20 µg of total protein, a value that is comparable with the highest HSS levels detected in the leaf at stage II, with a maximum value of 39 ng. The delay between the highest levels of HSS (stage II) and the peak of PA accumulation (stage VI) results most likely from two factors:

(1) the need to transport PAs from their site of synthesis in the young leaf into the inflorescence, and (2) the finding that PA biosynthesis in species of the Boraginales seems to be less channeled than in other PA-producing species, as shown by (Frölich et al., 2007) using radioactively labeled putrescine as a tracer.

The maximal incorporation of tracer into PAs took more than 2 weeks, with a temporary accumulation of pathway intermediates such as homospermidine or a polar uncharacterized compound. The drastic decrease of PA levels at stage VII might have various causes. One explanation could be the abscission of the petals, which was observed at this stage. PAs in the petals might be a strategy to fend off nectar robbers such as short-tongued bumblebees of the genus *Bombus* (Irwin & Maloof, 2002; Utelli & Roy, 2001). Nectar robbers bite a hole in the petal tube to reach nectar without actually entering and pollinating the flower (Castro et al., 2008). Another explanation for the drop of PA levels could be the degradation of PAs in these tissues or the translocation of PAs from the inflorescences to other tissues of the plant, as PA *N*-oxides are highly mobile and can easily be translocated from one tissue to another (Hartmann et al. 1989). Further studies should elucidate the dynamics of PA levels in these reproductive structures.

2.3 Discussion

In this study, we show that comfrey has two PA biosynthetic sites that differ with respect to their function (i.e. the roots as a well-characterized organ of PA biosynthesis and young leaves that are in the direct vicinity of a developing inflorescence). The roots in comfrey are responsible for constitutive PA production, most likely for the protection of the vegetative parts of the plant. Confirmation that the whole PA pathway is expressed in the roots has been obtained from root cultures that are able to produce PAs (Frölich et al., 2007). A link between growth and PA biosynthesis should guarantee a constant ratio between PA and biomass, a phenomenon that we also observed for PA-producing species of other lineages (Anke et al., 2004; Niemüller et al., 2012). In contrast, the young leaves subtending an inflorescence with unopened flower buds characterized in this study provide an additional PA supply for the reproductive tissues within the flowers of comfrey, a pattern observed previously for PA-producing *Phalaenopsis* spp. (Orchidaceae). In *Phalaenopsis* spp., specific structures within small flower buds, but not of open flowers,

produce PAs during flower development, boosting PA levels up to about 6 mg g⁻¹ fresh weight (Anke et al., 2008). The assumption, in comfrey, that PA biosynthesis in the young leaf also is of functional importance is supported by the incorporation rate of labeled putrescine into PAs of almost 10% (Table I). This incorporation rate is remarkable, bearing in mind that putrescine is not only a precursor for PA biosynthesis but also part of the highly dynamic polyamine pool of primary metabolism, including essential functions such as growth, development, and biotic and abiotic stress responses (Alcázar et al., 2010; Evans & Malmberg, 1989; Gill & Tuteja, 2010; Tiburcio et al., 2014). As HSS evolved independently in *Symphytum* and *Phalaenopsis* (Nurhayati et al., 2009; Reimann et al., 2004) the selection pressure that resulted from the need to protect the reproductive structures against herbivores

obviously resulted in a similar regulation of PA biosynthesis in these two lineages. The protection of reproductive structures is a phenomenon that is often observed in the plant kingdom and that is in good accordance with the optimal defense theory (McKey, 1979). The pattern of HSS expression in PA-producing angiosperms is highly variable. Nonetheless, several PA-producing plants show similarities in HSS expression. The vicinity of the vascular tissue to cells involved in PA biosynthesis is a motif found not just in the roots and leaves of *Symphytum* spp. but also in other PA-producing plants, such as *C. officinale* (also Boraginaceae), expressing HSS in the endodermis and the pericycle of the roots, or in *Senecio* spp. (Asteraceae), in which HSS is expressed in cells directly next to the phloem. In *Senecio* spp., the phloem has been shown to be the tissue by which PAs are transported from the site of synthesis to the shoot, where they are then efficiently allocated to the inflorescences, the major site of storage (Hartmann et al., 1989; Moll et al., 2002). Moreover, a link between alkaloid biosynthesis and the vascular tissue has been described for other plant systems, such as for the early steps of monoterpene indole alkaloid biosynthesis (Burlat et al., 2004), for the biosynthesis of morphine in opium poppy (Bird et al., 2003; Weid et al., 2004) and for tropane alkaloid biosynthesis in solanaceous plants (Kanegae et al., 1994; Suzuki et al., 1999).

Despite the probability that HSS, and most likely the complete pathway of PA biosynthesis, evolved several times independently in various lineages of the angiosperms (Anke et al., 2008; Kaltenecker et al., 2013; Reimann et al., 2004) the similarity between the PA structures produced is remarkable. Not only is the bicyclic ring system characteristic for all PAs, namely the necine base, identical with respect to their structure and stereochemistry between unrelated plant lineages, but also the complete PA molecules (Hartmann & Witte, 1995). Similar selection pressures probably forced the evolution of similar, almost identical traits (Pichersky et al., 2006). In this study, we have shown that the strategy of using a second auxiliary site for PA biosynthesis to protect floral structures also evolved independently in two distantly related species, extending the aspect of convergent

evolution from molecular structures to the regulation of the whole pathway. Further work will be needed to analyze the evolutionary mechanisms underlying the repeated recruitment, optimization, and integration of PA biosynthesis into the metabolism of the plant.

2.4 Materials and Methods

2.4.1 Plant Material

Comfrey (*Symphytum officinale*) was grown in pots with a mixture of TKS2 (Floragard) and lava granulate at a ratio of 3:1 in the Botanical Gardens Kiel from April to September.

2.4.2 RNA Isolation and Quantification of Transcripts

For transcript analyses of leaves in relation to their positions in the shoot system, plant samples were pulverized in liquid nitrogen with mortar and pestle before total RNA was extracted with Trizol (Invitrogen, Life Technologies) according to the manufacturer's protocol, but with two additional phase separation steps involving the addition of 200 μ L of chloroform to the aqueous phase followed by phase separation via centrifugation. Finally, RNA was washed twice with ice-cold ethanol (75% [v/v] in water). A subsequent lithium chloride (2 M final concentration) precipitation (16 h and 4°C) and two additional washing steps with ice-cold ethanol were then performed to remove possible inhibitors of the following RT reactions. RNA was dissolved in RNase-free water, and RNA integrity and purity were tested by agarose gel electrophoresis and by 260/280-nm and 260/230-nm ratio measurements using a NanoDrop 1000 UV/VIS spectrometer. One microgram of total RNA was used as a template for RT with an oligo(dT)₁₇ primer (Supplemental Table S1) and RevertAid Premium Reverse Transcriptase (Thermo Scientific). For the transcript quantification of HSS in leaves subtending inflorescences at various developmental stages, a

slightly modified protocol for total RNA isolation was employed. Instead of washes with ethanol, RNA was diluted 1:1 with 100% ethanol and loaded on spin columns from the Direct-zol RNA MiniPrep Kit (Zymo Research). Samples were further processed as recommended by the manufacturer, including an optional on-column DNase I digestion. For transcript quantification, 1.5 µg of total RNA was used for RT as described previously. To test for contaminating genomic DNA, control reactions were prepared without reverse transcriptase and used as a template in control PCRs (Supplemental Fig. S5). For semiquantitative PCR (sqPCR), GoTaq-DNA polymerase (Promega) with deoxyribonucleotide triphosphates (0.2 mM each) and primers (0.2 µM each) was used, and aliquots were taken after 20, 25, 30, and 35 cycles to ensure sampling before PCR product formation reached saturation (Supplemental Fig. S1). Products were analyzed on a 2% (w/v) agarose gel. Quantitative real-time PCR was performed in a Rotor-Gene Q System (Qiagen) with GoTaq qPCR Master Mix (Promega) following the manufacturer's protocol. Melting curve analyses were undertaken to distinguish specific PCR products from primer dimers or unspecific PCR products. The calculation of the relative transcript levels of HSS was carried out by comparative Ct methods ($2^{-\Delta\Delta C_t}$ for Fig. 10B and $2^{-\Delta C_t}$ for Fig. 10B; (Schmittgen & Livak, 2008)). Actin served as the reference gene to normalize expression levels. For both sqPCR and qRT-PCR, an annealing temperature of 60°C was used. Primer pairs were P1 and P2 (for HSS) and P3 and P4 (for actin; Supplemental Table S1). The actin-specific primers resulted from an actin-encoding sequence amplified with a pair of degenerate primers (P5 and P6) designed according to an alignment of the actin-encoding sequences of *Arabidopsis* (*Arabidopsis thaliana*), as described previously (Sievert et al., 2015). For the cloning of PCR products, the pGEM T-easy vector (Promega) was employed according to the manufacturer's protocol followed by transformation into chemically competent *Escherichia coli* TOP10 cells (Invitrogen) for vector propagation. Plasmids were sequenced at MWG Eurofins to confirm the identity of the amplification products.

2.4.3 Protein-Blot Analysis of Comfrey Leaves

Samples were pulverized in liquid nitrogen with pestle and mortar. Protein was extracted with phosphate-buffered saline supplemented with 5% (m/v) polyvinylpyrrolidone and 2.5% (w/v) sodium ascorbate to prevent protein precipitation by polyphenols. Ten to 20 μg of total protein per sample was mixed with SDS loading buffer and separated by SDS-PAGE followed by semidry blotting and immunodetection as described previously (Anke et al., 2008). The polyclonal antibody was affinity purified against recombinant HSS of comfrey (Niemüller et al., 2012). MultiMark Multi-Colored Standard (NOVEX), PageRuler Plus Prestained Protein Ladder (Thermo Scientific), and PageRuler Prestained Protein Ladder (Thermo Scientific) were used as protein mass standards as indicated in the figure legends. After immunodetection, PVDF membranes were stained with PageBlue Protein Staining Solution (Thermo Scientific) to ensure that equal protein amounts were loaded on each lane. For the relative quantification of protein levels by densitometry, we used the software ImageJ (version 1.48) with 25 ng of recombinant HSS protein as the reference (Schneider et al., 2012).

2.4.4 Immunohistochemical Staining of HSS in Leaf Cross Sections

For the immunohistochemical localization of HSS in leaf cross sections, young leaves were harvested and the tip and the base were cut off to be used as reference tissue, whereas the central part of the leaf was cut into pieces of ~ 1 cm side length before being immersed in ice-cold fixation buffer according to (Anke et al., 2008). The reference tissue of each leaf was pulverized in liquid nitrogen, and total RNA was extracted and transcribed to cDNA as described above. Each reference tissue was tested by sqPCR for the presence of HSS transcripts. The fixed central regions of positively tested leaves were dehydrated in an ethanol series and embedded in Technovit 7100 (Heraeus Kulzer). Sections of 3 to 4 μm thickness were cut on a microtome (HM3555S; Microm) and mounted on adhesive microscope slides

(SuperFrost; Thermo Fisher Scientific). Immunodetection with HSS-specific antibodies and specificity tests with recombinant HSS and DHS of comfrey were carried out as described previously (Niemüller et al., 2012).

2.4.5 Radioactive Tracer Feeding Experiments and Product Analysis

To test the capacity of detached leaves of comfrey to produce PAs, [^{14}C]putrescine (3.95 GBq mmol $^{-1}$; GE Healthcare) was used as a tracer. Two young leaves (~3.5 cm in length) next to an inflorescence with developing flower buds were cut from the plant and transferred into a 1.5-mL reaction tube containing the tracer dissolved in 1 mL of tap water (169 kBq). The leaves were incubated in a light/dark regime of 12 h/12 h (light of ~1,000 lux) at room temperature. Once the liquid was almost completely taken up, the same volume of tap water without tracer was added. After 4 d, the leaves were frozen in liquid nitrogen and stored at -50°C . Both leaves were pulverized in liquid nitrogen with mortar and pestle and extracted in 1.5 mL of 0.05 M H $_2$ SO $_4$ by being vortexed for 3 min at room temperature. After centrifugation (10 min at 5,000g), zinc dust was added in excess to the supernatants, which were then stirred for 3 h for the complete reduction of alkaloid *N*-oxides. As SCX-SPE purification has been shown to be suitable for the enrichment of PAs (Colegate et al., 2005), the samples were further centrifuged (10 min at 5,000g) and then applied to SCX-SPE cartridges (Phenomenex) equilibrated with 6 mL of methanol and 6 mL of 0.05 M H $_2$ SO $_4$. After each column had been washed with 12 mL of water and 12 mL of methanol, the alkaloids were eluted by applying 3 × 6 mL of methanol containing 5% (v/v) NH $_4$ OH. All elution fractions were combined, the solvent was vaporized, and the residue was dissolved in 2 mL of methanol. The supernatant was transferred in equal parts into two vials, dried, and stored at -20°C . For hydrolysis, one of the samples was incubated in 2 N sodium hydroxide for 3 h at 60°C , and the solvent was vaporized. For HPLC analyses, the hydrolyzed and the nonhydrolyzed samples were dissolved in 50 μL of methanol. Each step of the extraction process was monitored via scintillation counting (Tri-Carb LSC; Perkin Elmer) to calculate the ratio of incorporated [^{14}C]putrescine.

Radio-HPLC measurements were performed on a Merck-Hitachi L-6200 instrument with solvent A (100 mM phosphate buffer, pH 7.5) and solvent B (acetonitrile) at a ratio of 85:15 with a flow rate of 1 mL min⁻¹. Aliquots of 20 µL of sample were injected, and fractions were collected every 30 s for comparison of the hydrolyzed and the nonhydrolyzed extract and every 15 s for comparison of the hydrolyzed extract with retronecine and with hydrolyzed and nonhydrolyzed monocrotaline standards (Roth). The radioactivity of the fractions was quantified by scintillation counting. Radiolabeled retronecine was obtained by the hydrolysis of [¹⁴C]senecionine (Lindigkeit et al., 1997)

For TLC, Silicagel G-25 TLC plates (Merck) were developed in a mobile phase containing ethyl acetate, isopropyl alcohol, and ammonium hydroxide (25% [v/v]; 45:35:20). Radioactivity was detected using a radioactivity TLC detector (RITA; Raytest). Compounds scraped from the TLC plate were eluted with the mobile phase, dried, and dissolved in 50 µL of methanol for GC-MS analysis. GC-MS data were obtained with a Shimadzu GC-2010 chromatograph equipped with a 15 m Optima-1 MS capillary column coupled to a quadrupole mass spectrometer (Fisons MD800). Electron-impact mass spectra were recorded at 70 eV. Gas chromatography conditions were as follows: injector, 250°C; temperature program, 60°C for 3 min and 60°C to 300°C at 6°C min⁻¹; carrier gas, helium at 1 mL min⁻¹. GC-MS data for retronecine were as follows:

Retention index (Kovats) (Ri), 1,478 (on the Optima-1 MS capillary column); and mass-to-charge ratio, 155 [M⁺]. For the mass spectrometry spectrum, mass-to-charge ratio and (relative intensity) were as follows: 80 (100), 111 (74), 155 (45), 94 (37), 68 (34), 93 (33), 82 (31), (30), 67 (29), and 106 (25).

2.4.6 Quantification of Total PAs in Inflorescences

Total PAs were extracted from lyophilized inflorescences, hydrolyzed, and reduced to obtain the necine base retronecine as described for the tracer feeding experiment. For quantification of the necine base, the sum parameter method involving silylation of the necine base followed by GC-MS was applied according to (Kempf et al., 2008). Retronecine from hydrolyzed monocrotaline served as the external standard.

2.4.7 Accession Numbers

Sequence data from this article have been deposited in the GenBank/EMBL data libraries under accession number [LT631489](#), *comfrey* partial mRNA for actin (*act* gene).

2.5 Acknowledgments

We thank Dr. Dorothee Langel for help in designing the radioactive tracer feeding experiments; Jan Baur, Margret Doose, Brigitte Schemmerling, and Karina Thöle for support in the laboratory; and Dr. Elisabeth Kaltenecker, Dr. Jessica Garzke, and Annika Jonathas for helpful comments on the article.

3. Radioactive Tracer Feeding Experiments and Product Analysis to Determine the Biosynthetic Capability of Comfrey (*Symphytum officinale*) leaves for Pyrrolizidine Alkaloids

Thomas Stegemann, Lars H. Kruse, Dietrich Ober

Detailed author contributions are listed at the end of the thesis.

3.1 Abstract

This protocol delivers a method to determine the biosynthetic capability of comfrey leaves for pyrrolizidine alkaloids independently from other organs like roots or flowers.

The protocol applies and combines radioactive tracer experiments with standard and modern techniques like thin layer chromatography (TLC), solid-phase extraction (SPE), high-performance liquid chromatography (HPLC) and gas chromatography-mass spectrometry (GC-MS).

Keywords: Tracer, Radio-HPLC, Radio-TLC, SPE, GC-MS, Alkaloid, Plant-organ specificity

3.2 Background

Comfrey roots are known to be able to synthesize pyrrolizidine alkaloids (Frölich et al., 2007) and the key enzyme for biosynthesis, homospermidine synthase (HSS), was localized in the endodermis cells. In addition to this site of synthesis, there have been hints that also leaves of a certain developmental stage might be able to produce pyrrolizidine alkaloids (Niemüller et al., 2012). Therefore, a protocol was developed to determine the biosynthetic capability of comfrey leaves to synthesize pyrrolizidine alkaloids independently from other plant organs.

3.3 Materials and Reagents

- 1 epT.I.P.S® pipette tips (Eppendorf, catalog number: 0030000730)
- 2 Strata SCX 500 mg/6 ml tubes (Phenomenex, catalog number: 8B-S010-HCH)
- 3 Scintillation vial 4 ml (Carl Roth, catalog number: HEE8.1)
- 4 1.5 ml microcentrifuge tube (SARSTEDT, catalog number: 72.706.700)
- 5 2 ml microcentrifuge tube (SARSTEDT, catalog number: 72.695.500)
- 6 Scalpel (Carl Roth, catalog number: AH88.1)
- 7 Microcapillary pipette, volume 1-5 µl (Sigma-Aldrich, catalog number: Z611239)
- 8 Silica gel G-25 TLC plates 20 x 20 cm (Merck, catalog number: 1003900001)
- 9 Verex Vial Kit 9 mm, µVial i3 (Phenomenex, catalog number: AR0-9974-12)

- 10 Hamilton syringe 25 µl (Hamilton, catalog number: 80400)
- 11 Fresh comfrey leaves from a flowering plant (size about 3.5 cm in length)
- 12 Liquid nitrogen
- 13 [1,4-14C]Putrescine (3.95 GBq/mmol, Amersham Int., catalog number: CFA.301, since the end of Amersham Int., [1,4-14C]Putrescine is still available at PerkinElmer, catalog number: NEC150000MC)
- 14 [12C]Putrescine (Carl Roth, catalog number: 4141.2)
- 15 Scintillation cocktail, Rotiszint eco plus (Carl Roth, catalog number: 0016.3)
- 16 Acetonitrile (Carl Roth, catalog number: 7330.1)
- 17 Methanol (Carl Roth, catalog number: P717.1)
- 18 Ammonia solution 30% (Carl Roth, catalog number: CP17.1)
- 19 Sulphuric acid solution volumetric, 0.05 M (VWR, catalog number: 319589-500ML)
- 20 Zinc dust (Carl Roth, catalog number: 9524.2)
- 21 Sodium hydroxide (NaOH) (Carl Roth, catalog number: 6771.1)
- 22 Potassium phosphate dibasic (K₂HPO₄) (Carl Roth, catalog number: T875.1)
- 23 Potassium phosphate monobasic (KH₂PO₄) (Carl Roth, catalog number: P018.1)
- 24 [14C]Retronecine
- 25 Note: It was prepared according to (Hartmann et al., 2001; Lindigkeit et al., 1997).
- 26 Ethyl acetate (Carl Roth, catalog number: 6784.1)
- 27 2-Propanol (Carl Roth, catalog number: 9866.2)
- 28 5% ammonia in methanol (see Recipes)
- 29 100 mM phosphate buffer, pH 7.5 (see Recipes)
- 30 Mobile phase TLC (see Recipes)

3.4 Equipment

- 1 Pipettes (Eppendorf, model: Research® plus, catalog number: 3123000063)
- 2 Microscale
- 3 Fume hood (Thermo Fisher Scientific, catalog number: 1363)
- 4 Vacuum manifold for SPE (Agilent Technologies, catalog number: 5982-9110)
- 5 Lamp (Carl Roth, catalog number: 2986.1)
- 6 Mortar and pestle (Carl Roth, catalog number: NT80.1)
- 7 Vortex shaker (IKA, model: Vortex 2)
- 8 Micro stir bars (Carl Roth, catalog number: 0955.1)
- 9 Magnetic stirrer (IKA, model: lab disc [white])
- 10 Optima 1 MS GC column (MACHEREY-NAGEL, catalog number: 726205.15)
- 11 Minispin Microcentrifuge (Eppendorf, catalog number: 5452000018)
- 12 Radioactivity thin-layer-chromatography detector (RITA, Raytest, Straubenhardt)
- 13 Tri-Carb 2910 TR LSC Low Activity Liquid Scintillation Analyzer (PerkinElmer)
- 14 LiChrograph HPLC (Merck-Hitachi) connected to a fraction collector
Pharmacia Frac-100 (GE Healthcare Life Science)
- 15 EC 250/4 NUCLEOSIL® 120-5 C18 HPLC column (MACHEREY-NAGEL,
catalog number: 720041.40)
- 16 Developing chambers for TLC (Carl Roth, catalog number: 3133.1)
- 17 Shimadzu GC-2010 gas chromatograph with SSL injector (Shimadzu, model:
GC-2010)
- 18 Shimadzu AOC-20i Auto-injector (Shimadzu, model: AOC-20i)
- 19 Fisons MD 800 quadrupole mass spectrometer

3.5 Software

- 1 XCalibur 1.1 (Thermo Fisher Scientific, Dreieich, Germany)
- 2 GinaStar TLC (Raytest, Straubenhardt)
- 3 QuantaSmart™ 4.0 (PerkinElmer)

3.6 Procedure

5.6.1 Radioactive tracer feeding experiments

A

1) 169 kBq of [1,4-¹⁴C]putrescine solution is transferred into a 2 ml microcentrifuge tube and evaporated to dryness.

Note: Make sure to follow the official guidelines for the work with radioactivity.

2) 0.04 μ mol of [¹²C]putrescine is weighed on a microscale and transferred into another 2 ml microcentrifuge tube.

Note: The purpose of using also a [¹²C]putrescine parallel to tracer is to give you the ability of using an equally-treated sample to analyze with hyphenated techniques, like mass spectroscopy, in later stages of this experiment.

3) 1 ml of tap water is added to each of the tubes of Step A1 and Step A2. Take 5 μ l of the [¹⁴C]putrescine solution that is mixed with 3 ml of scintillation cocktail and the radioactivity is quantified using the Tri-Carb LSC (Tri-Carb Count Conditions for ¹⁴C nuclides are: 'Nuclide: ¹⁴C, Quench Setting Low Energy: ¹⁴C; Count Time (min): 5; Count Mode: Normal; Assay Count Cycles: 1; Repeat Sample Count: 1; #Vials/Sample: 1; Calculate % Reference: Off').

Notes:

a For safety reasons, make sure to mark the tubes according to the kind of putrescine that is in solution ([¹²C] or [¹⁴C]) to avoid mix-up of tubes. This labeling should be continued at every consecutive step.

b Any commercially available liquid scintillation counter machine can be used; the mentioned program is used every time radioactivity has to be quantified.

c Keep in mind to always run a blank without any radioactive tracer within a quantification of radioactivity to quantify the background.

4) Two young comfrey leaves subtending an inflorescence with unopened flower buds are cut from a comfrey plant. Immediately place one leaf in the microcentrifuge tube containing the [^{14}C]putrescine solution, the other in the tube containing the [^{12}C]putrescine solution (Figure 11).

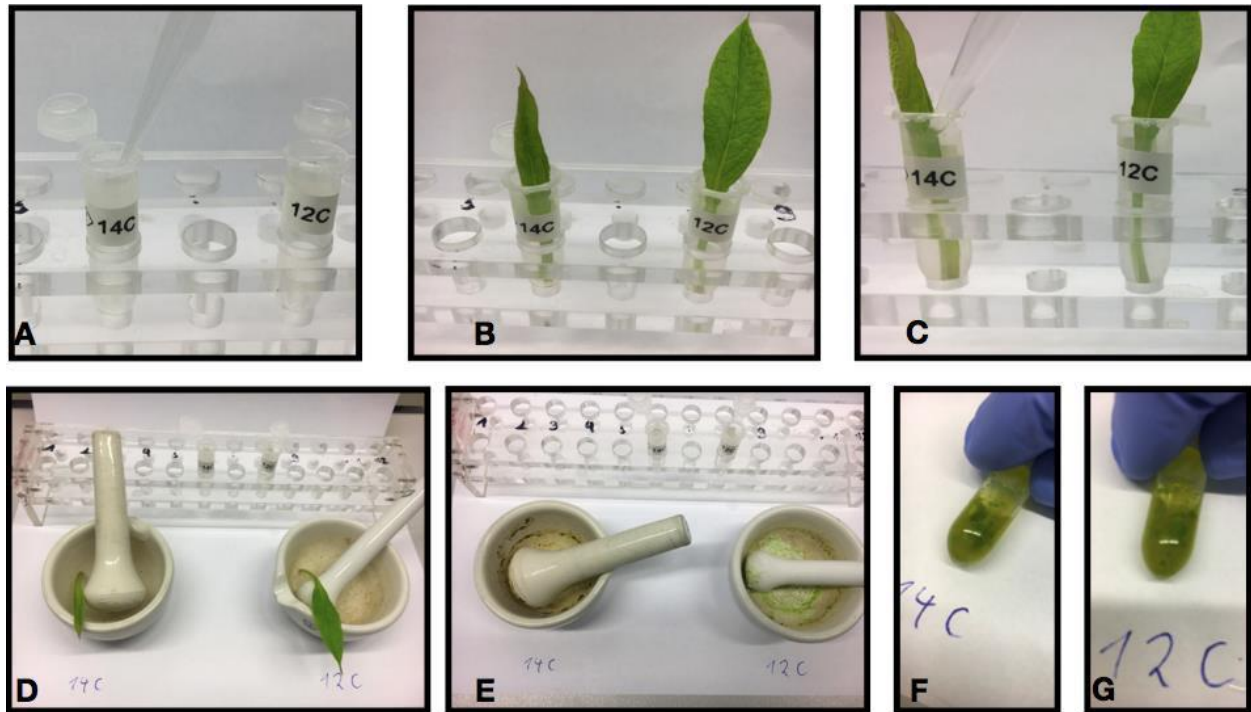


Figure 11: Workflow of tracer feeding and extraction. A. Steps A1 to A3, showing the preparation of the tracer in the microcentrifuge tubes. B. Step A4, showing the incubation of the leaves in the [^{12}C]- and [^{14}C]-tracer solution. C. Steps A6 to A8 refilling the tube with tap water to avoid desiccation of the leaf. D and E. Steps A9 to A10 showing pulverization of the leaves and transfer of the powder into 2 ml microcentrifuge tubes. F and G. Steps A11 to A12 showing acidic extraction of the leaves.

5) The leaves in the tubes are placed under a 12 h/12 h light/dark regime under the lamp with an intensity of ca. 1,000 lux.

6) As soon as the water is taken up by the leaves, another 1 ml of tap water is added. Avoid the petiole to dry out.

7) After addition of the tap water to the [^{14}C]putrescine-containing tube, an aliquot of 5 μl is mixed with 3 ml of scintillation cocktail and the radioactivity is quantified using the Tri-Carb LSC.

8) Steps A6 and A7 are repeated for four days. After the final addition of 1 ml of tap water to the tube, the amount of radioactivity taken up by the leaf in the [^{14}C]putrescine solution is calculated using this formula:

$$\text{uptake in percent} = (169 \text{ kBq} - [\text{kilo Becquerel present in last measurement} \times 200 + \text{amount of radioactivity measured in the } 5 \mu\text{l steps}]) / 169 \text{ kBq} \times 100.$$

9) Both leaves are frozen separately in liquid nitrogen and pulverized with mortar and pestle.

Note: The mortar and the pestle will retain plant debris in their pores. Especially the mortar and pestle used with the leaf sample incubated with [^{14}C]putrescine has to be treated carefully after use to decontaminate residual radioactivity.

10) Each of the pulverized leaves is transferred into a 2 ml microcentrifuge tube (labeled [^{14}C]-leaf and [^{12}C]-leaf, respectively).

11) 1.5 ml of 0.05 M H_2SO_4 is added to each of the two samples in the centrifuge tubes.

12) The closed tubes of Step A11 are vortexed for 3 min at room temperature and the cell debris is separated by centrifugation (10 min, 5,000 x g).

13) The supernatants of Step A12 are transferred, each, into a fresh 2 ml microcentrifuge tube containing a micro stir bar.

14) An aliquot of 5 μl is taken from each tube of Step A13, mixed with 3 ml of scintillation cocktail and the radioactivity of the sulphuric extract is quantified via Tri-Carb LSC.

15) In each tube of Step A13 a spatula tip of zinc dust is added and stirred for three hours on a magnetic stirrer.

Note: Zinc dust reduces the alkaloid N-oxides present in your sample to the tertiary alkaloid and may result in formation of foam rising in your tube. Avoid spilling of your sample.

16) Each tube of Step A15 is centrifuged (10 min, 5,000 x g) and the clear supernatant is applied to a Strata SCX-SPE cartridge positioned on the vacuum manifold. The cartridges were conditioned with 6 ml of methanol and equilibrated with 6 ml of 0.05 M H₂SO₄ prior to use.

Notes:

a Since there is most likely residual radioactivity in the Zinc make sure to dispose the Zinc as solid radioactive material.

b After each treatment, the Strata SCX-SPE cartridge is dried by applying vacuum for an additional minute to the cartridge.

17) An aliquot of 5 μ l of the flow-through of each of the Strata-SCX cartridges is mixed with 3 ml of scintillation cocktail to quantify the radioactivity that is incorporated into non-alkaloid metabolites using the Tri-Carb LSC (Figure 12).

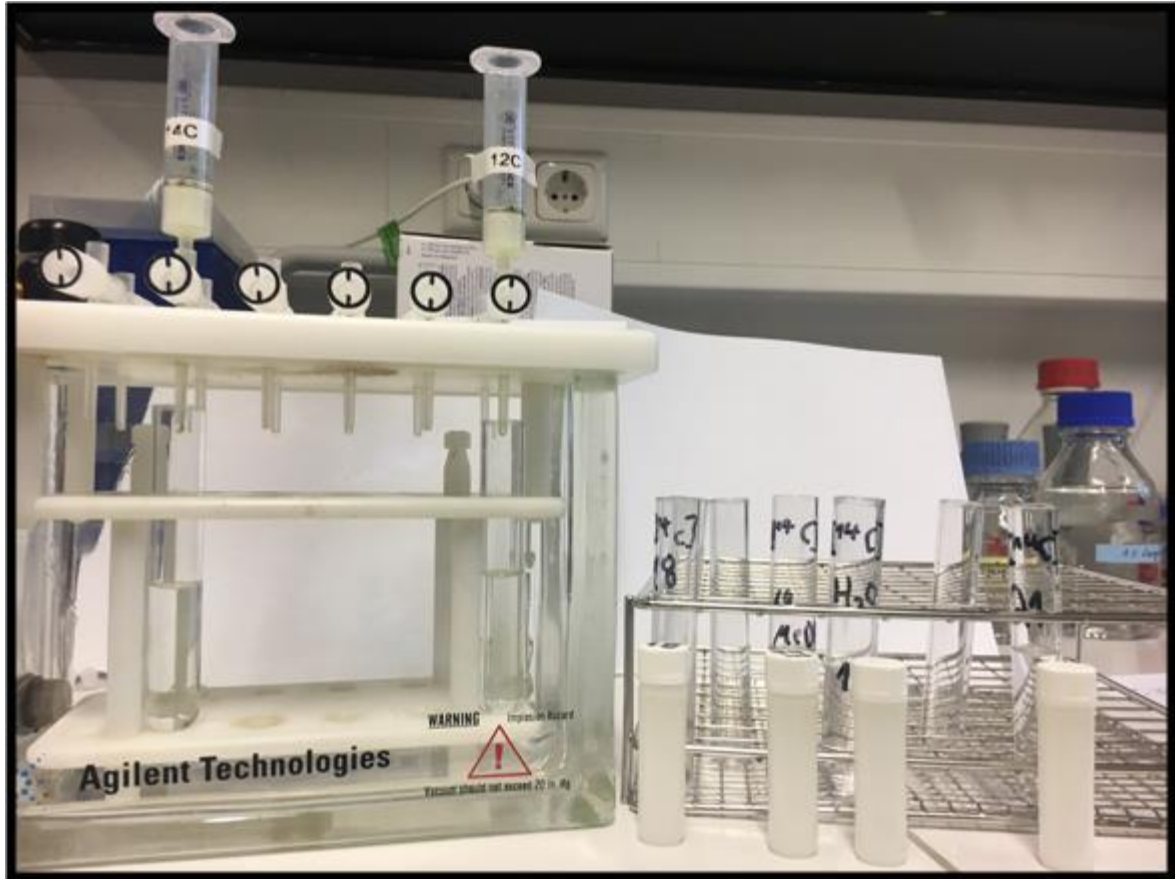


Figure 12: Solid phase extraction setup. Steps A17 to A21 are shown. On the left: SPE cartridges assembled onto the vacuum manifold loaded with sample. On the right: test tubes of the vacuum manifold with their label and the scintillation vials.

18) The loaded Strata SCX-SPE cartridges of Step A16 are washed on the vacuum manifold first with 12 ml of deionized water and then with 12 ml of methanol.

19) An aliquot of 5 μ l of the flow-through from the washing steps of each of the Strata-SCX cartridges is mixed with 3 ml of scintillation cocktail to quantify the radioactivity using the Tri-Carb LSC.

20) The washed cartridges of Step A18 are eluted using the vacuum manifold with a glass tube positioned under each of the two cartridges by applying three times 6 ml of methanol containing 5% (v/v) of ammonia (Recipe 1). The three elution fractions of each cartridge are combined.

21) An aliquot of 5 μ l of the combined elution fractions is mixed with 3 ml of scintillation cocktail to quantify radioactivity that was incorporated into the alkaloid compounds using the Tri-Carb LSC.

Note: The cartridge will most likely retain some radioactive molecules (very strong bases), make sure to dispose properly.

22) The solvent of the combined elution fractions in both tubes of Step A20 is evaporated.

23) The dry residue of the [^{14}C]-labeled sample (Step A22) is dissolved in 2 ml of methanol and divided into equal parts by transfer 1 ml in each of two 2 ml microcentrifuge tubes. The tubes are labeled (#24a) and (#24b).

24) The methanol of both samples (tubes #24a and #24b) is evaporated.

26) The dry residue of sample #24a is dissolved in 50 μ l of methanol and stored at -20 $^{\circ}\text{C}$ (to be used in Step A31).

27) The dry residue of sample #24b is dissolved in 2 ml of 2 N NaOH. The tube is closed and heated in a heating block at 60 $^{\circ}\text{C}$ for 3 h. Afterwards the tube is opened and the solvent evaporated over 2 days under a fume hood (see Notes 1 and 2)

28) The dry residue of the [^{12}C]-labeled sample of (Step A 23) is dissolved in 2 ml of 2 N NaOH. The tube is closed and incubated in a heating block at 60 $^{\circ}\text{C}$ for 3 h. Afterwards,

the tube is opened and the solvent evaporated over 2 days under a fume hood (see Notes 1 and 2).

29) The dry residue of hydrolyzed samples of Step A27, labeled with [¹⁴C], and Step A27, labeled with [¹²C], are dissolved in 50 µl of methanol, each, and stored at -20 °C (to be used in Steps A34 and B1).

Tracer feeding experiment: recovery of applied radioactivity		
Parameter	Radioactivity	Percentage of Recovered Radioactivity
	<i>kBq</i>	
Total radioactivity applied	169	100
Crude extract (sulfuric acid)	25	16
Crude extract after reduction	27	16
Extract purified via SCX-SPE (PA enrichment)	15	8

Figure 13: Example of the tracer surveillance. Data according to Kruse et al. (2017).

30) The HPLC column is equilibrated with 85% solvent A (100 mM phosphate buffer, pH 7.5, Recipe 2) and 15% solvent B (acetonitrile) at 1 ml/min for 1.5 h.

31) The fraction collector Frac-100 is equipped with 4 ml scintillation vials.

32) 20 µl of the sample from Step A25 is transferred with a Hamilton syringe into the rheodyne injector-loop of the LiChrograph HPLC and the valve is changed to the inject position. The fraction collector is programmed to a fraction size of 500 µl.

33) After the HPLC run finished (25 min), 3 ml of scintillation cocktail is added to each fraction collected in the scintillation vials. The vials are closed and radioactivity is quantified with the Tri-Carb LSC (Figure 14).

34) The HPLC column is reequilibrated after the run for 1.5 h as described in Step A30.

- 35) Steps A31 to A34 are repeated with the [^{14}C]-labeled sample from Step A29.
- 36) Steps A30 to A33 are repeated with the [^{14}C]retronecine standard.
- 37) An aliquot of 10 μl of the remaining [^{14}C]-labeled sample from Step A29 is mixed in a 1.5 ml microcentrifuge tube with 10 μl of the [^{14}C]retronecine standard.
- 38) Steps A30 to A33 are repeated with the sample of Step A36.

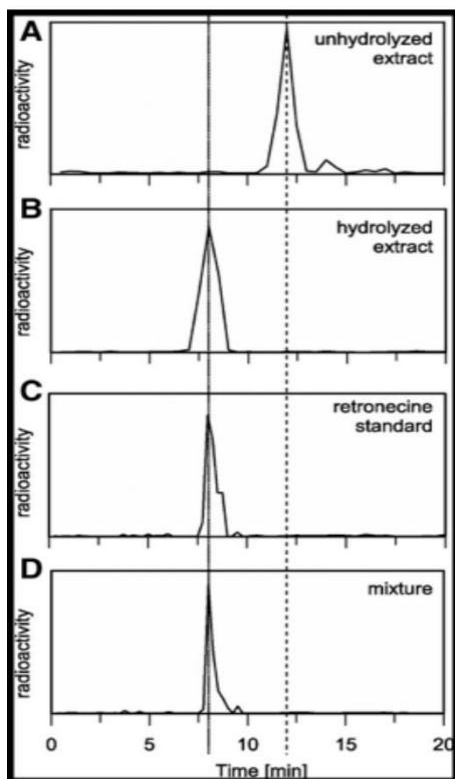


Figure 14: Example of a plotted radio-chromatograms. **A.** The unhydrolyzed purified extract of Step A32. **B.** The hydrolyzed purified extract of Step A34. **C.** The [^{14}C]retronecine standard of Step A35. **D.** Mixture of standard and hydrolyzed extract of Step A37. Data according to Kruse et al. (2017).

3.6.2 Product analysis

B

- 1) The 20 μl remaining of the [^{14}C]-labeled sample from Step A28 is applied as aliquots of 5 μl onto a TLC plate by using the micro capillary pipette. Make sure that the solvent is completely evaporated before applying the next aliquot. This lane is labeled [^{14}C].

- 2) The complete [^{12}C]-labeled sample from Step A28 is applied to the lane parallel to that of Step B1 in the same manner as described in Step B1. The lane is labeled [^{12}C].
- 3) The TLC is developed in a presaturated TLC developing chamber with 20 ml of mobile phase (ethyl acetate: isopropyl alcohol: ammonium hydroxide [30%, v/v]: 45:35:20, Recipe 3).
- 4) The TLC plate is dried under a fume hood overnight.
- 5) The radioactivity of the TLC plate is detected using the RITA system with GinaStar TLC software. The area of the [^{12}C]-lane that is parallel to the radioactive spot of the [^{14}C]-lane is scrapped off including the area 1 cm above and 1 cm below with a spatula into a 2 ml microcentrifuge tube (Figure 15).

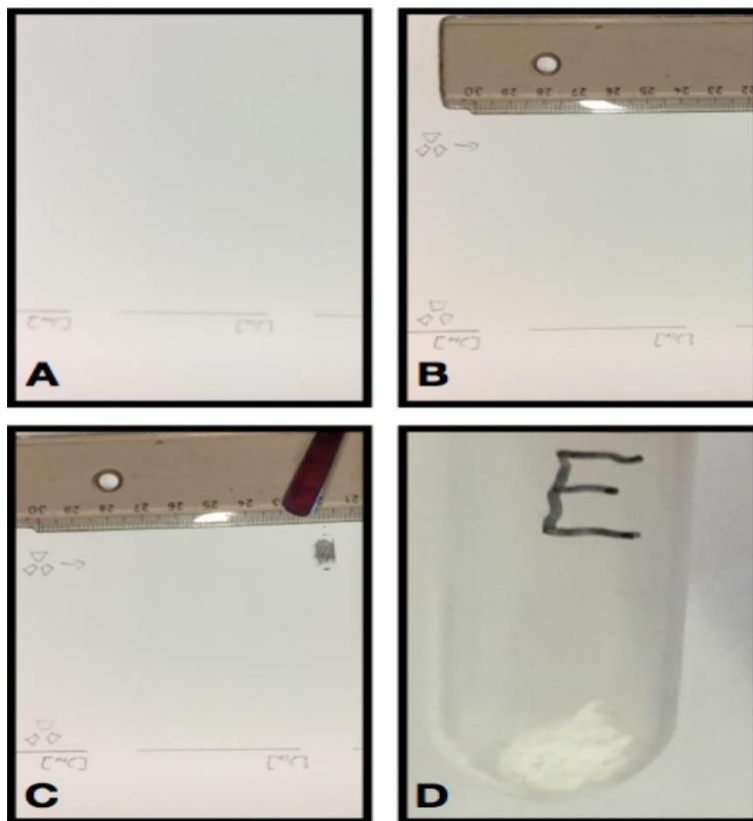


Figure 15: Workflow for product analysis. A. Steps B1 to B4 41 showing the developed TLC. B. Step B5 showing the spots labeled after detection of radioactivity with the RITA system. C. Step B5 showing the spot on the [^{12}C]-TLC lane that is parallel to the radioactivity spot and is scrapped off. D. Steps B5 to B6 show the silica gel powder scraped off the TLC plate and transferred to a 2 ml microcentrifuge tube.

- 6) The silica gel powder of Step B5 is suspended by adding 1 ml of the mobile phase to the microcentrifuge tube. The sample is shaken vigorously and centrifuged (1 min,

5,000 x g). The supernatant is transferred into a fresh 2 ml microcentrifuge tube and evaporated under a fume hood.

7) Step B6 is repeated three times with transfer of the supernatant into the same 2 ml microcentrifuge tube to ensure full extraction.

8) The dry residue resulting from Step B7 is dissolved in 25 μ l of methanol and transferred into a μ Vial for GC-MS analysis. 1 μ l is injected with the AOC-20i auto-injector and electron-impact mass spectra are recorded at 70 eV. Gas chromatography conditions are as follows: injector: 250 °C; injection mode splitless; splitless time 1 min, temperature program: 60 °C for 3 min and 60 °C to 300 °C at 16 °C min⁻¹; carrier gas, helium at 1 ml min⁻¹ (Figure 6).

Note: Any commercially available GC-MS system can be used for this purpose, a direct injection of the radioactive area is not recommended, by reason of the risk for contaminating expensive equipment and of the non-availability of ¹⁴C-labeled reference spectra.

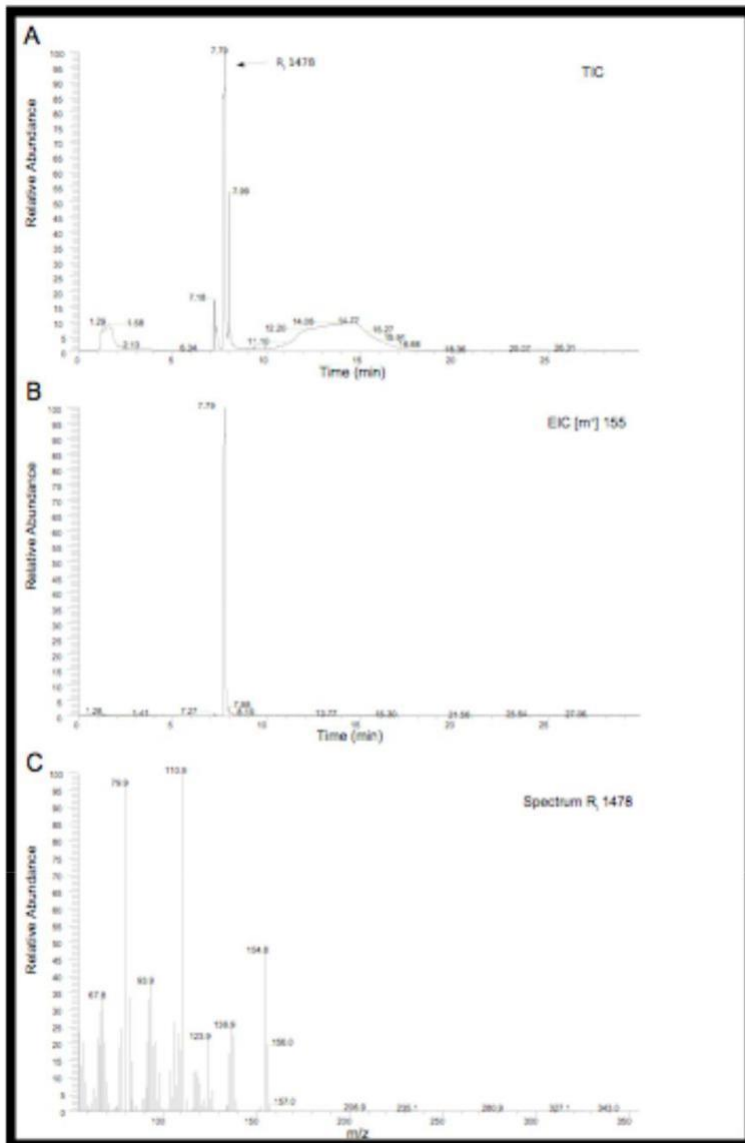


Figure 16: Example of a GC-MS run. A. Showing the total ion chromatogram (TIC) of the sample measured at Step B8. B. Showing the extracted ion chromatogram for the molecular weight of hydrolyzed pyrrolizidine alkaloids from comfrey. C. Showing the mass spectrum at the retention index 1,478, the largest peak of the TIC and EIC, identified as retronecine by comparison with literature and NIST database. Data according to (Kruse et al., 2017).

3.6.3 Data analysis

1) The data resulting from measurement of radioactivity of the sample aliquots with the Tri-Carb LSC in Steps A1 to A8 allow calculation of the total uptake of [^{14}C]putrescine as a tracer by the comfrey leaves given in decays per minute (dpm).

2) The radioactivity is calculated using the following formula:

$$\text{Total Radioactivity [dpm]} = (\text{measured radioactivity}) [\text{dpm}] \times (\text{total volume}) [\mu\text{l}]/5$$

3) The values for radioactivity resulting from aliquots taken in Steps A14 to A21 allow conclusions about the chemical properties of the metabolites that incorporated radioactivity: The amount of radioactivity in the sulfuric extract indicates the amount of radioactivity incorporated into water soluble and acidic extractable molecules. As they eluted from the SPE with ammoniacal methanol they are most likely weak bases as, for example, alkaloids (Figure 13).

4) The HPLC runs of Steps A30 to B1 do not require an HPLC detector since the radioactivity measured for the individual fractions is plotted against the fraction time point and thereby delivering a direct radio-chromatogram. This can be done by using standard data-processing software like Microsoft Excel, Apple Numbers or Libre Calc or manually on paper. The resulting peaks deliver insights if the SPE-purified molecules that incorporated tracers carry side chains that are esterified to the [^{14}C]-labeled core structure originating from the tracer. A comparison with standards is already the first evidence for a possible incorporation of putrescine into alkaloids.

5) The GC-MS total ion chromatogram of the compounds extracted from the TLC spot will further be processed, in the case of pyrrolizidine alkaloids, by extracting the ion 155 m/z representing the $[\text{M}]^+$ molecule of the retronecine core structure. In the case of a single peak, the EI mass spectrum of this peak allow comparisons with spectral libraries like NIST or data previously published of pyrrolizidine alkaloids.

3.6.4 Notes

1) Make sure to close the tubes properly. For safety reasons, it is recommended to put some weight on the cap of the tubes to avoid them being opening by the heat.

2) This process can take very long depending on the laminar air flow of the fume hood and can be speeded up by mixing the water with methanol in a 1:1 ratio, or by using a nitrogen flow or a centrifugal evaporator.

3.7 Recipes

1 5% ammonia in methanol

In a volumetric flask, 16.67 ml of 30% ammonia solution is added to 83.33 ml of methanol

2 100 mM phosphate buffer, pH 7.5

2.449 g KH_2PO_4 and 14.143 g K_2HPO_4 are weighed into a volumetric flask and made up to 1 L with deionized water

3 Mobile phase TLC

In a beaker, 45 ml of ethyl acetate is mixed with 35 ml of 2-propanol and 20 ml of 30% (v/v) ammonia solution. The mobile phase has to be prepared fresh prior to use

3.8 Acknowledgments

This work was funded by a DFG grant given to Dietrich Ober. We thank Dr. Dorothee Langel for her input and ideas contributing to this method. We thank Dr. Christoph Gelhaus and Maren Hartelt, Kiel University, for help in implementing this method. The authors declare no conflict of interest.

4. Specific Distribution of Pyrrolizidine Alkaloids in Floral Parts of Comfrey (*Symphytum officinale*) and its Implications for Flower Ecology

Thomas Stegemann, Lars H. Kruse, Moritz Brütt, Dietrich Ober

Detailed author contributions are listed at the end of the thesis.

4.1 Abstract

Pyrrolizidine alkaloids (PAs) are a typical class of plant secondary metabolites that are constitutively produced as part of the plant's chemical defense. While roots are a well-established site of pyrrolizidine alkaloid biosynthesis, comfrey plants (*Symphytum officinale*; Boraginaceae) have been shown to additionally activate alkaloid production in specialized leaves and accumulate PAs in flowers during a short developmental stage in inflorescence development.

To gain a better understanding of the accumulation and role of PAs in comfrey flowers and fruits, we have dissected and analyzed their tissues for PA content and patterns. PAs are almost exclusively accumulated in the ovaries, while petals, sepals, and pollen hardly contain PAs. High levels of PAs are detectable in the fruit, but the elaiosome was shown to be PA free. The absence of 7-acetyllycopsamine in floral parts while present in leaves and roots suggests that the additional site of PA biosynthesis provides the pool of PAs for translocation to floral structures. Our data suggest that PA accumulation has to be understood as a highly dynamic system resulting from a combination of efficient transport and additional sites of synthesis that are only temporarily active. Our findings are further discussed in the context of the ecological roles of PAs in comfrey flowers.

4.2 Introduction

Pyrrolizidine alkaloids (PAs) are a class of secondary metabolites that occur in certain, distantly related families of the angiosperms. They are part of the plant's chemical defense against herbivores (Hartmann & Witte, 1995; Langel et al., 2011). It is estimated that 3 % of all plants contain PAs (Smith & Culvenor, 1981) with occurrences for example in some families of the Boraginales order, the Asteraceae, Apocynaceae, Convolvulaceae, Orchidaceae, or the genus *Crotalaria* within the Fabaceae (Hartmann & Witte, 1995; Langel et al., 2011). Studies on homospermidine synthase (HSS), the first specific enzyme of PA biosynthesis, showed that PA biosynthesis is a convergent trait

being recruited several times independently in the various PA-producing lineages (Kaltenegger et al., 2013; Dietrich Ober & Hartmann, 1999; Reimann et al., 2004).

Immunolocalization with HSS-specific antibodies showed highly variable expression patterns of HSS in the various PA-producing lineages, suggesting that PA biosynthesis is restricted to certain specific cells and certain developmental stages (Anke et al., 2004; Moll et al., 2002; Niemüller et al., 2012).

Within the Boraginales, PA-producing species are found in the Boraginaceae and the Heliotropiaceae with well-established model systems for studies of PA biosynthesis (Frölich et al., 2007; van Dam et al., 1995). Molecular analyses of HSS-encoding genes suggest an origin of PA biosynthesis before separation of these two families (Luebert et al., 2016; Niemüller et al., 2012; Reimann et al., 2004). However, also within these two families HSS expression is varying between species. HSS was localized in cells of the lower leaf epidermis of *Heliotropium indicum*, (Heliotropiaceae), in cells of the endodermis and pericycle in the case of *Cynoglossum officinale* (Boraginaceae), and only the cells of the endodermis in *Symphytum officinale* (Boraginaceae). For *S. officinale*, studies on root cultures have shown that roots of *S. officinale* have the capacity to express the complete pathway of PA biosynthesis (Frölich et al., 2007). Therefore, roots have been interpreted as the exclusive site of PA biosynthesis, from where the alkaloids are distributed into the aerial parts of the plant (Frölich et al., 2007). Recently, we have been able to show that *S. officinale* has, in addition to the roots, a second site of PA biosynthesis, viz., young leaves subtending developing inflorescences. The expression of HSS correlated with an accumulation of PAs in the inflorescence, suggesting an efficient transport of PAs from the leaf to the inflorescences, probably as part of a chemical protection of the reproductive structures in the flower (Kruse et al., 2017).

In plant secondary metabolism it is a well-known phenomenon that the site of synthesis might be very different from the site of accumulation (see Table 1). But in contrast to the cell-specific analyses of HSS expression, data on the distribution of PAs within a plant are scarce. Only for selected plant species detailed information is

available (e.g. *Senecio* sp., Table 1), while for other species the tissues harvested for PA analysis are often only separated as below-ground material (roots, rhizomes) and aerial parts (leaves, axis, flower). Moreover, limited information is available about the developmental stage of the plant or the season of harvest. As PAs are an integral part of the plant's ecology (Hartmann & Ober, 2000, 2008), a more detailed understanding of PA accumulation patterns is required. Although PA biosynthesis is known to be constitutive, recent results of Kruse et al. (2017) suggest that besides the transport of metabolites additional sites of synthesis during specific developmental stages can result in highly variable patterns of PA accumulation. Especially, different floral tissues involved in pollinator attraction and/or defense against herbivores warrant further studies. In order to understand the dynamics of PA accumulation within the reproductive tissues of *S. officinale* we analyzed various tissues of the flower and fruits and discuss the results regarding their implications to the ecology of the plant.

Table 1

Overview about site of PA synthesis (according to HSS expression) and major site of PA accumulation of selected PA-producing plants

Species (Family)	Site of biosynthesis	Main site of PA accumulation	Ref.
<i>Jacobaea vulgaris</i> (Asteraceae, Senecioneae)	endodermis and adjacent cortex cells	flowers	a, b
<i>Senecio vernalis</i> (Asteraceae, Senecioneae)	endodermis and adjacent cortex cells	flowers	c, d
<i>Eupatorium cannabinum</i> (Asteraceae, Eupatorieae)	cortex parenchyma	flowers	e
<i>Phalaenopsis</i> sp. (Orchidaceae)	apical meristem and flower buds	flowers	f, g
<i>Heliotropium indicum</i> (Heliotropiaceae)	lower leaf epidermis	flowers	a, h
<i>Symphytum officinale</i> (Boraginaceae)	root endodermis and bundle sheath cells of specialized leaves	root, flowers	a, i
<i>Cynologossum officinale</i> (Boraginaceae)	endodermis and pericycle	inflorescences	a, j, k
<i>Crotalaria spectabilis</i> (Fabaceae)	nodules	leaves, seeds	l, m

a (Niemüller et al., 2012), b (Witte et al., 1990), c (Hartmann & Zimmer, 1986), d (Moll et al., 2002), e (Anke et al., 2004), f (Anke et al., 2008), g (Frölich et al., 2007), h (Catalfamo et al., 1982), i (Kruse et al., 2017), j (Pfister et al., 1992), k (van Dam et al., 1995), l (Irmer et al., 2015), m (A. E. Johnson et al., 1985)

4.3 Methods and Material

4.3.1 Plant Material

Flowers, leaves, and roots of *S. officinale* were collected in the Botanical Garden of Kiel University. Since it was not possible to harvest fruits of *S. officinale* from our population, fruits were purchased from a commercial vendor (Rühlemann's, <http://www.kraeuter-und-duftpflanzen.de/>).

4.3.2 Plant Dissection and Pollen Harvest

More than 100 individual flowers of *S. officinale* were dissected immediately after harvest, frozen in liquid nitrogen, and freeze-dried. The same was done with leaves and roots of three biological replicates. Dissected floral tissues included sepals, petals, ovaries, and styles with stigma. To harvest pollen of *S. officinale*, stamens were detached with forceps and slightly shaken above a pre-weighted microcentrifuge tube. This process was repeated until the yield was quantifiable to 10 mg on a microscale. Pollen and pollen-depleted stamens were analyzed separately. Elaiosomes were separated from the fruits using precision forceps, by which the elaiosome was removed carefully by slight agitation. To estimate the variability of the weight of the individual floral parts (sepals, petals, and ovaries), whole flower and fruits, 10 individual weightings of each were recorded and the standard deviation was calculated. In addition, complete, undissected flowers have been analyzed. Fig. 1 shows a scorpioid cincinnus, the typical inflorescence of *S. officinale* (A), a longitudinal section of a flower (B), and the flower structures resulting from dissection (C to H). Fig. 2 shows fruits with elaiosomes of *S. officinale*.

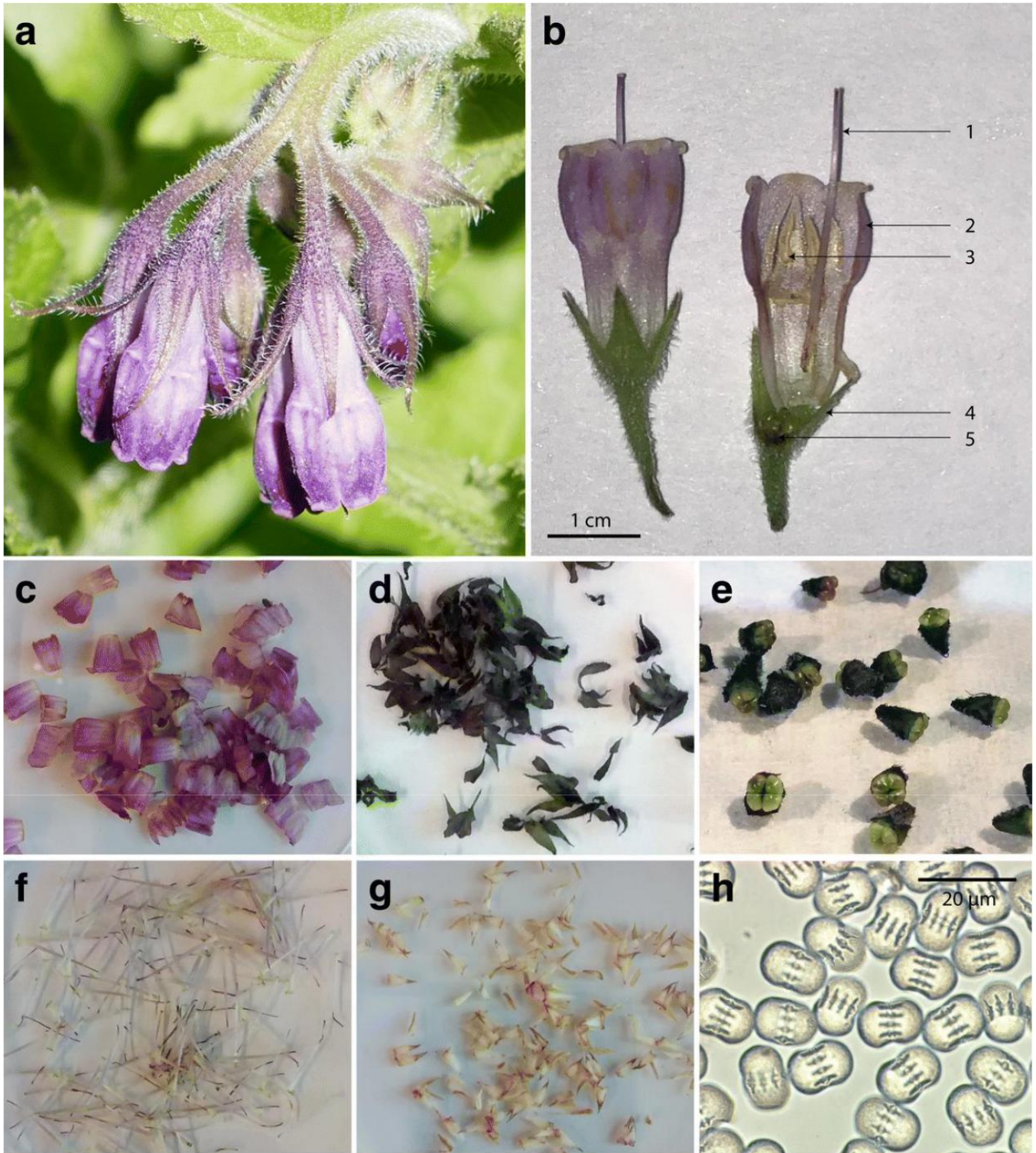


Figure 17: Flower of *Symphytum officinale* and individually sampled tissues. **A**, Overview of a typical inflorescence of *S. officinale* with flowers in different developmental stages. **B**, Details of an open flower showing the sampled tissues that are indicated by arrows and numbers. Styles (1), petals (2), anthers (3), sepals (4), and ovaries (5) were individually dissected from various flowers for PA level quantification. **C to H**, collected flower structures used for PA quantification. **C**, Petals, of which five form a corolla tube. **D**, Sepals. **E**, Ovaries. **F**, Styles. **G**, Stamina. **H**, Microscopic image of collected stephanocolporate pollen with phase contrast. The picture was assembled from several individual images by focus stacking with the software Picolay (www.picolay.de)

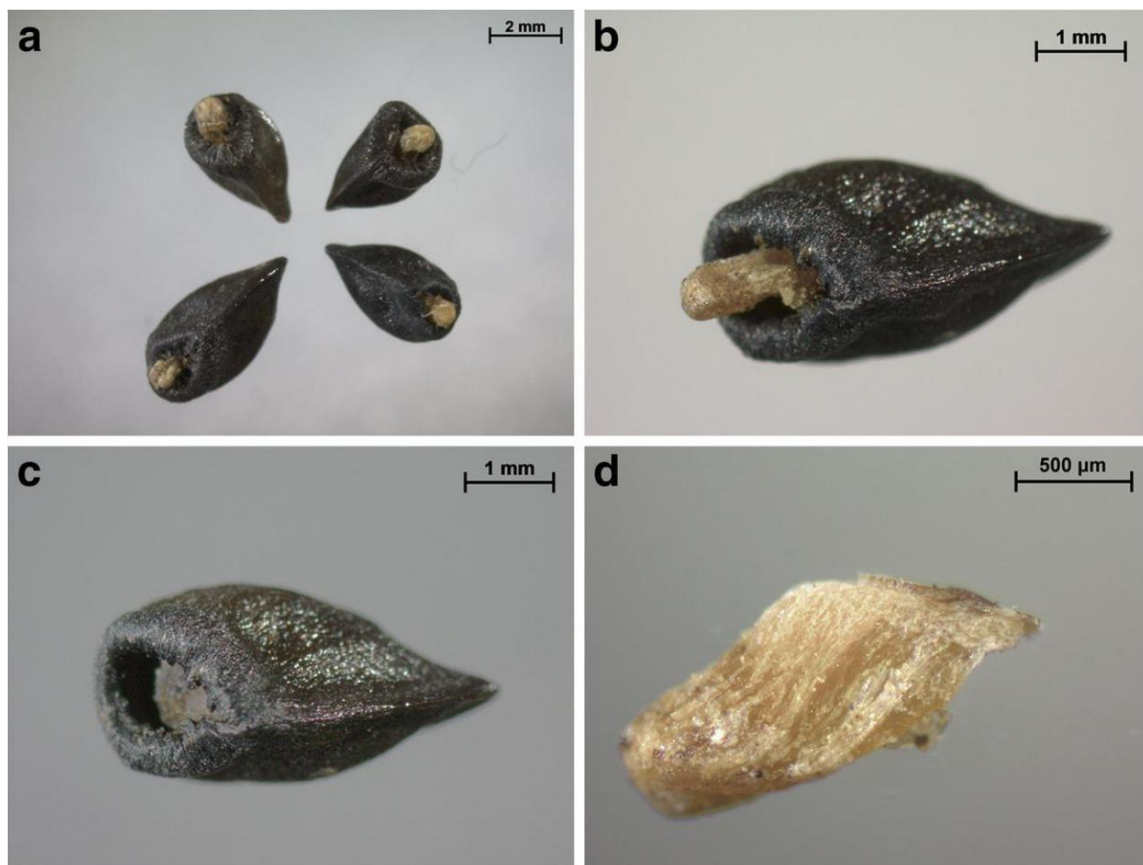


Figure 18: Fruits with elaiosomes of *S. officinale*. **a**, Schizocarp fruit separating into four individual nutlets. **b**, Single nutlet with attached elaiosome seated in a cavity of the pericarp. **c**, Single nutlet after removal of the elaiosome. **d**, isolated elaiosome used for PA quantification

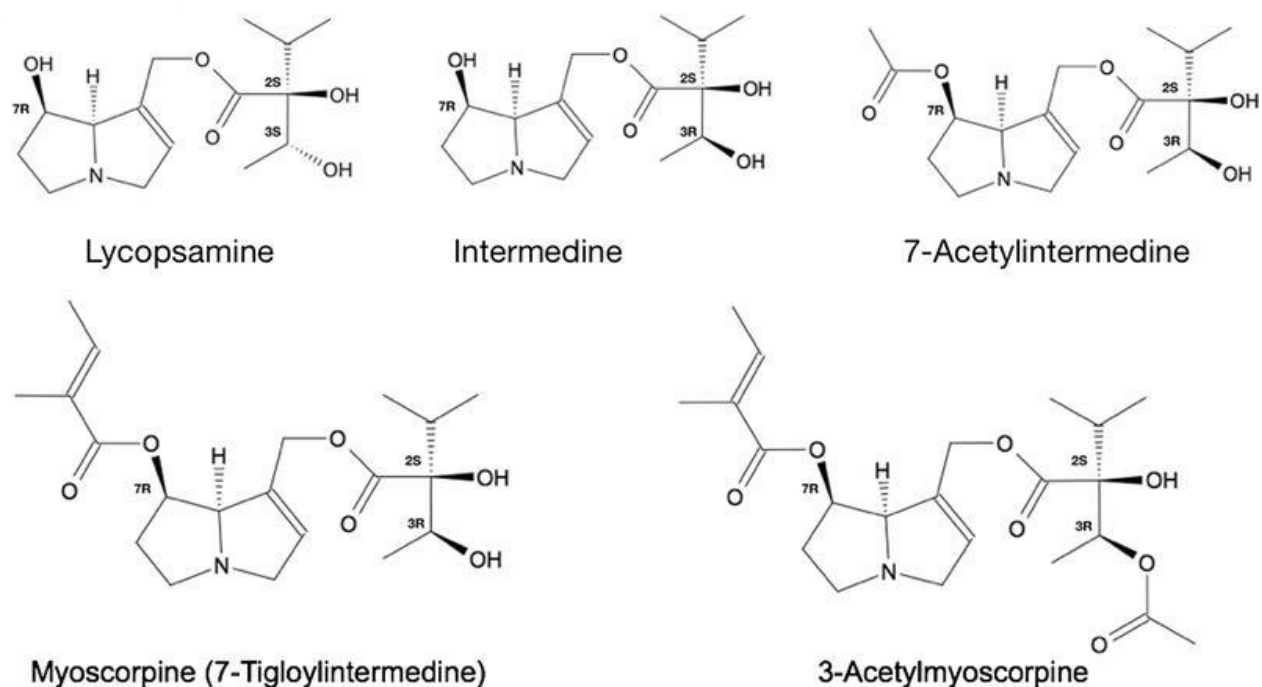


Figure 19: Structures of PAs detected in flowers of *S. officinale* (according to (Hartmann & Witte, 1995))

4.3.3 Alkaloid Extraction and Solid Phase Extraction

Of all samples except the pollen (10 mg) and elaiosomes (13 mg) 70 to 100 mg dry weight of pooled material were ground with a pestle and mortar in liquid nitrogen and the fine powder was transferred into 50 ml tubes and extracted overnight in 10 ml of 0.05 M H₂SO₄ under constant agitation. After centrifugation the extract was purified by solid phase extraction (Strata-SCX® cartridges) according to Kruse *et al.* (2017). After elution the sample was dried overnight and dissolved in 100 µl of methanol before being split into two equal parts for qualitative and quantitative analysis.

4.3.4 Sample Preparation for the Identification of PAs

For qualitative PA analyses, 50 µl of purified alkaloid extracts were acidified and reduced with zinc dust to reduce PA *N*-oxides to their respective tertiary form according to Stegemann *et al.* (2018). Afterwards the tertiary alkaloids were alkalized

and extracted from the aqueous phase with chloroform according to (Kowalczyk & Kwiatek, 2017), dried overnight and solved in 50 μ l of methanol for GC-MS analysis.

4.3.5 Quantification of PAs

For quantitative PA analyses, PA levels were determined as retronecine equivalents. Specifically, 50 μ l of purified alkaloid extracts were reduced and hydrolyzed with LiAlH₄ solution, before the resulting necine base (retronecine) was derivatized and quantified via GC-MS according to (Kempf et al., 2008), "sum parameter method"). For quantification of PA *N*-oxides, the sample resulting from solid phase extraction was resolved in water containing 0,1% (v/v) formic acid and analyzed by LC-MS.

4.3.6 GC-MS Analysis

The measurements were done on a TraceDSQ system (Trace Ultra GC coupled to a Dual Stage Quadrupole Mass Spectrometer, ThermoFisher Scientific) equipped with a split/splitless (SSL) injector. GC conditions applied were: 60 °C for 5 min, 60 °C to 300 °C at 5 °C/min, injector temperature 280 °C, carrier gas helium: 1 ml/min, injection mode: splitless, and splitless time of 1 min. MS-spectra were recorded at 70 eV and ion source temperature of 230 °C. All analyses were carried out in triplicate. RI values according to (Kováts, 1958) were calculated by co-chromatography of alkane standards. Identification of alkaloids and derivatives were done via spectra and RI value comparison with NIST database, an in-house database, and literature.

4.3.7 LC-MS Analysis

Measurements were done on a LCMS 8030 system (Shimadzu). Mobile Phase A: 50 mM sodium acetate, pH = 5; mobile phase B: acetonitrile. Injection volume: 10 μ l. Separation was done using a Accucore XL C18 column (250 mm \times 3 mm, particle size 4 μ m, ThermoFisher Scientific) with a flow rate 1 ml/min. Starting conditions of the HPLC were 50% A and 50% B for 15 min, followed by a linear gradient from 50 to 60% B over 10 min and from 60 to 95% B for 40 min. Electrospray ionization was done with the following parameters: IS voltage, 5500 V; nebulizer gas, 50 psi (nitrogen); source temperature, 650 $^{\circ}$ C. PA *N*-oxides have been quantified of those PAs identified before by GC-MS and given as ratio *N*-oxide to tertiary PA.

4.4 Results

4.4.1 Total PA Levels in Various Flower and Fruit Tissues of *S. officinale*

The data in Table 2 show that almost all PAs are accumulated in the ovaries with almost 3 μ g alkaloid per individual ovary (retronecine equivalents). The PAs remain in this tissue since in the ripe fruit PA levels of more than 8 μ g are reached (calculated for four mericarps [nutlets] that result from separation of the schizocarp). PA concentrations decrease during fruit ripening, most likely due to enlargement of the ripening fruit. Only minor amounts of PAs have been detected in sepals, petals, and pollen. No PAs were found in stamina after removal of the pollen or in the elaiosomes of the ripe fruits.

Table 2

Total PA levels and concentration in various flower and fruit tissues of *S. officinale*

Plant organ	Biomass [mg DW per individual flower]	Total PAs a		Ratio of <i>N</i> -oxides to tertiary PAs
		Content* [ng per individual flower]	Concentration [ppm DW/ppm FW]	
Sepals	1.2 ± 2.0/	tr	tr	–
Petals (corolla tube)	4.4 ± 3.2	85 ± 64	17/6	96:4
Stamina	< 1.0	–	–	
Pollen	b	b	14/14	
Ovaries	4.4 ± 1.6	2836 ± 942	638/98	95:5
Styles with stigma	< 1.0	–	–	
Complete flower	8.5 ± 1.2	2075 ± 132	243/41	95:5
Fruits composed of four nutlets (single nutlet)	46.0 ± 3.6 (11.5 ± 0.9)	8424 ± 636	183/18 3	92:8
Elaiosome	0.37	–	–	

tr traces (< 1 ng), *DW* dry weight, *FW*

fresh weight --, not detectable

*The content per individual flower is based upon application of the average weight of the respective flower parts per flower in relation to concentration. The standard deviation is based on calculation of an average weight of those flower parts taken from ten individual flowers

- a) Total PA levels refer to retronecine equivalents
- b) The weight of the pollen of a single flower cannot be determined

PA Pattern in Various Flower and Fruit
Tissues of *S. officinale*

Structures of PAs detected in flowers of *S. officinale* are given in Fig. 3. As the ovaries are the main site of PA accumulation, their PA pattern is the same as that of the complete flower.

No change in the PA pattern is detectable during fruit development (Table 3). 7-Acetylintermedine represents two third of the PA content, while intermedine and lycopsamine account for approx. 15%, each. This alkaloid pattern with 7-acetylintermedine, intermedine, and lycopsamine as major PA components is well in accordance with the PA pattern determined for leaves and roots of *S. officinale* (Table 3). In contrast, in pollen and petals, PAs are stored exclusively as myoscorpine, while in other tissues myoscorpine and 3-acetylmyoscorpine are only detectable in traces.

Table 3Pattern of PAs in various tissues of *S. officinale*

PA	Petals	Pollne	Ovaries	Fruits	Whole flower	Leaves	Roots
7-Acetylintermedine	tr	tr	67%	67%	64%	47%	44%
7-Acetyllycopsamine	tr	tr	tr	tr	tr	35%	29%
Intermedine	tr	tr	15%	15%	15%	12%	14%
Lycopsamine	tr	tr	17%	17%	16%	5%	12%
Myoscorpine	99%	99%	tr	tr	2%	tr	tr
3-Acetylmyoscorpine	tr	tr	tr	tr	1%	tr	tr

Values are given in percent of the total amount of PAs detected in this tissue *tr* traces (< 1 ng)

4.5 Discussion

According to the literature, *S. officinale* contains PAs in all parts of the plant, but information about PA distribution within certain organs is scarce. Mütterlein and Arnold describe a detailed analysis of the roots of *S. officinale*, a study motivated to provide a risk analysis of the pharmaceutical most relevant parts of the plant (Mutterlein & Arnold, 1993). *S. officinale* is a medicinal plant traditionally used externally for the treatment of disorders of the locomotor system (Staiger, 2012). While information about PA distribution in roots of *S. officinale* is well established, no information is available about the PA distribution in the other ecological relevant parts, e.g. the flower.

Recently, we have observed that during flower development of *S. officinale* a second site of PA biosynthesis is switched on in small leaves subtending a developing inflorescence. This additional site of PA biosynthesis was interpreted as a mechanism that boosts PA levels especially for the reproductive parts of the flower (Kruse et al.,

2017). Such a strategy was also postulated for the orchid *Phalaenopsis* that produces PAs in the tips of aerial roots, but increases PA levels in the flower by a second site of synthesis in the small flower buds (Anke et al., 2008; Kruse et al., 2017) studied PA levels at various stages of inflorescence development and found that a few days after the transcript level of HSS showed a peak in the subtending leaf, PA levels reached a maximum in inflorescences, in which all flowers were open and those flowers that had opened first began to darken. This observation suggests a transport of PAs from the subtending leaf into the inflorescence. In the next analyzed stage of inflorescence development, when the flowers withered, PA levels dropped to values comparable to that of an inflorescence with unopened flower buds. To explain this drop of PA levels in the transition stage from flower to fruit set we speculated that PAs might have been accumulated in flower structures that get lost during fruit development like the petals or the stamina. High PA levels in petals could protect the flower from nectar robbers like short-tongued bumblebees that are unable to access the nectar through the long tubular flowers, but, instead, rob the nectar through little holes they bite into the base of the corolla. Or the pollen might be the structures that contain the bulk of PAs, as high PA concentrations are reported from related species like *Echium vulgare* (Boraginaceae, (Boppré et al., 2008)) and might be interpreted as protection of the pollen that, as the male gametophyte, produces the male gametes. To test these two hypotheses, we analyzed the individual flower structures of *S. officinale* for their PA content and PA pattern.

Our data show that in flowers of *S. officinale* almost all PAs are located in the ovary (Table 2). As the total amount of PAs in the fruits is even higher, translocation of PAs has to continue also during fruit ripening. This observation is well in accordance with the optimal defense theory that suggests that deterring chemicals are stored preferably in those parts of a plant that need best protection, e.g. young leaves or reproductive structures (McKey, 1979). *S. officinale* is a perennial plant that produces dry schizocarp fruits that are separating into four mericarps (“nutlets”, (Luebert et al., 2016)). At the base of the nutlets elaiosomes are formed that attract ants as part

of the zoochorous fruit dispersal (Peters et al., 2003). PAs should not be present in the elaiosomes as they have been described as efficient chemicals to deter ants (Hare & Eisner, 1993; Iyengar & Eisner, 1999). Indeed, elaiosomes proved to be PA-free (Table 2). Therefore, the drop of PA levels observed by (Kruse et al., 2017) cannot be explained to the loss of PA-rich flower structures. Other factors have to be responsible for the observed drop of PA-levels later in inflorescence development in the study of (Kruse et al., 2017). As many flowers of *S. officinale* are sterile (Ge-Ling et al., n.d.), a remobilization of PAs might occur if fruit set fails.

Our qualitative data show that the PA bouquet in the flowers of *S. officinale* is similar, but not identical to data previously described in the literature for roots and shoots with intermedine- and lycopsamine derivatives as major components (Brauchli et al., 1982; Mutterlein & Arnold, 1993). Echimidine, a PA described to be present in hybrids and closely related species of *Symphytum*, but not in *S. officinale* (Mutterlein & Arnold, 1993), was not detectable. The observation that there is a slight shift in the PA pattern, namely the absence of 7-acetyllycopsamine in the floral structures, suggests that the PAs transported to the floral structures do not come from the PA pool of the vegetative parts of the plant (older leaves and roots), but from a different site, most likely from the young leaves subtending developing inflorescences, where PAs have been shown to be synthesized during flower development (Kruse et al., 2017)

Several publications suggest that PA producing plants protect their pollen with PAs, as repeatedly contaminations of honey with PAs were detected (Betteridge et al., 2005; Cramer et al., 2013; Kempf et al., 2008). Also species of the Boraginaceae, including *S. officinale*, are discussed to be responsible at least for parts of these contaminations (Mudge et al., 2015). We found only very low concentrations of PAs in pollen of *S. officinale*, an observation that is well in accordance with data of PA levels in pollen of *Echium plantagineum* (Boraginaceae) of about 6 to 28 ng/mg (Boppré et al., 2008). Of note, in pollen of the closely related species *Echium vulgare* PA levels of about 900 ng/mg (Kempf et al., 2010) and even 14,000 ng/mg (Boppré

et al., 2008) have been detected. Different PA levels are also described for *Senecio* species. In pollen of *Senecio ovatus* 155 ng/mg have been detected (Boppré et al., 2008), while in *Jacobaea vulgaris* (syn. *Senecio jacobaea*) levels of 180 to 800 ng/mg (Boppré et al., 2008) and of 3000 ng/mg (Kempf et al., 2008) have been reported. In PA producing *Crotalaria sagittalis* (Fabaceae) no PAs have been detected in pollen (Kempf et al., 2010). High variability of detected PA levels is not restricted to floral structures. Analyses of PA levels of roots of *S. officinale* varied from 1380 to 8320 ng/mg (Couet et al., 1996) and from 450 to 5990 ng/g (Mutterlein & Arnold, 1993). Our data suggest some degree of variation of PA levels. The high PA concentration in the ovaries and the flower (638 ng/mg and 243 ng/mg, respectively) are considerably lower than the peak value detected in the inflorescences with open flowers by Kruse et al. though still higher than that described for other stages of inflorescence development (Kruse et al., 2017). This difference might be due to the fact that we harvested the flowers for this study in the advanced growing season (July instead of May, same year) and that we harvested and pooled about 100 individual flowers while Kruse et al. (2017) analyzed three biological replicates independently.

The biosynthesis of PAs is regarded as a constitutive defense mechanism that is coupled to plant growth. If no further biomass is produced, PA biosynthesis is switched off (Anke et al., 2004; Sander & Hartmann, 1989). Therefore, the observed variability of PA levels between different parts of the plant, between individuals, and between samples harvested at different time points during the growing season shows a much more complex pattern than anticipated before. Tests for an inducibility by application of methyl jasmonate to three PA-producing species of the Boraginales, including *S. officinale*, showed no effect on transcript nor on PA levels (Sievert et al., 2015) though there are some reports suggesting an induction of PAs. For example, *C. officinale* plants, of which 50% of the leaf biomass was removed, showed a 2-fold higher PA concentration in the leaf base than in the removed leaf tips (van Dam et al., 1993). In hairy roots of *Echium rauwolfii* PA induction by application of methyl jasmonate was described (Abd El-Mawla, 2010). The only well-characterized example, in which PA

biosynthesis is dependent on an external factor, is the fabaceous genus *Crotalaria* that produces PAs only after nodulation (Irmer et al., 2015).

Our data suggest that even though PA accumulation is part of a constitutive defense strategy, quantification of PA levels can always be only a glimpse of the metabolic state of the plant. The different developmental stages with their specific physiology including efficient transport processes and additional temporary sites of synthesis show unique PA levels, suggesting that this variability might have been selected in evolution. What kind of implications these dynamics in PA metabolism have for the ecology of the plant is currently not completely understood and will require further investigations of alkaloid mediated interaction between plants and animals involved in pollination, fruit dispersal, and herbivory.

4.6 Supplemental Table

Supplemental Table 1. GC-MS data of PAs identified in this study.

Alkaloid	RI	[M] ⁺	characteristic ion m/z (rel. abundance)
7-Acetylintermedine	2371	341	180(100), 120(65), 181(25), 93(23), 136(20), 121(18), 179(17)
7-Acetylycopsamine	2389	341	180(100), 120(65), 181(25), 93(23), 136(20), 121(18), 179(17)
Intermedine	2190	299	138(100), 93(38), 94(25), 139(25), 137(18), 136(11), 95(10)
Lycopsamine	2209	299	138(100), 93(36), 94(24), 139(23), 137(15), 136(13), 95(10)
Myoscorpine	2512	355	220(100), 93(60), 136(52), 83(41), 121(35), 141(20), 221(18)
3-Acetylmyoscorpine	2594	423	220(100), 120(70), 136(56), 93(54), 94(41), 121(31), 141(23), 221(13)

5. Variance of Pyrrolizidine alkaloid-content and gene transcription in *Heliotropium indicum*

Thomas Stegemann, Dietrich Ober

Botanisches Institut, CAU Kiel;

Detailed author contributions are listed on the end of this thesis.

5.1 Abstract

Pyrrolizidine alkaloids (PAs) are secondary metabolites that are constitutively produced by the indian heliotrope (*Heliotropium indicum*) to defend against herbivores. Previously, using this well-established model-system a subtractive transcriptomic approach was used to identify new candidate genes for PA biosynthesis. While previous studies focused on the average content of PAs in whole plants or even whole harvests of *H.indicum*, the variation between individuals and even between different parts of an individual were neglected. By analysing the PA content in individual leaves of different individuals the intraspecific variation of PAs was analyzed. Our data suggest that the content of PAs between individual leaves and has to be taken into account when using leaves of *H.indicum* as a model system for studies on the physiology and regulation of PA biosynthesis. To test for correlation of PA levels and the expression level of homospermidine synthase, the first specific enzyme of PA-biosynthesis, transcript levels have been quantified. In this data set the transcript levels of a candidate gene, encoding a copper-dependent amine oxidase, putatively involved in oxidation of homospermidine were included. The data show a large variability between individual leaves on a PA and a transcript level. Furthermore a coregulation of *hss* and the candidate gene was observed. Based on our data knock-down or even knock-out experiments have to be designed with care to avoid misleading interpretations of PA and transcript levels.

5.2 Introduction

Pyrrolizidine alkaloids (PAs) as secondary metabolites are part of the chemical defense strategy of plants (Hartmann & Witte, 1995). They appear within various plant lineages and families leading to the estimation that 3% of all plants do contain PAs (Smith & Culvenor, 1981).

Studies on the biosynthesis of PAs have demonstrated the homospermidine synthase (HSS) to be the first pathway specific enzyme (Ober & Hartmann, 1999). HSS is responsible for transferring an aminobutyl moiety from putrescine to spermidine

creating the PA precursor homospermidine (Böttcher et al., 1994). Biomimetic experiments with homospermidine suggest that a copper-containing amine oxidase (CuAO) is involved in PA biosynthesis (Robins, 1995). Although immunolocalization of HSS was performed, the site of PA accumulation has been reported to differ from the site of synthesis (reviewed in Stegemann et al., 2019). This characteristic is not only valid for PAs but also for many other group of plant secondary metabolites (Shitan et al., 2015).

Heliotropium indicum as a member of the Heliotropiaceae family has been established as model for studies of PA biosynthesis over the last years (Frölich et al., 2007; Sievert et al., 2015). Recently a method was reported that allows the identification of candidate genes of PA biosynthesis in *H. indicum* (Sievert et al., 2015). This method is based on the observation that HSS is localized in the lower leaf epidermis (Niemüller et al., 2012) and the hypothesis that other enzymes of PA biosynthesis are also cell-specific expressed in the same cell type. In a subtractive approach the transcriptome of the upper leaf transcriptome was subtracted from that of the lower leaf transcriptome to provide a set of candidate transcripts that might be involved in the PA biosynthesis.

The biosynthesis of PAs is classified as a constitutive defense mechanism, meaning the PA production is depending on biomass growth of the plant (Anke et al., 2004; Sander & Hartmann, 1989). Recent investigations of *Symphytum officinale*, a member of the Boraginaceae family suggest that the quantification of PAs are always just a glimpse of the actual metabolic state of the plant (Stegemann et al., 2019).

Possible approaches to confirm candidates would require for example knock-downs of the respective genes by methods like RNA interference (RNAi), through virus-induced gene silencing (VIGS) (Liscombe & O'Connor, 2011) or knockout experiments for example using CRISPR/Cas9. Using knock-down experiments highly variable PA levels might be a problem in the data interpretation. To provide more sophisticated bases for the intraindividual variation of PA levels in *H. indicum* we analyzed the alkaloid content and the transcript levels of hss and CuAO candidate gene in individual leaves of selected plant individuals.

5.3 Results & Discussion

To test for the intraspecific variation of PAs in *H. indicum* different leaves of one or more individuals were analyzed with respect to PA concentration and transcript levels of the genes encoding HSS and CuAO, that is discussed to be involved in the biosynthesis of the PA backbone structure, the necine base. For this purpose it was sufficient to analyze total PA content, using sum-parameter method (Kempf et al., 2010; Kowalczyk & Kwiatek, 2017) instead of analyzing the alkaloid pattern. As all PAs known to occur in *H. indicum* leaves do possess retronecine as necine base the reduction and hydrolysis steps as part of the sum-parameter method convert all alkaloid structure into the same building block. Increasing the sensitivity for the overall PA content.

5.3.1 Intraspecific variation of PA concentration in leaves of *H.indicum*

Using one individual of *H. indicum* the variation of PA concentration in 5 different leaves was tested. The data show a unexpected difference in PA levels (Fig 20). While in leaf III only 24.48 µg PA/g (fresh weight) were found, leaf V contained 6124.15 µg/g. This is a 300-fold difference in alkaloid content. A certain degree of variation was also observed in *S. officinale* which was in parts explained by a second site of PA biosynthesis in a specific leaf subtending the inflorescence (Kruse et al., 2017). In addition the comparison of individual leaves of *S. officinale* with data in the literature of *Symphytii herba* suggests also a high level of variation (Stegemann et al., 2019).

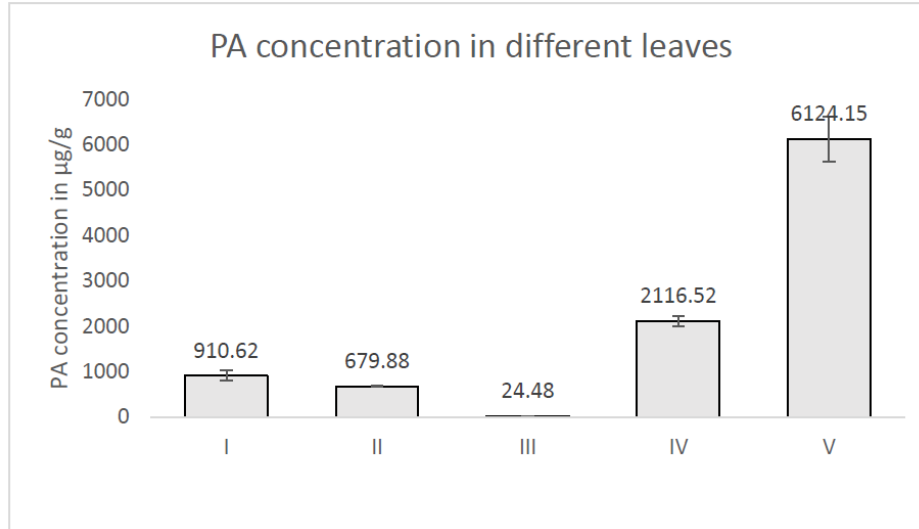


Figure 20: PA concentration in individual leaves of a *H. indicum* individual. PAs were quantified as retronecine-equivalents using GC-MS after reduction and hydrolysis of PAs (sum-parameter method). The bars represent the PA concentration of each leaf (n=3, technical replicates)

5.3.2 Intraspecific variation of hss-transcripts in leaves of *H.indicum*

To test whether the observed variation of PA concentrations in the individual leaves of *H. indicum* is also represented on the transcript level of *hss*, an even larger number of leaves of two plant individuals was tested. For this, the relative transcription of *hss* to that of the ubiquitin (*ubq*) housekeeping gene was measured via RT-qPCR. Figure 21 shows that the relative transcription of *hss* in 11 different leaves showed values vary between below 0.0001 and to about 0.2. This data show that the transcription level of PA-biosynthetic genes in leaves of *H. indicum* could differ by a factor of 2000 in wild types of *H. indicum*. The fact that PA-levels and transcript levels of *hss* show strong variation between individual leaves suggests that the whole pathway of PA biosynthesis is affected.

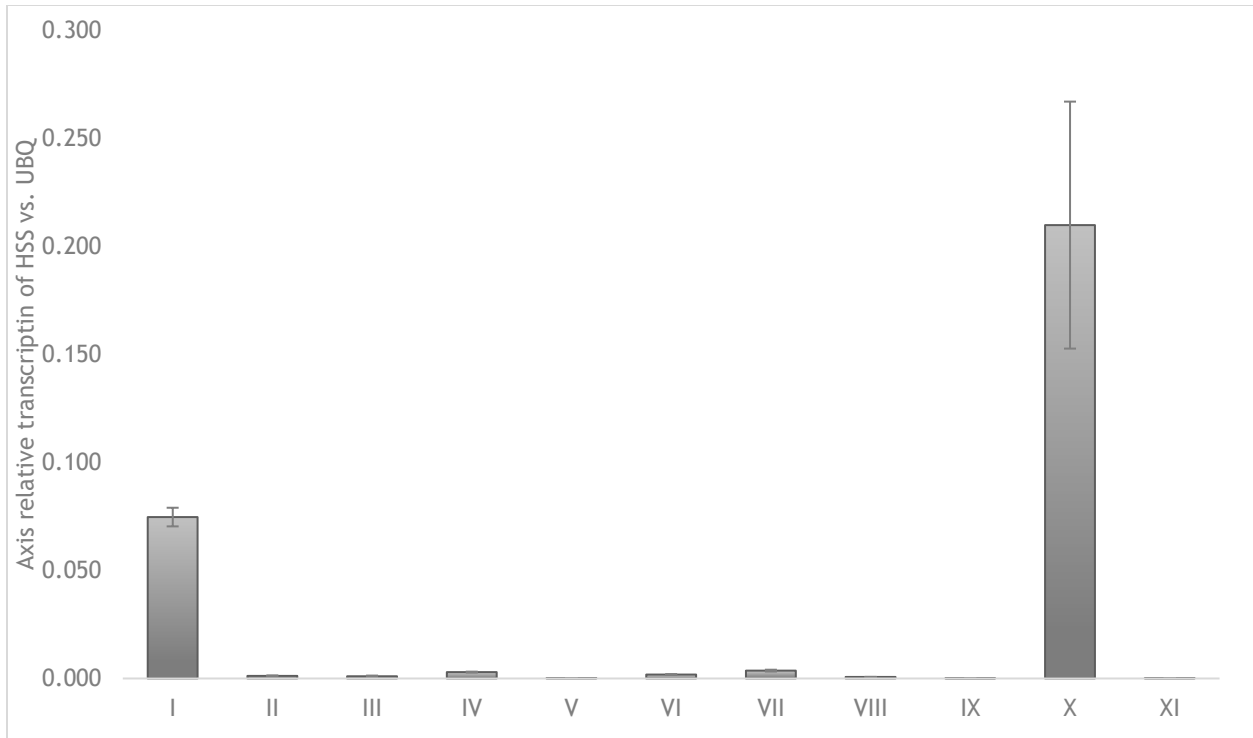


Figure 21: Levels of *hss* transcript in individual leaves of two *H. indicum* plants. Transcript levels were quantified by RT-qPCR using *ubq* reference gene. Each bar (I-XI) represents a single leaf of *H. indicum* analyzed in triplicate.

5.3.3 Intraspecific variation of possible candidate gene-transcription in leaves of *H.indicum*

Based on the hypothesis that the whole pathway of PA-biosynthesis shows strong variation between individual leaves we postulate that other enzymes of PA biosynthesis should show a similar pattern of variation as the *hss*. Therefore, we selected a candidate gene encoding a copper-containing amine oxidase (CuAO) from data generated by the subtractive transcriptomic approach. This enzyme could be responsible for the postulated oxidation of homospermidine in the PA-biosynthesis (Sievert et al., 2015). To be able to compare the transcript levels of *hss* and the candidate gene we used the same leaves for transcript quantification of the *cuao* as for *hss*. Fig 22 shows indeed a similar degree of variation of the relative *cuao* transcript level as for the *hss* ranging between values of 0.001 and 0.67. Of note, as for *hss*,

also for *cuao* the leaf number X is the one with the highest transcript levels followed by leaf number I. The same is true for the leaf number IX showing the lowest relative transcript level.

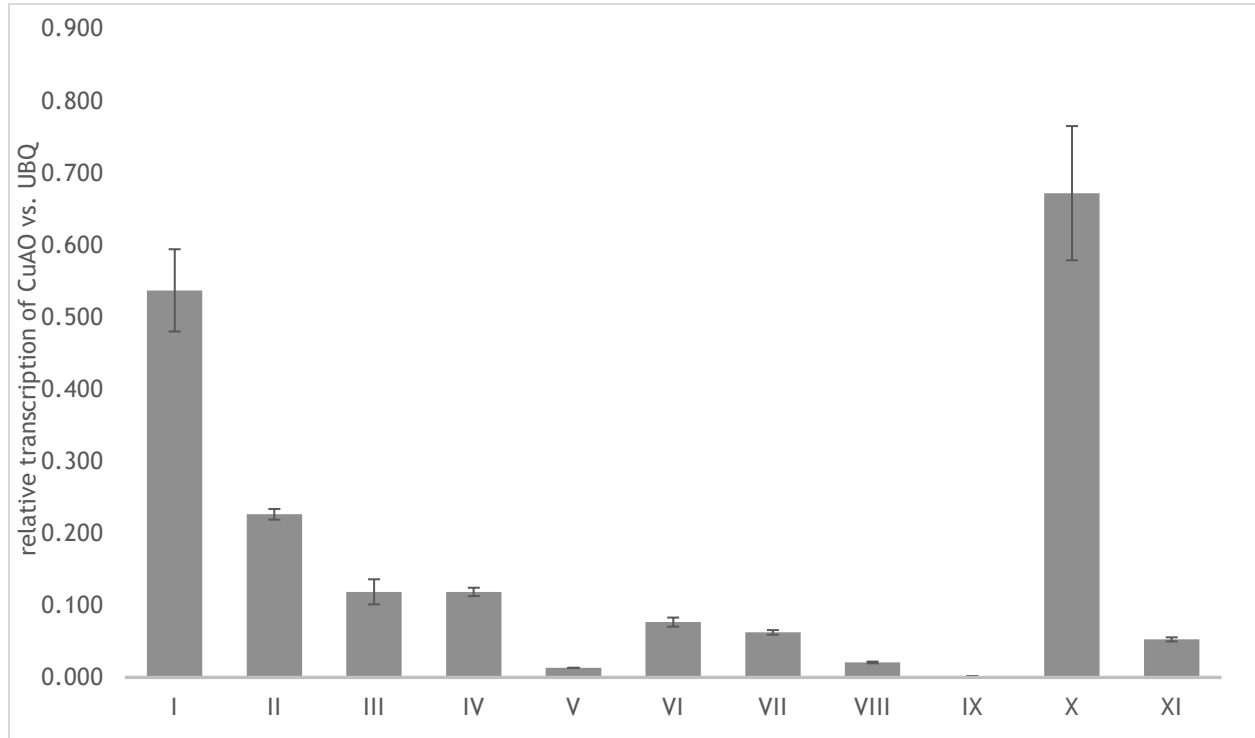


Figure 22: Levels of *cuao* transcript in individual leaves of two *H.indicum* plants. Transcript levels were quantified by RT-qPCR using *ubq* reference gene. Each bar (I-XI) represents a single leaf of *H. indicum* analyzed in triplicate.

5.3.4 Possible correlation of *hss* and *CuAO*

Using the analyzed relative transcript levels of *hss* and *cuao* we tested the hypothesis of coregulation by creating a scatter plot (Fig 23.). Statistical analyses resulted in a Pearson coefficient of 0.932. This high value indicates a strong correlation of the analyzed values. Presuming that the candidate is indeed involved in PA biosynthesis this obvious coregulation with HSS could be used for two purposes.

Firstly, for identification of candidates the test for coregulation with HSS will provide first support for the involvement of the candidate in PA biosynthesis.

Secondly, the observed strong variation of transcript levels between individual leaves bares the risk of misinterpretation, if strategies for downregulation for example by RNAi are used. This variation might result in non-significant effects. The analyses of relative transcript levels based on HSS as a reference for PA biosynthesis would compensate the natural variation in expression levels. Further studies have to prove that the candidate used in the study, i.e. CuAO is indeed involved in PA biosynthesis. This would WEG BEREITEN for identification of further candidates.

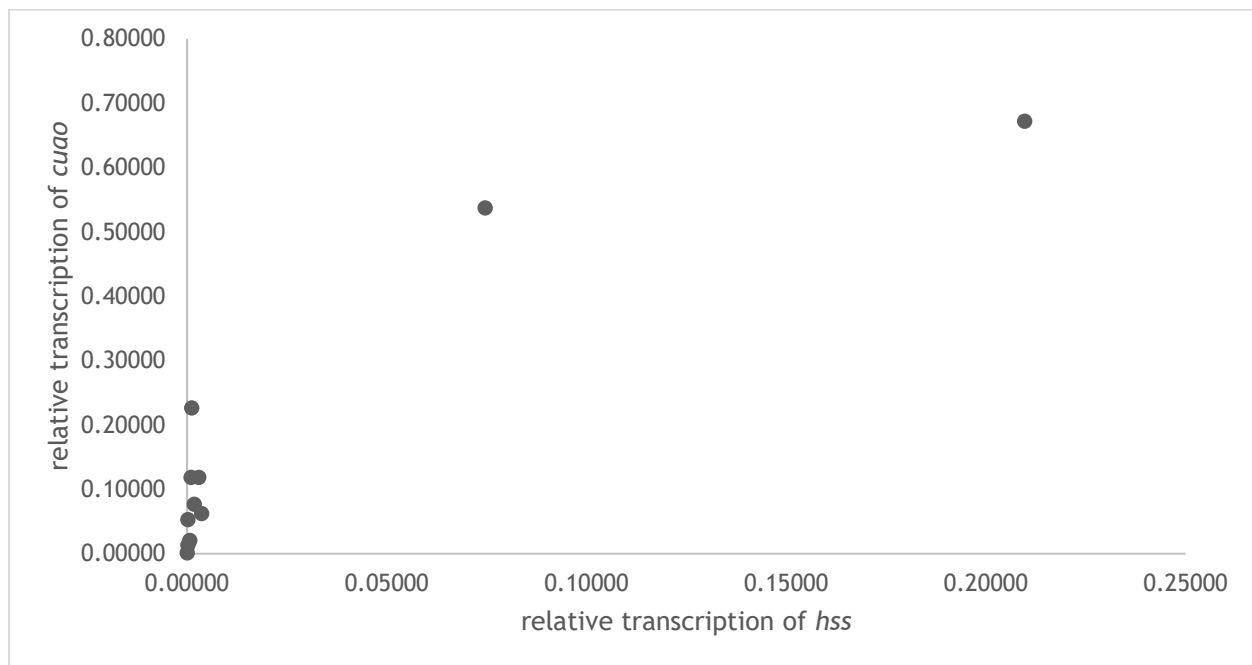


Figure 23: Scatterplot of relative transcript levels of *hss* (Fig. 21) vs. *cuao* as a candidate gene (Fig. 22).

5.4 Experimental

5.4.1 Plant material

Plants of *H. indicum* were grown in the greenhouse of Kiel Botanic Gardens under 12h/12h lighting conditions. Plants were grown for 4-6 weeks till they reached the post 4-6 leaves stadium.

5.4.2 Quantification of PAs

Leaves of *H.indicum*, were harvested and grounded via mortar and pestle under liquid nitrogen. The powder was divided by three to achieve technical replicates in this analysis. The method for quantification of PAs was the same as described in (Stegemann et al., 2019).

5.4.3 Quantification of transcript levels

Leaves of *H. indicum* were cut and directly frozen with liquid nitrogen. The leaves were grounded with mortar and pestle under liquid nitrogen and the RNA extracted with Trizol-Reagent Trizol (Invitrogen, Thermo Fisher Scientific) according to the manufacturer's protocol. The whole RNA extraction process was described previously (Kruse et al., 2017). For transcript quantification, 0.5-1.5 µg of total RNA was used for RT-qPCR as described previously (Kruse et al., 2017).

5.4.4 Primers

The primers used for HSS transcripts and UBIQ transcripts are described previously (Sievert et al., 2015), while the primers for the CuAO transcripts are listed in primer table of the next chapter.

6. Double oxidation of homospermidine by a copper-containing amine oxidase results in a pyrrolizidine backbone

Mahmoud Mohamed^{1,*}, Thomas Stegemann^{1,*}, Christian Sievert¹, Lars H. Kruse^{1,5}, Ulrich Girreser², Serhat Çiçek³, Manfred Nimtz⁴, Dietrich Ober¹

* shared first authorship

¹ Botanical Institute and Botanic Gardens, Kiel University, Kiel, Germany

² Institute of Pharmaceutical Chemistry, Kiel University, Kiel, Germany

³ Institute of Pharmaceutical Biology, Kiel University, Kiel, Germany

⁴ Cellular Proteome Research, Helmholtz Centre for Infection Research, Braunschweig, Germany

⁵ Present address: Plant Biology Section, School of Integrative Plant Sciences, Cornell University, Ithaca, NY 14853, USA

6.1 Abstract

Copper-containing amine oxidases (CuAOs) are described of all kingdoms of life and are described to be involved in many physiological processes. CuAOs oxidize mono- and polyamines to the respective aldehydes. From the plant *Heliotropium indicum* we describe a CuAO, named homospermidine oxidase (HSO), that prefers the triamine homospermidine over other amines as substrate and oxidizes both primary amino groups in a single reaction. As a result, a bicyclic structure, 1-carboxypyrrolizidine, is formed. Tracer feeding and virus-induced gene silencing experiments suggest that 1-carboxypyrrolizidine is an intermediate in the biosynthesis of the necine base moiety of

pyrrolizidine alkaloids, a class of natural compounds produced by the plant as part of the chemical defense against herbivores. Transient expression of HSO in tobacco leaves allowed biochemical characterization of this unusual enzyme.

6.2 Introduction

Polyamines are aliphatic molecules with two or more amino groups that are involved in central processes such as cell growth and proliferation, regulation of gene expression and translation, membrane stabilization, and apoptosis (Ballas et al., 1983; Besford et al., 1993, 1993; Michael, 2016; Seiler & Raul, 2005). Moreover, in plants, polyamines are involved in cell signaling and in responses to abiotic and biotic stresses (Kusano et al., 2008; Liu et al., 2015; Sobieszczuk-Nowicka et al., 2019).

These processes require a stringent control of polyamine levels that is realized, among others, by copper-containing amine oxidases (CuAOs, EC 1.4.3.22), a group of ubiquitous enzymes that catalyze the oxidation of primary amino groups using preferentially diamines (putrescine and cadaverine) and polyamines (spermidine and spermine) as substrates. In the addition to the amine levels, the production of hydrogen peroxide during the enzymatic reaction is responsible for a plethora of secondary effects. In plants, these effects include cell-wall reinforcement and lignification during maturation, pathogen invasion and symbiotic interaction, wound healing, root development, as well as signaling processes resulting in the activation of defense gene expression or induced stomatal closure in response to drought (Cona et al., 2006) (Angelini et al., 2010; Fraudentali et al., 2019; Groß et al., 2017; Wisniewski et al., 2000).

Also the aminoaldehydes resulting from CuAO-mediated oxidation of polyamines were shown to be important intermediates in various pathways. These include the formation of 4-aminobutyric acid (GABA), a metabolite that participates in various physiological processes, and the biosynthesis of alkaloids, a class of biological active compounds often involved in plant defense (Hartmann, 2008; M. Wink et al., 1998).

CuAOs are quinoproteins in which a specific tyrosine residue is post-translationally modified to topaquinone (TPQ) by a self-catalytic process requiring enzyme-bound Cu(II)

(Johnson et al., 2007). The TPQ is involved in the oxidative deamination of primary amines into the corresponding aldehydes with the formation of hydrogen peroxide and ammonia (Lunelli et al., 2005). CuAOs are sensitive to inhibition by carbonyl-group reagents like hydroxyethylhydrazine or other substituted hydrazines that interact with the TPQ cofactor (Padiglia et al., 1998). The structure of CuAOs has been solved from eubacteria, yeast, mammals, and plants and is remarkably conserved. The active sites are buried deeply in each of the subunits of the homodimer. They are linked to the surface of the enzyme by a substrate channel, of which the length and the width vary (Guss et al., 2009). The size of this channel is discussed to have strong influence on substrate specificity (Chang et al., 2010).

Pyrrolizidine alkaloids (PAs) are a class of so-called secondary metabolites that are part of the plant's chemical defense against herbivores and that are produced in various unrelated lineages of the angiosperms (Hartmann & Ober, 2008; Kaltenecker et al., 2013; Reimann et al., 2004). They are esters of a bicyclic necine base with one or more necic acids (Hartmann & Ober, 2000). It is estimated that about 3% of all plants produce PAs (Smith & Culvenor, 1981), which are, mainly due to their hepatotoxicity, responsible for severe intoxications by contaminations of herbal products used for nutrition or medical purposes (Authority, 2007; (Allgaier & Franz, 2015)). A better understanding of the biosynthetic route of PAs is a prerequisite for improved risk management. In the first specific step of PA biosynthesis an aminobutyl moiety of spermidine is transferred to putrescine, both deriving from the natural polyamine pool. This reaction is catalyzed by homospermidine synthase (HSS), the so far only characterized enzyme of PA biosynthesis that was shown to have evolved by independent gene duplication events in the various PA-containing plant lineages (Kaltenecker et al., 2013; Dietrich Ober & Hartmann, 1999; Reimann et al., 2004). The next step of the pathway should involve the oxidation of homospermidine at both primary groups, reactions for which CuAOs ("diamine oxidases") have already been proposed in early studies (Böttcher et al., 1993; Grue-Sorensen & Spenser, 1983; Khan & Robins, 1985). Some of the arguments for the involvement of a CuAO in homospermidine oxidation are (i) the fact that PA biosynthesis is blocked by typical inhibitors of CuAOs like hydroxyethylhydrazine resulting in an accumulation of homospermidine (Böttcher et al., 1993), (ii) the observation that in a

biomimetic experiment the incubation of homospermidine with CuAO of pea seedlings and catalase for six days followed by an incubation with an alcohol dehydrogenase resulted in the formation of detectable amounts trachelanthamidine, the saturated bicyclic ring structure of PAs (Robins, 1982), and (iii) the similarity of the postulated reaction with that of already characterized CuAOs, especially with those involved in the formation of a heterocyclic ring system as part of various alkaloidal backbone structures from polyamine precursors (Hashimoto et al., 1990; Heim et al., 2007).

Cyclization after oxidation of the primary amino groups is generally regarded as a spontaneous reaction (Liebisch et al., 1969). These CuAO-mediated cyclizations have been described for the biosynthetic pathways of nicotine (Heim et al., 2007; Katoh et al., 2007) and tropane alkaloids (Hashimoto et al., 1990) both using *N*-methylputrescine as substrate and, using cadaverine as substrate, for the biosynthetic pathways of piperidine alkaloids in *Sedum* species (Gerdes & Leistner, 1979), Lycopodium alkaloids (Ma & Gang, 2004), and quinolizidine alkaloids (Wink & Hartmann, 1979; Yang et al., 2017). In all of these cases monocyclic structures are formed after oxidation of a single primary amino group.

A homospermidine oxidase (HSO) postulated as second step in PA biosynthesis should accept homospermidine as substrate. Studying the substrate specificity of bovine serum albumin oxidase (BSAO), Houen et al. (2005) tested also homospermidine as substrate and showed that the product was 1-(4'-aminobutyl)-pyrrolinium, *i.e.* a monocyclic structure that resulted from the oxidation of only one of the two primary amino groups. That this monocyclic iminium ion is an efficient precursor for the necine base of PAs in PA-producing plants was already shown in early tracer feeding studies (Denholm et al., 1991). However, for PA biosynthesis, both primary amino groups of homospermidine have to be oxidized by one or two CuAOs to allow the formation of the characteristic bicyclic pyrrolizidine of the necine base moiety.

To identify candidates for a HSO in PA biosynthesis, we have used a subtractive transcriptomic approach (Sievert et al., 2015). A prerequisite for such an approach is the fact that the enzymes involved in PA biosynthesis are only expressed in specific cells. Analyzing HSS in various PA-producing lineages, it was shown that expression is

restricted to specific cells (Anke et al., 2004, 2008; Moll et al., 2002; Niemüller et al., 2012) and to specific developmental phases (Kruse et al., 2017). For *Heliotropium indicum* (Indian heliotrope, Heliotropiaceae), HSS was localized exclusively in the cells of the lower leaf epidermis and in the epidermis of shoots while no expression was observed in the upper epidermis (Niemüller et al., 2012). Assuming that not only HSS, but the complete PA biosynthesis is localized in these cells, the subtraction of the transcriptome of the upper epidermis from that of the lower epidermis should result in an enrichment of PA-specific transcripts.

Here we show that one of the sequences identified by subtractive transcriptomics encodes HSO that catalyzes the second step of PA biosynthesis. HSO is a CuAO that, in contrast to other CuAO-encoding sequences of *H. indicum*, is co-expressed with HSS. Characterization of HSO after transient expression in *Nicotiana benthamiana* showed a high specificity for homospermidine that is oxidized at both primary amino groups allowing spontaneous formation of the pyrrolizidine backbone of PAs. Knock-down studies of HSO by virus-induced gene silencing (VIGS) showed significantly reduced PA levels and confirm the involvement of HSO in PA biosynthesis..

6.3 Results

6.3.1 Identification of a putative homospermidine oxidase

In *H. indicum*, a plant native to Asia, it was shown that HSS is expressed exclusively in non-specialized cells of the lower leaf epidermis of young leaves and the shoot, but not in the upper leaf epidermis (Niemüller et al., 2012). Expecting that not only the first specific step of the pathway, but the complete pathway is expressed in these cells, cDNA of single cells of the lower and the upper epidermis was used for a subtractive transcriptomic approach to enrich PA-specific sequences (Sievert et al., 2015). The approach resulted in the identification of five partial transcripts encoding CuAO-like proteins (CuAO1 to 5). To test these candidates for a co-expression with HSS, we used cells of the upper and lower leaf epidermis isolated by laser capture microdissection microscopy to obtain micro amounts of cDNA for quantitative reverse transcription polymerase chain reaction (qRT-PCR) analyses (Sievert et al., 2015). The transcript levels for CuAO1 were about 8-fold higher in the lower than in the upper leaf epidermis, a pattern similar to that observed for

HSS nominating the CuAO1 as a potential candidate for a homospermidine oxidase (HSO) (Figure 24). Transcript levels of the other CuAO candidates differed in the lower and upper epidermis only by the factor not higher than 2. One of these sequences, CuAO2, was selected to be included in the further characterization for comparative reasons.

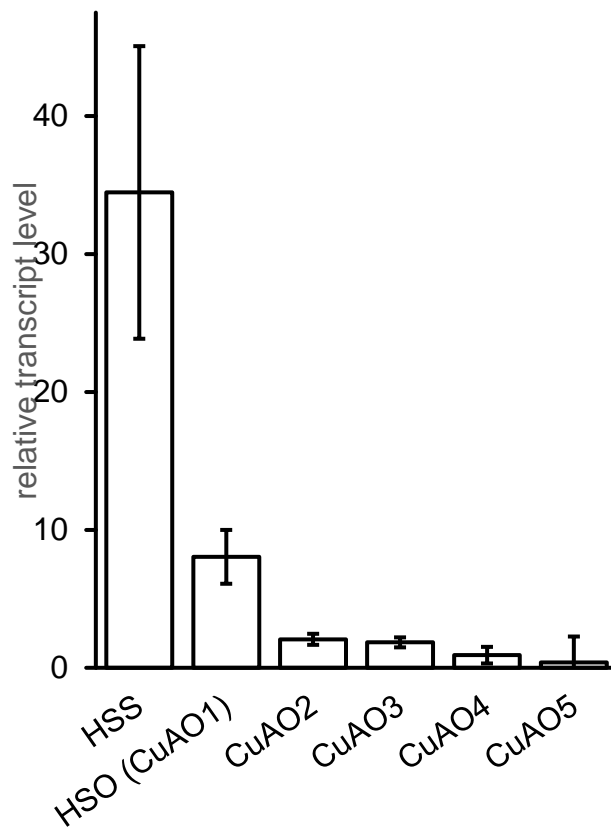


Figure 24: Relative transcript levels of the HSS- and CuAO-coding genes in the lower versus the upper leaf epidermis. Quantification by qRT-PCR was performed with cDNA from cells isolated by laser capture microdissection microscopy of the upper and lower leaf epidermis. Values > 1 indicate a higher transcript level of the respective gene in the lower leaf epidermis than in the upper leaf epidermis. The values were normalized using the genes for actin, ubiquitin, and elongation factor 1 α as references.

The transcript of HSO and CuAO2 are 1986 bp and 2304 bp long, respectively. According to the SignalP-5.0 server, the HSO protein is predicted to possess a *N*-terminal signal peptide of 21 amino acids in length. The tyrosine residues predicted to be post-translationally modified to TPQs are at amino acid positions 405 and 492 in HSO and CuAO2, respectively.

Since heterologous expression of HSO in *E. coli* failed using systems described earlier for expression of *N*-methylputrescine oxidase from tobacco (Heim et al., 2007; Katoh et al., 2007), the transient expression system using *N. benthamiana* was used for expression of *C*-terminal strep-tagged proteins with the pH7WG2D binary vector (Karimi et al., 2007). Quantification of transcript levels in infiltrated tobacco leaves by qRT-PCR

and of protein levels by gel blot analysis and by a photometric assay for CuAO-mediated formation of hydrogen peroxide suggested day 4 and day 6 after infiltration as the optimal time point for protein extraction of HSO and CuAO2, respectively (Figure 29). After affinity purification, HSO showed unequivocal activity with homospermidine with optimum pH of 7.2. The observation that HSO activity was completely abolished in the presence of 2-hydroxyethylhydrazine, an inhibitor of TPQ-dependent amine oxidases, gives further support for HSO to be a typical CuAO. Furthermore, the HSO turned out to be completely inactive after we replaced the precursor of the TPQ, the tyrosine at position 405, by a phenylalanine using site-directed mutagenesis.

Electrospray ionization tandem mass spectrometry (ESI-MS/MS) of peptides resulting from digestion of HSO with trypsin allowed us to detect TPQ as a phenylhydrazine adduct in the octadecapeptide (TVLTL^SSN^YDYVIDYEFKK) with the expected mass increment of 120 that was derived from phenylhydrazine-treated HSO (data not shown). In addition, ESI-MS/MS confirmed that of five potential *N*-glycosylation sites within HSO (positions 48, 52, 492, 576, 603) at least at the positions 48, 52, and 576 mainly Man₈GlcNAc₂ structures were detected in addition to other high-mannose-type *N*-glycans as the prominent type of glycosylation (data not shown). The peptide containing the predicted position 492 was only found unmodified

6.3.2 Substrate specificity and kinetic properties of HSO

To test whether homospermidine is the preferred substrate of HSO, the substrate specificity was analyzed using several diamines and polyamines including those which have been described for CuAOs of plant origin. For comparison, the CuAO2 was included in these analyses, as this enzyme does not show co-expression with HSO. Using substrate concentrations of 1 mM in a photometric assay with a crude desalted protein extract of tobacco leaves expressing HSO and CuAO2, respectively, it was shown that homospermidine is the best substrate for HSO, while spermine and putrescine were the less accepted ones (Figure 25). In contrast, for CuAO2, putrescine is the best accepted substrate. The presence or position (*N*- or *C*-terminal) of the strep-tag showed no influence on substrate preference of CuAOs as tested with CuAO2.

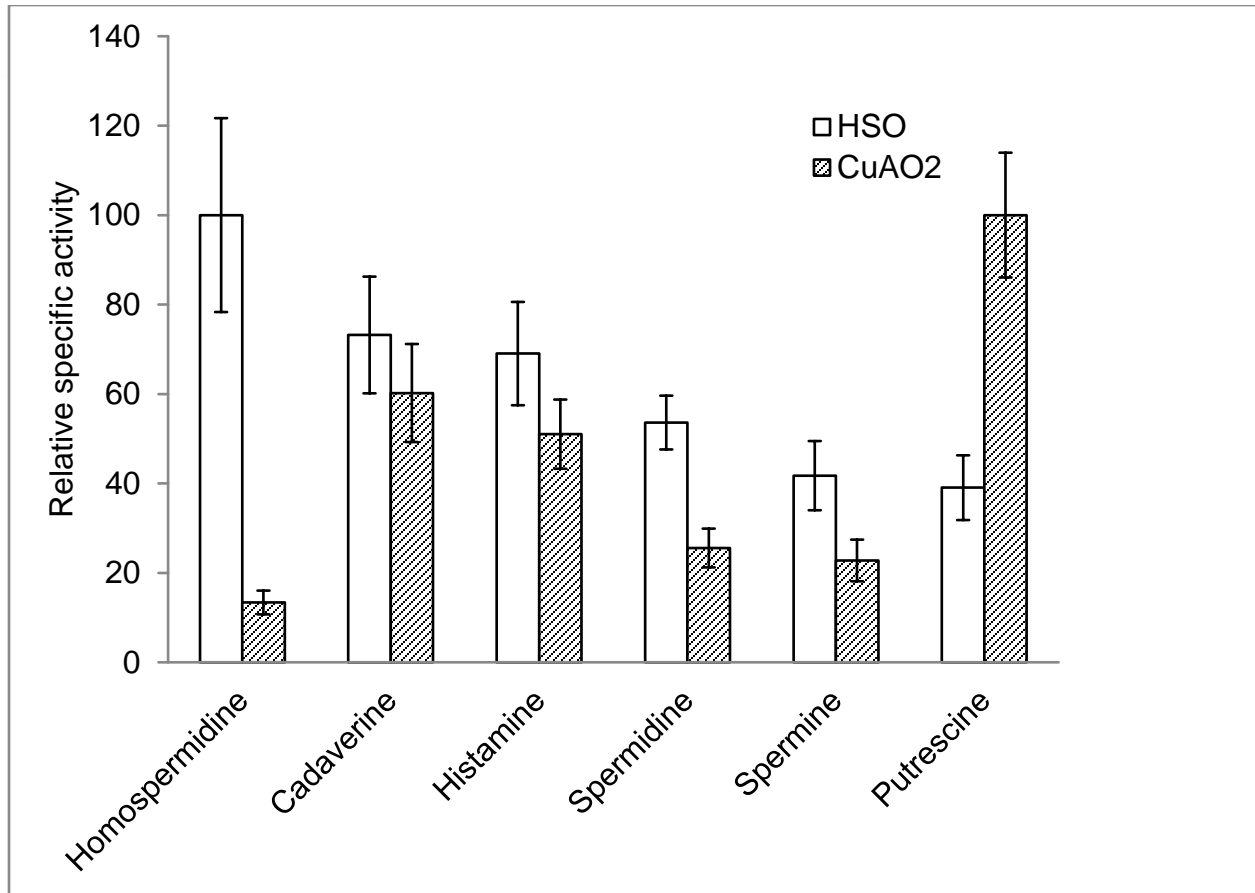


Figure 25: Substrate specificity of HSO and CuAO. Desalted protein extracts of tobacco leaves transiently expressing HSO and CuAO2, respectively, have been incubated with different polyamines (1 mM each, columns represent the mean of three independent expression experiments). 100% correspond to 164.0 pkat/mg for HSO and to 67.4 pkat/mg for CuAO2.

Using affinity purified enzyme preparations for enzyme kinetics of HSO, homospermidine, spermidine, and putrescine were used as substrates in concentrations ranging from 20 μ M to 10 mM (Figure 26). We observed a strong substrate inhibition for HSO with putrescine at concentrations higher than 150 μ M and for homospermidine at concentrations higher than 9 mM. No inhibition was observed for spermidine, but with this substrate the maximum activity was less than 20% of that observed with higher concentrations of homospermidine. Kinetics of CuAO2 with putrescine as its most preferred substrate showed substrate inhibition at concentrations higher than 9 mM similar to that observed for HSO with homospermidine. Due to the fact that substrate

inhibition occurs, we estimated apparent K_M -values using the Lineweaver-Burk plot only for the data area without prominent effects of inhibition (Table 1). While K_M -values for homospermidine (34 and 67 μM) and spermidine (66 and 80 μM) are in the same range, the value for putrescine was considerably higher (466 μM , calculated only for 20 to 150 μM). For CuAO2 the K_M -value for putrescine was estimated to be 4 mM.

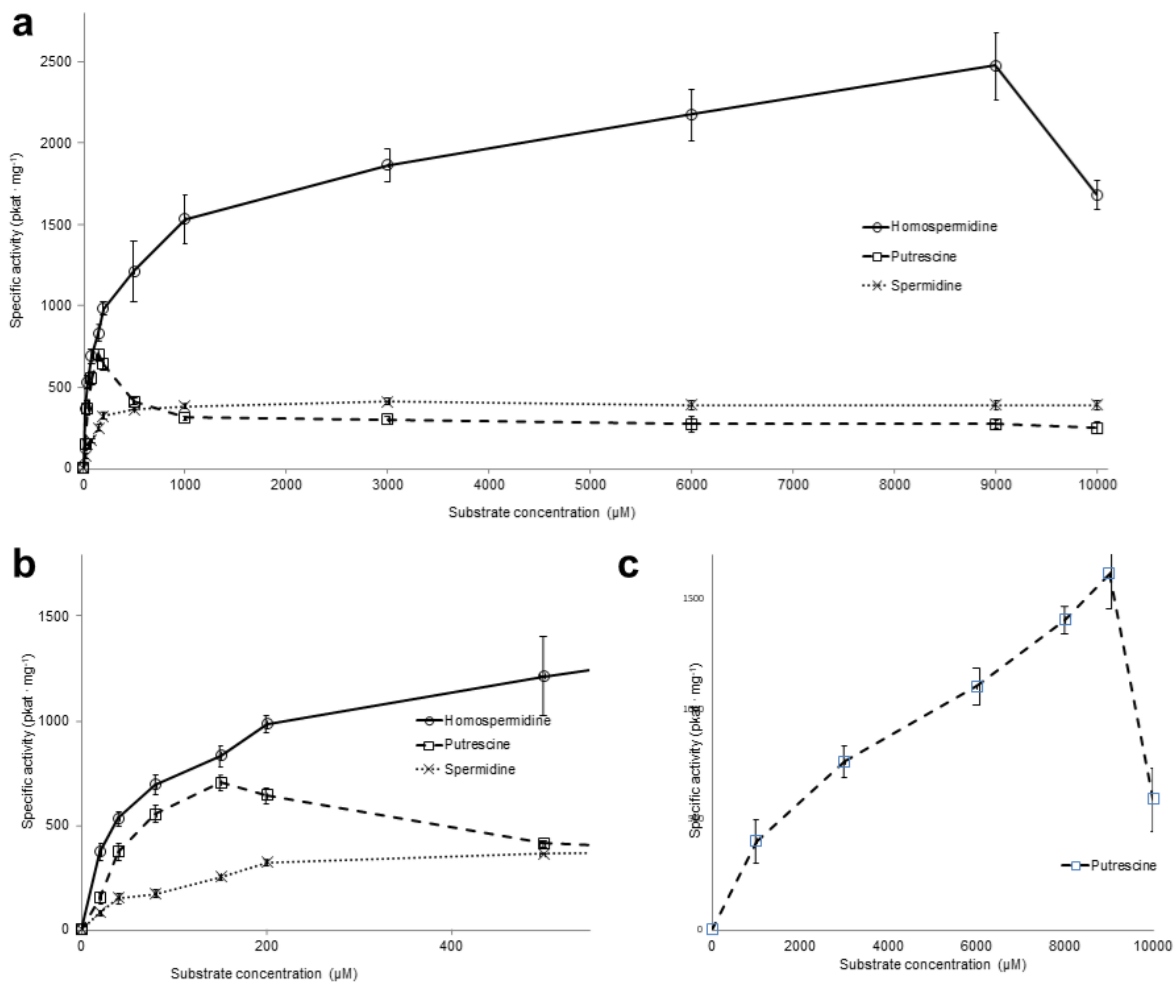


Figure 26: Substrate kinetics. The specific activity of affinity-purified HSO and CuAO2 was analyzed at various substrate concentrations (0 to 10 mM). **a** HSO was tested with homospermidine, spermidine, and putrescine as substrates as these are described to occur in relevant amounts in *H. indicum* (Frölich et al., 2007). **b** Detail of a for substrate concentration from 0 to 500 μM . **c** CuAO2 was tested with putrescine as the most preferred substrate. All data points represent the mean values \pm s.d. for three experiments.

Table 1. Kinetic data of HSO and CuAO.

Enzyme	Substrate	K _M [μM] ¹	(range of substrate conc.)	Spec. activity [pkat mg ⁻¹] ²
HSO	Homospermidine	81	(0-150 μM)	2480 (at 9 mM)
		81	(0-9 mM)	
	Spermidine	136	(0-150 μM)	411 (at 3 mM)
		95	(0-9 mM)	
	Putrescine	836	(0-150 μM)	702 (at 150 μM)
CuAO2	Putrescine	6700	(0-9 mM)	1610 (at 9 mM)

¹ calculated according to Lineweaver-Burk plot for the range of substrate concentrations only before substrate inhibition become prominent (0 to 9 mM for homospermidine and spermidine, 0 to 150 μM for putrescine and, for comparative reasons, also of homospermidine and spermidine.

² determined for the substrate concentration with the maximum activity before substrate inhibition become prominent

6.3.3 HSO is involved in PA biosynthesis

To confirm that HSO is involved in PA biosynthesis *in planta* a virus-induced gene silencing (VIGS) approach was used. Young leaves of ten week old *H. indicum* plants were inoculated with *A. tumefaciens* harboring the VIGS-construct for HSO (in pTRV2) or the pTRV2 empty vector as negative control, both with pTRV1 that is responsible for the replication and systemic spread of the virus in the plant. After 14 days the relative transcript levels of the genes encoding HSO, and HSS were estimated and alkaloid levels quantified in a single leaf that developed after infection. In these analyses transcript levels of *hss* served as a marker to compensate for different rates of PA biosynthesis in individual leaves that are not due to the knock-down. Successful knock-downs, identified by a lower *hso/hss*-transcript ratio, showed significantly lower alkaloid levels (Figure 27). This data gives strong support for the interpretation that HSO is involved in PA biosynthesis.

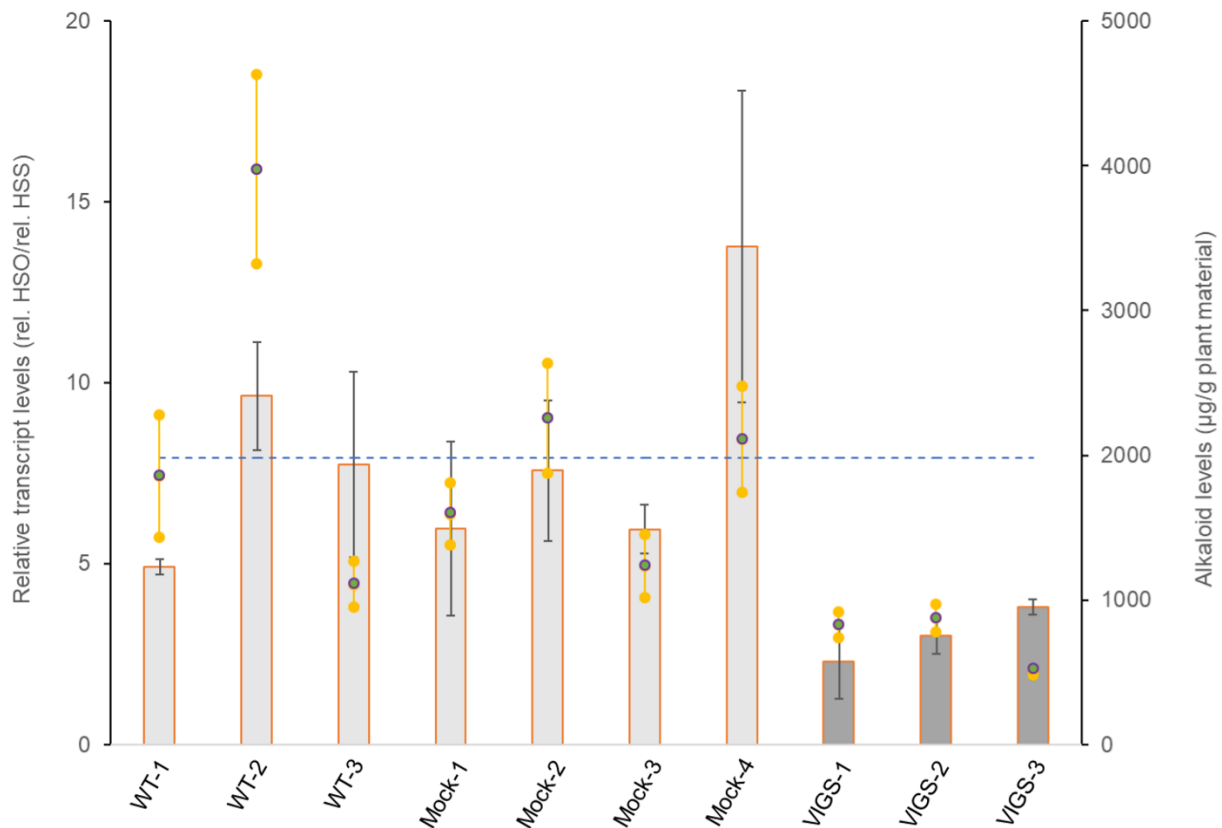


Figure 27: Virus-induced gene silencing analysis of HSO in *H. indicum*. Plants infected with pTRV2-vector constructs for HSO or the pTRV2 vector control (mock) have been analyzed in comparison to wild-type plants. Three leaves have been taken per individual and analyzed in triplicate. To compensate for variation in the level of PA biosynthesis in individual leaves, HSS transcript levels served as reference. Therefore, bars represent the ratio of HSO/HSS transcript levels, each standardized using the transcript level of ubiquitin. In addition, the alkaloid content in the analyzed tissue is given by dots. Each bar and data point represent the mean \pm s.d. of 9 values (that is three technical replicates of three leaves per individual). The dashed line represents the mean of the relative transcript level of all control lines (wild-type and mock-lines). Statistical analyses show that the relative transcript levels and PA-levels of the HSO knock-downs were significantly lower than those of the wild-type and the mock control plants ($p=0.002$ and $p=0.011$, respectively).

6.3.4 HSO is sufficient for the formation of the methyl-pyrrolizidine backbone

To identify the HSO reaction product, the product was analyzed using 1D proton nuclear magnetic resonance spectroscopy (NMR). A similar reaction setup was described earlier by Houen et al. (2005) who observed with BSAO a partial conversion of homospermidine to a pyrrolinium ion. This resulted from oxidation of one of the primary amino groups of homospermidine (Figure 28). The NMR spectra resulting from HSO reaction showed a full turnover after 72 hours and resulted in a NMR spectrum not identical with that of Houen. Therefore, two-dimensional NMR experiments of the HSO reaction revealed the product to be 1-carboxypyrrolizidine (Figure 33). In addition, heteronuclear single quantum correlation (HSQC) experiments show that the product is, due to the two stereocenters present at the C1 and C8 of the 1-carboxypyrrolizidine, a diastereomeric mixture (Figure 28). In addition, ^{13}C -NMR showed the presence of a quaternary carboxylic acid function at the C9 group (Figure 34). To test for product stability at room temperature, the 1D proton NMR measurement was repeated after 3 and 7 days without any hints for degradation (Figure 35).

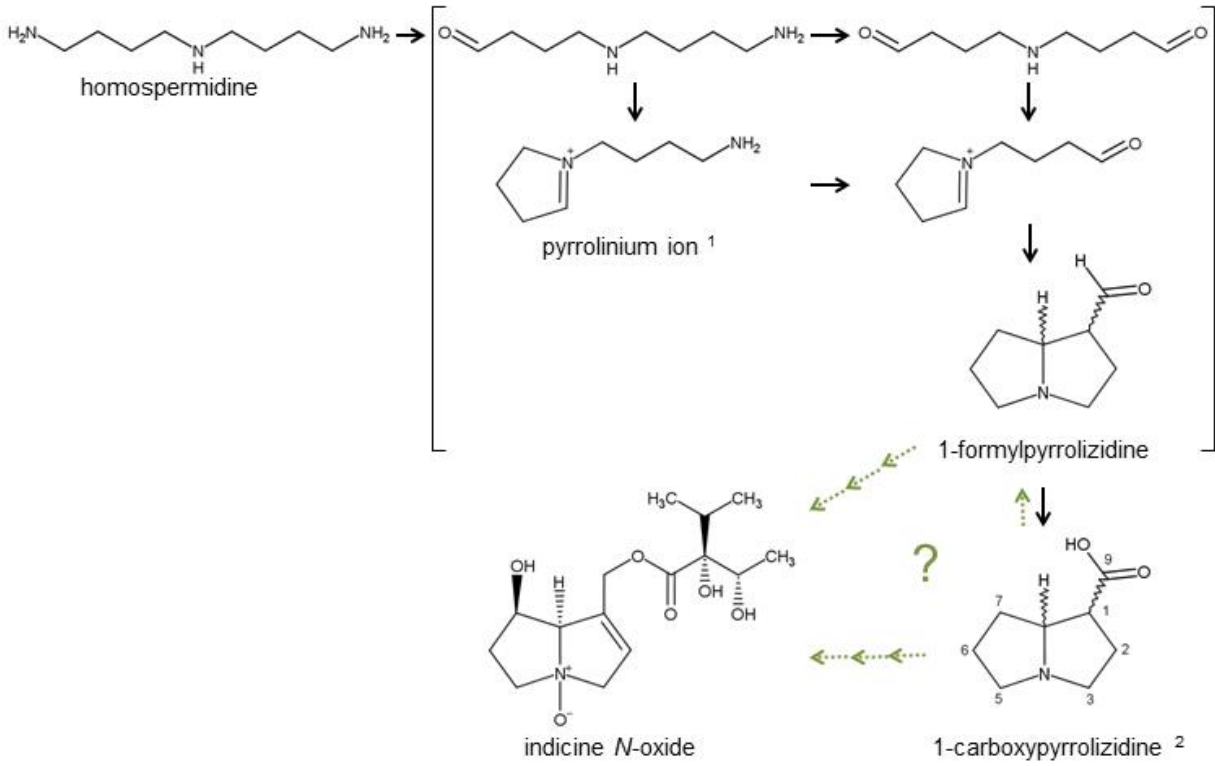
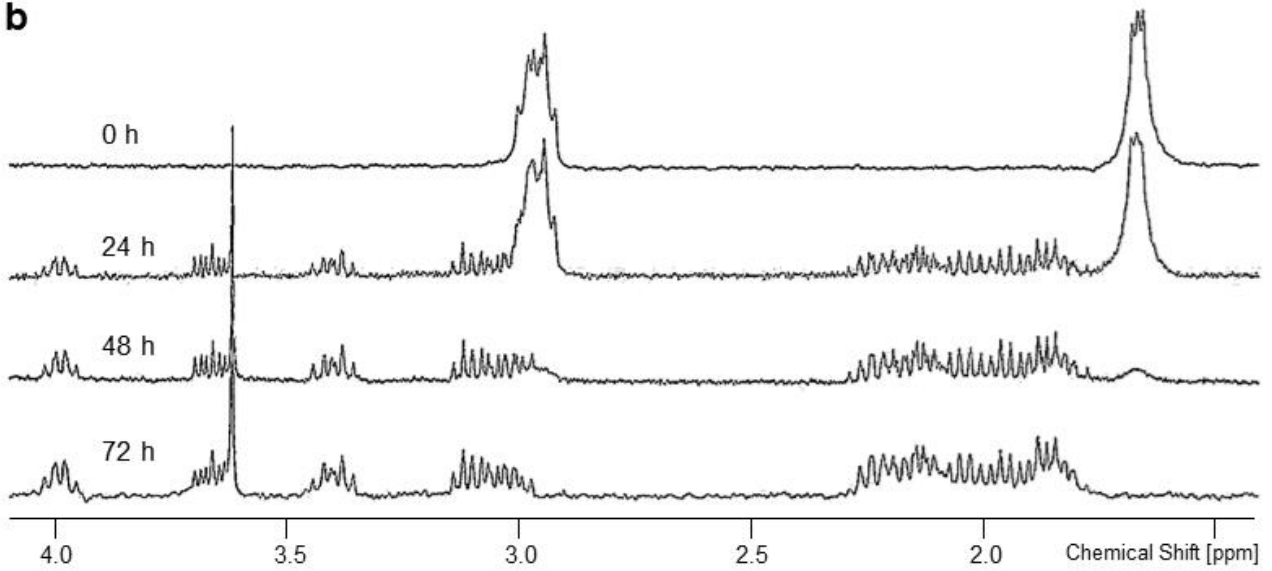
a**b**

Figure 28: HSO catalyzes the oxidation of both primary amino groups of homospermidine. **a** HSO-catalyzed conversion of homospermidine results in the formation of 1-carboxypyrrolizidine, a structure that was successfully incorporated into indicine N-oxide, a characteristic PA found in *H. indicum* leaves. Structures shown in square brackets are hypothetical intermediates of this reaction. The pyrrolinium ion resulting from oxidation of only one of the primary amino groups of homospermidine was shown previously to be the product after incubation with BSAO (Houen et al., 2005). The 1-formylpyrrolizidine, postulated in older literature (Khan and Robins, 1985), might also be a direct precursor for indicine N-oxide. The discussed biosynthetic routes are shown by dotted arrows. **b** Conversion of homospermidine by HSO analyzed by 1D proton NMR (in D₂O) at different time points of the enzyme reaction (0, 24, 48, 72 h). Spectra are shown for the region of 1.40 to 4.10 ppm. At the start of the enzyme reaction (0 h) the spectrum shows the hydrogen atoms (1.65 to 1.70 and 2.90 to 3.00 ppm) of homospermidine. At the end of incubation (72 h) no hydrogen atoms of homospermidine are detectable. Instead, the signals indicate the formation of 1-carboxypyrrolizidine.

1-Carboxypyrrolizidine - 1D proton NMR (500 MHz, D₂O, 25°C): 1.92 (2H, m), 2.03 (2H, m), 2.14 (2H, m), 2.23 (2H, m), 2.32 (2H, m), 3.48 (2H, m), 3.74 (1H, m), 4.06 (1H, m); ¹³C-NMR (126 MHz, D₂O, 25°C): 24.26, 27.33, 29.77, 51.62, 54.86, 59.40, 69.03, 181.65.

Using Direct Insertion Probe Electron Impact High Resolution Accurate Mass Spectrometry (DIP-EI HRAMS) the molecular weight of the reaction product was determined to be 155.09463. To confirm that the HSO-catalyzed oxidation results in the deamination of the two terminal primary amino groups, ¹⁵N-1H heteronuclear multiple-bond correlation spectroscopy (HMBC) experiments were performed with fully labeled [¹⁵N]homospermidine. Only signals from the secondary amino group of the precursor were observed (Figure 36).

6.3.5 Carboxypyrrolizidine is an intermediate of PA biosynthesis

To test if the 1-carboxypyrrolizidine resulting from HSO reaction with homospermidine is incorporated into PAs, the ^{15}N -labelled product was fed to fully developed leaves of *H. indicum* over a time period of three days. After alkaloid extraction of the leaves the PA pattern matched previously published data without any hints for artificial structures with stereoisomeric necine bases (Frölich et al., 2007). Non-natural isotopic shifts in the GC-MS spectra result from incorporation of ^{15}N and show that the carboxypyrrolizidine is indeed incorporated into PAs.

[^{14}N]Indicine: m/z (EI) 138 (999), 93 (524), 139 (377), 94 (348), 137 (116), 95 (103), 136 (92), 156 (88), 80 (76), 120 (67).

Indicine after feeding of ^{15}N -tracer: m/z (EI) 139 (999), 94 (480), 140 (332), 95 (274), 138 (225), 93 (100), 80 (91), 157 (86), 96 (83), 43 (64).

6.4 Discussion

CuAOs are found in all kingdoms of life. They are described to be responsible for polyamine homeostasis and detoxification, to produce hydrogen peroxide that acts directly or as signaling molecule in many physiological responses and to be involved in polyamine oxidation in metabolic pathways (Boyce et al., 2009; Medda et al., 1995). The latter function, the formation of aminoaldehydes, was shown to be a crucial step in various biosynthetic pathways of alkaloids, a class of natural compounds within plants that possess often drastic biological activities (Aniszewski, 2007). CuAOs were shown to be involved in the oxidation of *N*-methylputrescine in the formation of nicotine and tropane alkaloids and in the oxidation of cadaverine in the biosynthesis of quinolizidine alkaloids or piperine alkaloids. In all these cases, the oxidation of an amine is the prerequisite for the formation of *N*-containing heterocyclic structures characteristic for most groups of alkaloids (Aniszewski, 2007).

For PAs the involvement of one or more CuAOs (formerly called “diamine oxidase”) in the oxidation of the homospermidine was postulated since many years. Main arguments were

the type of reaction (Khan & Robins, 1985), the inhibition of this step by hydroxyethylhydrazin (Böttcher et al., 1993; Frölich et al., 2007), or a biomimetic experiment, in which the incubation of homospermidine with a CuAO of pea seedlings resulted in detectable amounts of a pyrrolizidine (Robins, 1989). Following this hypothesis we have been able to identify a CuAO of the PA-producing plant *H. indicum* (1) that has all characteristics of a typical CuAO including a TPQ and extensive glycosylation as posttranslational modifications; (2) that shows a preference for the substrate homospermidine that is oxidized at both primary amino groups to form a carboxypyrrolizidine, a compound that was readily incorporated into PAs in a tracer feeding experiment; and, (3) that is involved in PA biosynthesis, as down-regulation by VIGS results in decreased PA-levels; and (4).

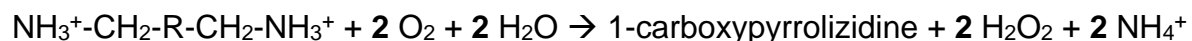
6.4.1 HSO has all characteristics of a typical CuAO

To express HSO, all tested *E. coli*-based expression systems failed to give soluble and active enzyme. These included also strategies using fusions with a GST-tag or a thioredoxin, two systems successfully used for the expression of *N*-methylputrescine oxidase of tobacco (Heim et al., 2007; Katoh et al., 2007). Transient expression in leaves of *N. benthamiana*, instead, resulted in the expression of active enzyme. This observation suggests that posttranslational modifications that are possible in a eukaryotic expression system might have a positive effect for the proper folding and activity of the recombinant protein. Such modifications could be the autocatalytic formation of the TPQ though this should not be dependent on a eukaryotic expression system, phosphorylations, and glycosylations. Extensive glycosylation is described for CuAOs of various organisms. For BSAO, an exhaustive deglycosylation was necessary to allow crystallization (Lunelli et al., 2005). For pea seedling amine oxidase it was estimated that between 3 and 14% of total molecular weight is due to carbohydrates that might enhance the stability of the protein or participate in protein-protein interactions (Medda et al., 1995; Tipping & McPherson, 1995). Though, having in mind that HSO was expressed heterologously in tobacco leaves and was not purified from its host *H. indicum*, the data from ESI-MS/MS analyses of tryptic peptides show that HSO is, at least, glycosylated at three out of five

predicted glycosylation sites with high-mannose-type *N*-glycans, structures also reported for other plant CuAOs (Franc et al., 2013). ESI-MS/MS showed also the expected mass shift of the phenylhydrazine-treated octadecapeptide harboring the in CuAOs highly conserved stretch of amino acids including the tyrosine precursor of TPQ at position 405 (T-x-x-N-Y-D/Q-Y, (Li et al., 1998)). Phenylhydrazine as well as hydroxyethylhydrazine are substituted hydrazines that are irreversible inhibitors of amine oxidases as they react with TPQ to a stable covalent adduct (Janes et al., 1992; Nagakubo et al., 2019; Padiglia et al., 1998). Therefore, the observation that HSO activity is lost after incubation with hydroxyethylhydrazine gives further support for the involvement of the TPQ in enzymatic activity just as the replacement of the TPQ precursor Tyr405 by a phenylalanine using site directed mutagenesis.

6.4.2 HSO catalyzes the oxidation of both primary amino groups of homospermidine

The formation of the bicyclic pyrrolizidine backbone that is characteristic for all plant-derived PAs requires the oxidative deamination of both primary amino groups of homospermidine. Therefore, it was unclear whether one or two CuAOs might be involved in the oxidation of homospermidine. Our data shows that HSO catalyzes the oxidation at both ends of homospermidine with a complete turnover to 1-carboxypyrrolizidine within 72 h at room temperature according to the following overall reaction:



Two-dimensional NMR of the HSO-catalyzed reaction did not give any hints for the formation of detectable amounts of an intermediate. We speculate that after the first oxidation, the product has to be released from the active site, so the second primary amino group can access the active site. Whether the substrate for the second oxidation is the open aldehyde or an already monocyclic intermediate remains open. Analyzing the substrate specificity of a CuAO of bovine serum, Houen et al. (2005) tested also homospermidine and showed by NMR that oxidation occurred at only one of the two primary amino groups resulting in the formation of an iminium ion, 1-(4'-aminobutyl)-pyrrolinium. Obviously, this product was no substrate any more for BSAO even though

this enzyme was shown to accept a wide array of substrates (Houen et al., 2005). Speculating that such a monocyclic structure is the substrate for the second oxidation of HSO, a wide substrate channel has to be postulated. Of note, the width of this substrate channel is one of the determinants discussed to be responsible for the substrate specificity of CuAOs including that of plants (Chang et al., 2010; Lunelli et al., 2005). Another factor is the presence of an attachment point in the substrate channel for a secondary amino group with a spacing of 3 to 4 CH₂ groups to the primary amino group bound in the active site (Houen et al., 2005).

Even though plant CuAOs have been described to be effective in the conversion of their substrates (Kumar et al., 1996), a complete conversion of the substrate homospermidine was unexpected, the more, as catalase that is continuously removing hydrogen peroxide from the reaction was not added in these analyses. Probably, non-enzymatic reactions push the reaction equilibrium to the product side. However, there are some cases of non-enzymatic reactions in nature (Keller et al., 2015) but these might also be reactions that occur *in vitro*. These are (1) the cyclizations forming the bicyclus and, (2), a possible oxidation of the reaction product by hydrogen peroxide. Structures described for CuAOs of various lineages show that there is not enough space within the active site for a cyclization process. It is more plausible to assume that cyclization is a spontaneous process after the aminoaldehyde is released from the enzyme. This idea is supported by the observation that the obtained 1-carboxypyrrolizidine is a diastereomeric mixture. As PAs extracted from *H. indicum* have a defined stereochemistry, it is most likely that cyclization is controlled *in planta* or that other mechanisms like isomerases are involved in PA biosynthesis. The second non-enzymatic conversion could be the oxidation of an aldehyde by hydrogen peroxide. As the products of CuAO-mediated deamination of primary amines are usually aldehydes, we expected the pyrrolizidine with an aldehyde group instead of the observed carboxylic group. Further studies have to show whether the detected carboxypyrrolizidine is an intermediate that occurs *in planta*, an idea supported by the fact that ¹⁵N-labelled 1-carboxypyrrolizidine produced by HSO is incorporated in tracer feeding experiments into PAs of *H. indicum*, or whether it is just occurring *in vitro*. Of note, derivatives of 1-carboxypyrrolizidine are described from various PA-containing plants, e.g. chysin, the corresponding methylester (Lang et al., 2001).

6.4.3 HSO is involved in PA biosynthesis and shows substrate preference for homospermidine

To test for the involvement of HSO in PA biosynthesis, we used VIGS to downregulate HSO in young plants of *H. indicum* and quantified PA levels. As PA biosynthesis is known to be quite variable within different tissues of the plant (Kruse et al., 2017; Stegemann et al., 2019), we quantified in addition to the transcript encoding HSO also the transcript of HSS. By comparing the relative expression levels of HSO and HSS with PA levels, cases in which low PA levels might be due to downregulation of the complete pathway should be eliminated. Indeed, in comparison to control lines (harboring the empty VIGS vector construct) and wild-type plants, the reduced levels of relative HSO expression correlate with lower levels of PAs (Figure 27).

Tests with various substrates showed that the preferred substrate of HSO is homospermidine, while CuAO2 prefers putrescine over all other substrates (Figure 25). Differences between the various substrates became even more obvious in the kinetic analyses with those substrates that are described by Frölich et al. (2007) to occur in *H. indicum* in concentrations ranging from 20 μM up to 10 mM (Figure 26). With homospermidine, HSO showed a specific activity of 2.5 nkat/mg at 9 mM, before the value decreased due to substrate inhibition. For putrescine, HSO showed a specific activity of 0.6 nkat/mg at 150 μM , a value similar to that for homospermidine in the same concentration, but is inhibiting already at concentrations higher than 150 μM . With spermidine no substrate inhibition was detected for HSO, but the observed specific activities remained low. Substrate inhibition was observed earlier for various CuAOs and was discussed to be due to a binding of cationic substrates to the reduced, catalytically incompetent form of the enzyme that results from the reductive half reaction (Holt et al., 2008; Ignesti, 2003). Furthermore, Ignesti (2003) postulated after sophisticated kinetic analyses of the CuAO of pig kidney with one- and two-substrate reactions that CuAOs have two substrate binding sites, one of which is the catalytic one. As a consequence, the use of the Michaelis-Menten approximation is not recommended for CuAOs. However, to allow rough comparisons in the efficiency of HSO we calculated apparent K_M -values for the lower polyamine concentration before substrate inhibition became prominent and refrained to calculate further kinetic constants. Based on this data the K_M -

values for triamines homospermidine (34 – 67 μM) and spermidine (66 μM) are much smaller than that for the diamine putrescine (466 μM). For several other plant CuAOs, like the CuAO of pea seedlings, diamines with a short chain length of 5 to 7 carbon atoms are the preferred substrates, characteristics that are most similar to the substrate specificity of CuAO2 that shows a K_M -value for putrescine of 6700 mM. For several CuAOs of *Arabidopsis* a preference for putrescine and spermidine is described (Fraudentali et al., 2019; Planas-Portell et al., 2013; Tavladoraki et al., 2016).

Analyses on the sequence of reactions by which putrescine as radioactive tracer is metabolized in PA-producing leaves of *H. indicum* revealed the transient accumulation of an unidentified “metabolite X” in the pathway between homospermidine and the necine base moiety of PAs (Frölich et al., 2007). We speculate that the “metabolite X” could be the product of HSO. Furthermore, the studies of Frölich et al. (2007) show that labelled homospermidine is only detectable in the young leaves after inhibition of HSO with hydroxyethylhydrazine but not without inhibition. This suggests that HSO is efficient in converting homospermidine and keeps homospermidine levels in the cell below the detection limit even though HSS has the capacity to produce significant amounts of homospermidine (Abdelhady et al., 2009). This suggests that HSO is not a rate limiting step of PA biosynthesis. In addition, Frölich et al (2007) confirmed a previous observation that after release of the inhibition, all homospermidine is incorporated into the necine base of PAs without any hints for degradation via other metabolic routes (Böttcher et al., 1993). This suggests that homospermidine might be protected from degradation for example by compartmentalization. Of note, HSO is predicted to possess an *N*-terminal targeting sequence for the endoplasmic reticulum. Further studies have to clarify the role of compartmentalization of HSO and PA biosynthesis also with respect to transport processes of polyamines that might be involved in the regulation of PA biosynthesis (Fujita et al., 2014).

6.4.4 Evolution of HSO

Gene duplications are a prominent mechanism that drives the development of new genes. For plant secondary metabolism several examples have been described that show

diversification and optimization after the duplication of genes involved in primary metabolism, including the CuAO involved in nicotine biosynthesis (Naconsie et al., 2014; Dietrich Ober, 2005). Most likely, also HSO originated from a gene encoding a CuAO involved in primary metabolism that was optimized in respect to its substrate specificity and reaction mechanism. Several models are proposed to explain the evolution of new functions, some of which postulate that the duplicated gene had already more than one activity before duplication (Conant & Wolfe, 2008; Depristo, 2007). For such a scenario, HSS, as the first specific enzyme of PA biosynthesis, is an illustrative example. It originated by duplication of a gene encoding deoxyhypusine synthase of primary metabolism, a gene that is involved in the posttranslational activation of the eukaryotic initiation factor 5A, but that was shown to possess also the ability to catalyze the formation of homospermidine ((Ober & Hartmann, 1999; 1999)). Such a bifunctionality can also be postulated for a CuAO of primary metabolism, as Robins (1989) showed that also the CuAO of pea seedlings was sufficient in a biomimetic experiment to catalyze the formation of the bicyclic pyrrolizidine. However, the report of Robins remains the only hint for such a side activity, as characterization of the substrate specificity of pea seedling amine oxidase described a preference for diamines with a short chain length but did not reveal any specificity for triamines including homospermidine in particular (Kumar et al., 1996; Lunelli et al., 2005). In another experiment, Abdelhady et al. (2009) expressed HSS under the control of a constitutive promotor in tobacco plants and detected high levels of homospermidine, but did not find any hints for the formation of the pyrrolizidine backbone structure of PAs. With our data, suggesting an *N*-terminal signal peptide for HSO, this observation might not be due to the absence of a CuAO accepting homospermidine at least in traces as the authors stated, but also to the localization of homospermidine and the CuAOs in different subcellular compartments.

6.5 Materials and Methods

6.5.1 Plant material and growth conditions.

Heliotropium indicum was grown in the greenhouse under conditions as described previously (Kruse et al., 2017). Seeds of *Nicotiana benthamiana* were sown in pots containing TKS®2 soil (Floragard, Germany) mixed with lava stones in a 3:1 ratio topped for germination with TKS®1 soil. Plants were grown in a climate chamber at 25°C, 65% humidity, 16/8 h light/dark cycle (206 $\mu\text{mol m}^{-1} \text{sec}^{-1}$). After two weeks, plants were fertilized (0.3%, v/v, Wuxal® Top N fertilizer, Aglukon, Germany) and treated with Novo Nem® F (ÖRE Bio-Protect, Schwentinental, Germany) for biological pest control till harvest.

6.5.2 Relative transcript quantification.

RNA extraction, cDNA synthesis, and relative transcript quantification of the genes encoding ubiquitin, HSS, HSO, and CuAO2 to CuAO5 were performed as described by Sievert et al. (Sievert et al., 2015) from cDNA isolated by laser capture microdissection microscopy and according to (Kruse et al., 2019) to test for effects of VIGS. Primer sequences are given in Supplemental Table 1.

6.5.3 Identification of complete open reading frame of HSO and CuAO2 and transient protein expression in *N. benthamiana*.

Suppression subtractive hybridization of cDNA preparations of the lower and the upper leaf epidermis of *H. indicum* resulted in an EST library, in which five transcripts of DAO-like sequences have been identified (Sievert et al., 2015). Of these sequences (CuAO1 to CuAO5) CuAO1 (=HSO) and CuAO2 were selected for transient expression in *N. benthamiana* plants. To obtain the full-length open reading frame the 3'-end and the 5'-end of the HSO and CuAO2, respectively, have been identified by using the rapid amplification of cDNA ends approaches as described (Nurhayati et al., 2009). Primers are given in Supplemental Table 1. For prediction of N-terminal signal peptides the

SignalP-5.0 server (Almagro Armenteros et al., 2019) and of *N*-glycosylation sites the GlycoEP server (Chauhan et al., 2013) were used. The complete ORF of HSO (CuAO1) and CuAO2 were amplified using primer pairs P24/P25 and P26/P27, respectively, introducing attB1 and attB2 recombination sites, a Kozak sequence (Kanagarajan et al., 2012) directly in front of the start-ATG, and C-terminal Strep®-tag II sequences (IBA, Göttingen, Germany). To test for a possible effect of the position of the Strep®-tag II, for CuAO2 also constructs with a *N*-terminal tag (P29/P30) and without any tag (P28/P29) were prepared. The resulting fragments were cloned into the binary vector pH7WG2D.1 (Karimi et al., 2007) with the Gateway system (Thermo Fisher Scientific) according to the manufacturer's instruction using the pDONR221 as entry vector. The resulting expression constructs were transformed into *Agrobacterium tumefaciens* strain GV3101/pMP90 (Koncz & Schell, 1986) by electroporation in addition to the empty pH7WG2D.1 vector as control and the pBIN61-P19 vector that was used to minimize posttranslational silencing effects by co-infecting the *N. benthamiana* plants.

For this, syringe agroinfiltration was performed using a method described by Broghammer et al. (2012) with modifications: The infiltration-medium (50 mM MES buffer, 2 mM Na₃PO₄, 0.5% glucose, 200 µM acetosyringone, pH= 5.6) was used to resuspend the pelleted agrobacteria harboring the vector plasmids before they were grown for 2.5 h at room temperature. After dilution of each culture to an OD₆₀₀ of 0.3 each of the cultures harboring the expression vector was mixed with the culture harboring the pBIN61-P19 vector in a ratio of 3:1 for infiltration of the leaves. Therefore, the abaxial surface of the leaves was gently scratched with a syringe needle and about 2 ml of the agrobacterium suspension was infiltrated in each leaf. Plants were placed in the climate chamber until harvest 4 and 6 days after infiltration for HSO and CuAO2, respectively.

6.5.4 Protein extraction and purification.

All steps were performed at 4°C if not otherwise stated. Leaf samples were frozen in liquid nitrogen, ground with mortar and pestle to a fine powder and 1 g was extracted in 5 ml of extraction buffer (100 mM Tris HCl pH 8, 150 mM NaCl, 5% (w/v) polyvinylpyrrolidone, 2.5% (w/v) sodium ascorbate, 1% (w/v) activated charcoal, 2% (v/v) Biolock® to prevent

binding of biotin to the affinity matrix) for 15 min at 4°C. After filtration of the extract via Miracloth® (Merck-Millipore) to remove cell debris, the extract was centrifuged at 20,000 g for 20 min and re-buffered to purification buffer (100 mM Tris HCl pH 8, 150 mM NaCl) to prepare the desalted crude protein extract. For affinity purification the extract was applied onto a Strep-Tactin®XT Superflow (IBA, Göttingen, Germany) according to the protocol of the manufacturer with a reduced flow rate of 7 drops/min. Protein concentration was estimated using the method of Bradford (1976) or, for the purified protein, by direct absorption using the Nanodrop 2000 UV-Vis Spectrophotometer (Thermo Fisher Scientific).

6.5.5 Protein gel blot analysis.

20 µg of the desalted crude protein extract were separated via SDS-PAGE using PageRuler Prestained Protein Ladder (Thermo Fisher Scientific) as protein mass standard. Blotting onto polyvinylidene fluoride membrane (Immobilon P; Millipore) and detection of the Strep-tag® II by the Strep-Tactin® AP conjugate (IBA) was done as described by the manufacturer with the modification that the membrane was blocked overnight at room temperature with Tris-buffered saline (TBS) supplemented with 0.1% (v/v) Tween 20, 0.1% (v/v) Triton and 3% (w/v) bovine serum albumin and incubation Strep-Tactin® AP Conjugate overnight at 4°C.

6.5.6 Microsequencing of HSO.

Affinity purified HSO was separated by SDS-PAGE (0.5 µg per lane), cut from the gel after staining with coomassie blue, washed three times with water. After digestion with trypsin the resulting peptides were subjected to ESI-MS/MS as described by Zorn et al. (2005)

6.5.7 Photometrical assay for CuAO.

Purified enzyme or the desalted crude protein extract were incubated in assay buffer (30 mM potassium phosphate buffer, pH 7.2) with polyamine substrates

(homospermidine, putrescine, spermine, spermidine, histamine, and cadaverine) at 30°C. Activity was quantified by monitoring hydrogen peroxide formation by color development according to Allain et al (1974). In the presence of horseradish peroxidase (5 U/ml, Carl Roth) the produced hydrogen peroxide oxidizes 4-aminoantipyrine that couples to sodium 4-hydroxybenzenesulfonate dihydrate (25 mM, Sigma-Aldrich) to form the quinoneimine dye ($\Delta\epsilon_{500} = 5.54 \text{ mM}^{-1} \text{ cm}^{-1}$) (Vojinović et al., 2004). Color formation was monitored continuously for 10 minutes using Swift-II software to ensure linear product formation.

6.5.8 Site directed mutagenesis.

For site-directed mutagenesis the construct containing the full ORF of HSO in the pDONR221 entry vector was amplified with the primer pair P31/P32 (Supplemental Table) to substitute the codon TAC by TTT resulting in the replacement of tyrosine by phenylalanine. The modified sequence was introduced into the pH7WG2D.1 destination vector before being expressed as described for the unmodified sequences.

6.5.9 Preparation of homospermidine and [¹⁵N]homospermidine

Homospermidine was prepared biosynthetically using heterologously expressed bacterial homospermidine synthase of *Blastochloris viridis* in *E.coli* (Tholl et al., 1996). In a total volume of 50 ml potassium phosphate buffer (50 mM, 2 mM DTT, 2 mM NAD⁺, pH 8.6) 5 mg of affinity purified bacterial HSS were incubated with 5 mmol putrescine at 37°C over night. After stopping the reaction by addition of 5.5 ml of 1.4 M hydrochloric acid, homospermidine was purified using ion exchange resin as described by Ober et al. (2003) and tested for complete removal of substrate by thin layer chromatography (Frölich et al., 2007). After evaporation of the solvent homospermidine trihydrochloride powder was washed three times with methanol at 4°C to remove minor impurities. Identity and purity of homospermidine was confirmed in CDCl₃ (Carl Roth, Karlsruhe, Germany) by 1D proton NMR, HMBC, and HSQC (Figure 33). The identical procedure was used to prepare [¹⁵N]homospermidine by using fully labelled [¹⁵N]putrescine (Sigma Aldrich) as substrate.

6.5.10 Virus-induced gene silencing in *Heliotropium indicum*

VIGS experiments were conducted according to Dinesh-Kumar et al. (2003). Briefly, an approx. 300 bp long sequence from the end of the open reading frame and the adjacent 3'-UTR of HSO was amplified using the primer pair P33/P34 (Supplemental Table), introducing overhangs that allowed restriction cloning into the *XhoI/NcoI*-linearized pTRV2 vector. The resulting construct, an empty vector control, and the pTRV1 vector were transformed into *A. tumefaciens* strain GC3101. For infection, young developing leaves of 10 week-old plants (usually having approximately 7 to 8 well-developed leaves) were used that showed a characteristic wrinkled surface structure (Fig. 32). Quantification of the transcript abundance of TRV coat protein in the developing inflorescences according to Broderick and Jones (2014) with primer pair P18/P19 suggested an optimal date for harvest 14 days after inoculation. Harvested leaves were ground to a fine powder in liquid nitrogen with mortar and pestle and used for RNA and alkaloid extraction. For quantification of the HSO transcript a primer pair was used that did not bind to that part of the sequence used for the VIGS construct (P35/P36). PAs have been quantified by GC-MS as described previously (Stegemann et al., 2019).

6.5.11 Enzymatic reaction for identification of the product 1-carboxypyrrolizidine

For a NMR-based identification of the product of the HSO-catalyzed conversion of homospermidine, a protocol was chosen that was described earlier for the identification of reaction products of bovine serum amine oxidase (Houen et al., 2005). Briefly, 0.2 mg purified HSO were incubated in a total volume of 0.7 ml in potassium phosphate buffer (10 mM, pH 7.2) supplemented with 60 μ l D₂O and 1 mM homospermidine as substrate for 72 h at room temperature. The reaction was monitored via 1D proton NMR at different time points. As this reaction showed a full conversion of the substrate, an upscaled version (by factor 10) of this protocol was also used to prepare [¹⁵N]carboxypyrrolizidine for tracer feeding experiments with [¹⁵N]homospermidine as substrate.

6.5.12 NMR analyses

1D proton NMR spectra for observation of the reaction process were recorded using a Bruker Avance III 300 NMR spectrometer (Bruker Daltonics) operating at 300 MHz and a 5 mm PABBO broad band probe with a z gradient unit. Measurements were performed at 293 K and the temperature was calibrated with a methanol- d_4 solution. For each sample automatic tuning and matching of the probe was performed as well as automatic shimming of the on-axis shims (Z to Z5). The automatic receiver gain adjustment mode was employed, resulting always in the same maximum value for the gain.

Two dimensional experiments were performed using a Bruker Avance 500 NMR spectrometer (Bruker Daltonics), operating at 500 MHz for the proton channel, 126 MHz for the ^{13}C channel and 60 MHz for the ^{15}N channel.

6.5.13 DIP-EI-HRAMS

For determination of the exact molecular weight of the HSO reaction product, the direct insertion probe technique using a QExactive GC-Obitrap Instrument (Thermo Fisher Scientific, Dreieich) with ion source temperature at 280°C, DIP with a rate of 20°C/s from 60°C to 300°C with an aluminum vial. Scans were performed at a resolution of 60.000 (200 m/z).

6.5.14 Tracer feeding experiments

For feeding experiments using the [^{15}N]carboxypyrrolizidine as tracer, the reaction product of the upscaled enzymatic reaction for product identification (see above) was purified. For this, the reaction was stopped by flash freezing in liquid nitrogen and freeze-dried. The lyophilisate was taken up in 0.1 N sulphuric acid (Carl Roth) and purified using a Retain-SPE-CX cartridge (1 g/50 ml, Thermo Fisher Scientific) according to the manufacturer's protocol. Both, wash and elution fractions, were freeze-dried and resolved in deuteriumoxide for product confirmation by 1D proton NMR. The product was stored at -20°C. For tracer feeding, a method was used as described earlier (Stegemann et al., 2018) with following modifications: [^{14}C]putrescine was replaced by

[¹⁵N]carboxypyrrolizidine and identification of PA patterns was done with GC-MS according to Stegemann et al. (2019).

6.6 Acknowledgments

This work was supported by the Deutsche Forschungsgemeinschaft (DFG) to D.O.. M.M. was recipient of a German Egyptian Research Long-Term Scholarship (GERLS).

6.7 Supplementary Table

No.	Primer sequence (5' to 3')	purpose
P1	Oligo(dT) (published in (Sievert et al., 2015))	cDNA synthesis
P2	UBQ <i>H. indicum</i> for (published in (Sievert et al., 2015))	qRT-PCR UBQ
P3	UBQ <i>H. indicum</i> rev (published in (Sievert et al., 2015))	qRT-PCR UBQ
P4	HSS <i>H. indicum</i> for (published in (Sievert et al., 2015))	qRT-PCR HSS
P5	HSS <i>H. indicum</i> rev (published in (Sievert et al., 2015))	qRT-PCR HSS
P6	GTCAAGACAAAAATGCAAACCAAAAGAGTG	qRT-PCR HSO for
P7	TCCATTGCTTCATCCAATGATCAATAC	qRT-PCR HSO for (VIGS)
P8	TAATAACGGTCCAACCACGTTTCCT	qRT-PCR HSO rev
P9	ACTATGTCACGAGTTTGAGTGAGC	qRT-PCR HSO rev (VIGS)
P10	CGGCTAACCATTTCTTTCATGTGC	qRT-PCR CuAO2 for
P11	ACTTTCTTGTTTCTCCAGGTTGTAGA	qRT-PCR CuAO2 rev
P12	CATGGGTTAAGCAAAATCGGTCTC	qRT-PCR CuAO3 for
P13	GAAGCATAAAACCGACGTGTTCC	qRT-PCR CuAO3 rev
P14	AACAGAGTCCGTGACATCATCAAA	qRT-PCR CuAO4 for
P15	CTAAAACCCACAGGCTTGTCAGG-	qRT-PCR CuAO4 rev
P16	GGAGGTTTACGGCGCAATTATAG	qRT-PCR CuAO5 for
P17	CTCTTCCTTTTTGATCCATTGCCA	qRT-PCR CuAO5 rev
P18	TTTGACAAGTCGGGCGGTC	qRT-PCR TRV coat protein for (VIGS)
P19	TATTCAGTGCCGCTAGTAACCC	qRT-PCR TRV coat protein rev (VIGS)
P20	TCCATTGCTTCATCCAATGATCAATAC	3'-RACE HSO for
P21	CAACCTATGTGCAATGGATCTTC	5'-RACE CuAO2 GSP1 rev
P22	GCAAGAGAGTGTAGAACCAAGC	5'-RACE CuAO2 GSP2 rev
P23	TAGAACCAAGCCCTCTCTTGG	5'-RACE CuAO2 GSP3 rev

P24	GGGGACAAGTTTGTACAAAAAAGCAGGCTCCACCATGAATTCACCTCTTAAATTTCTCCTC attB1 Kozak Binding region	<i>in planta</i> expression HSO for (C-term Strep tag)
P25	GGGGACCACTTTGTACAAGAAAGCTGGGTCTTATTTTTCGAACTGCGGGTGGCTCCAGCCGCC TCCACTTCACTGGTTGATTG attB2 Strep-Tag II Binding region	<i>in planta</i> expression HSO rev (C-term Strep tag)
P26	GGGGACAAGTTTGTACAAAAAAGCAGGCTCCACCATGGCCTCAACTTCGGAAAAAGCGA attB1 Kozak Binding region	<i>in planta</i> expression CuAO2 for (without tag, C-term Strep tag)
P27	GGGGACCACTTTGTACAAGAAAGCTGGGTCTTATTTTTCGAACTGCGGGTGGCTCCAAGCGCTG AGCTTGGCGATTAACTTGCACC attB2 Strep-Tag II Binding region	<i>in planta</i> expression CuAO2 rev (C-term Strep tag)
P28	GGGGACCACTTTGTACAAGAAAGCTGGGTCTTAGAGCTTGGCGATTAACTTGCACC attB2 Binding region	<i>in planta</i> expression CuAO2 rev (without tag)
P29	GGGGACAAGTTTGTACAAAAAAGCAGGCTCCACCATGGCTAGCTGGAGCCACCCGCAGTTCGAA AAAGGCGGCGCCTCAACTTCGGAAAAAGC attB1 Kozak linker Strep-Tag II spacer Binding region	<i>in planta</i> expression CuAO2 for (N-term Strep tag)
P30	GGGGACCACTTTGTACAAGAAAGCTGGGTCTTAGAGCTTGGCGATTAACT attB2 Binding region	<i>in planta</i> expression CuAO2 rev (N-term Strep tag)
P31	TTTAAGCAACTTTGATTATGTTATTGATTATGAATTCAAGAAAGCAGGC	site-directed mutagenesis HSO T405F for
P32	TAACATAATCAAAGTTGCTTAAAGTTAACACCGTTCTTGCAACAAGGC	site-directed mutagenesis HSO T405F rev
P33	TACGTCTCCCATGACCAAGTGAAGTGGAGTGAAGC BsmBI Binding region	VIGS HSO for
P34	TACGTCTCCTCGACCAAACCTGCAACGACCCA BsmBI Binding region	VIGS HSO rev
P35	TACGTCTCCCATGCGCCAAGCTCTAAAGTAATACATCC BsmBI Binding region	VIGS CuAO2 for
P36	TACGTCTCCTCGACGCAAAACATAACGACATATTAAGCG BsmBI Binding region	VIGS CuAO2 rev

6.8 Supplemental Figures:

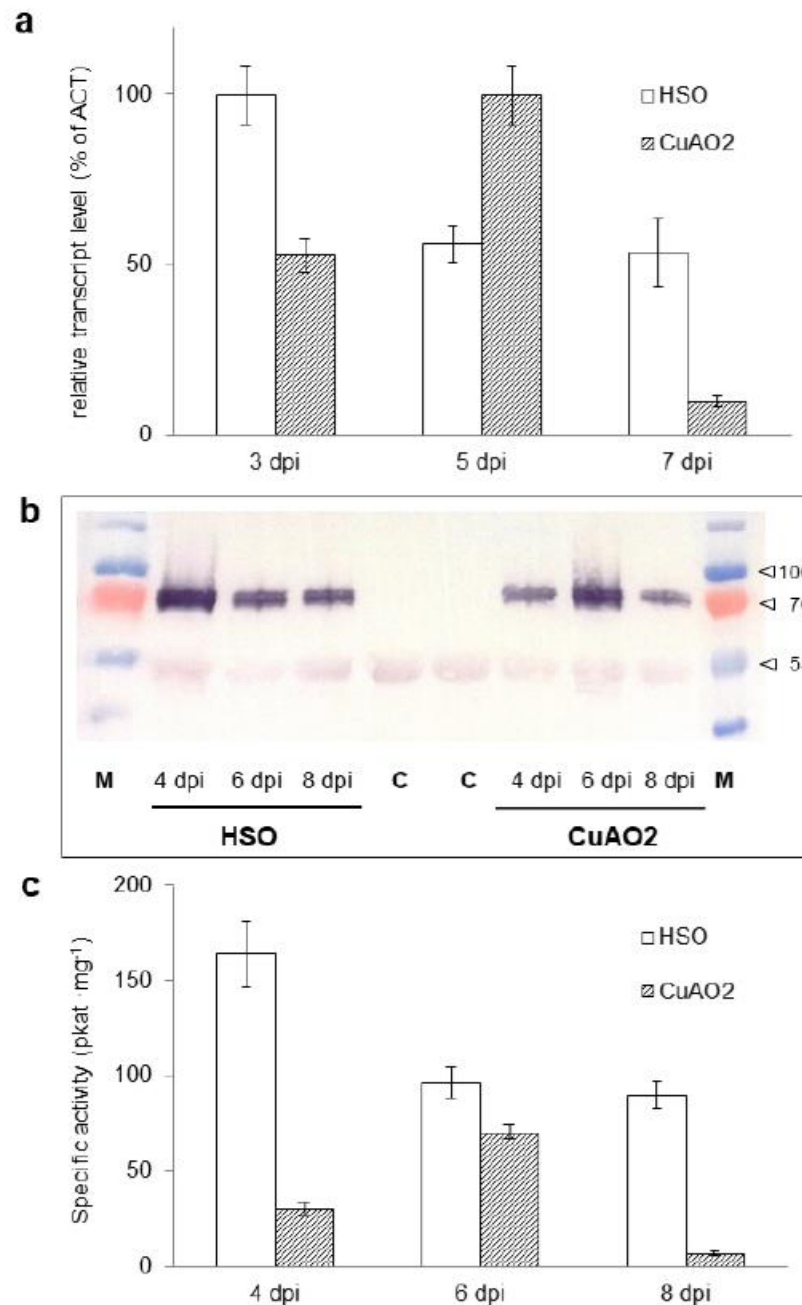


Figure 29: Estimation of expression levels after transient infection of *N. benthamiana* leaves in days after infection (dpi). **a** Transcript levels of HSO and CuAO2 relative to that of actin ($2^{-\Delta\Delta C_t}$ method) at 3, 5, and 7 days after infection. **b** Protein gel blot analysis of HSO and CuAO2 detected with the Strep-Tactin® AP conjugate that binds to the C-terminal Strep®-tag II at 4, 6, and 8 days after infection. M, PageRuler Prestained Protein

ladder (Thermo Scientific); C, Empty vector control. **c** Specific activity of HSO and CuAO2 with 1 mM homospermidine and 1 mM putrescine, respectively. The data in **a** and **c** represent the mean values \pm s.d. for 3 technical replicates.

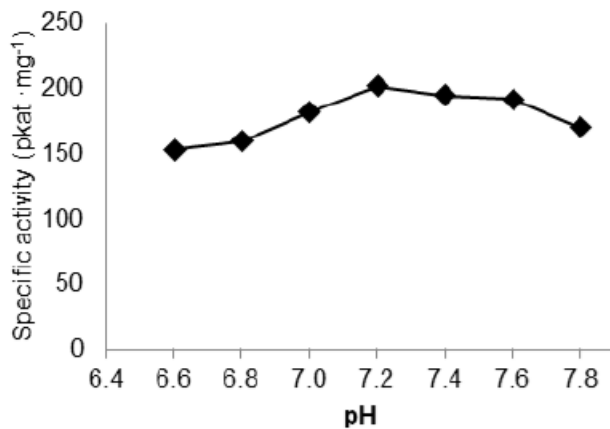


Figure 30: pH-Optimum of HSO. Crude protein extracts of tobacco leaves transiently expressing HSO have been desalted and rebuffered to 30 mM potassium phosphate buffer adjusted to the relevant pH. Assays were incubated with 1 mM homospermidine as substrate.

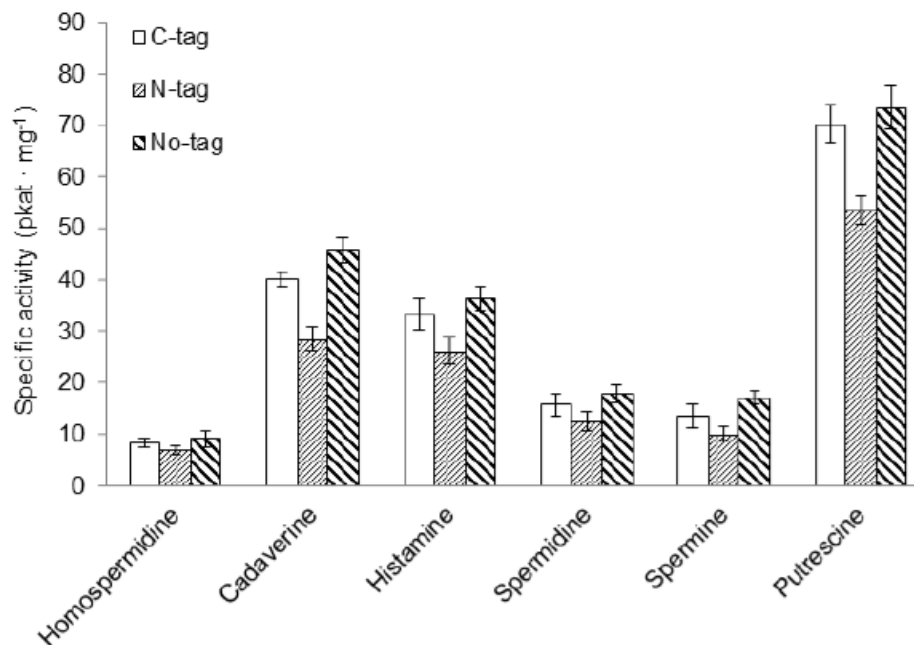


Figure 31: Influence of a Strep-tag II on the activity and substrate specificity of CuAO2. Specific activity of CuAO2 expressed without Strep-tag (No-tag), with N-terminal Strep-Tag II (N-tag), and with C-terminal Strep-tag II (C-tag). Desalted protein extracts of tobacco leaves transiently expressing CuAO2 have been incubated with different polyamines (1 mM each, columns represent the mean of three technical replicates).

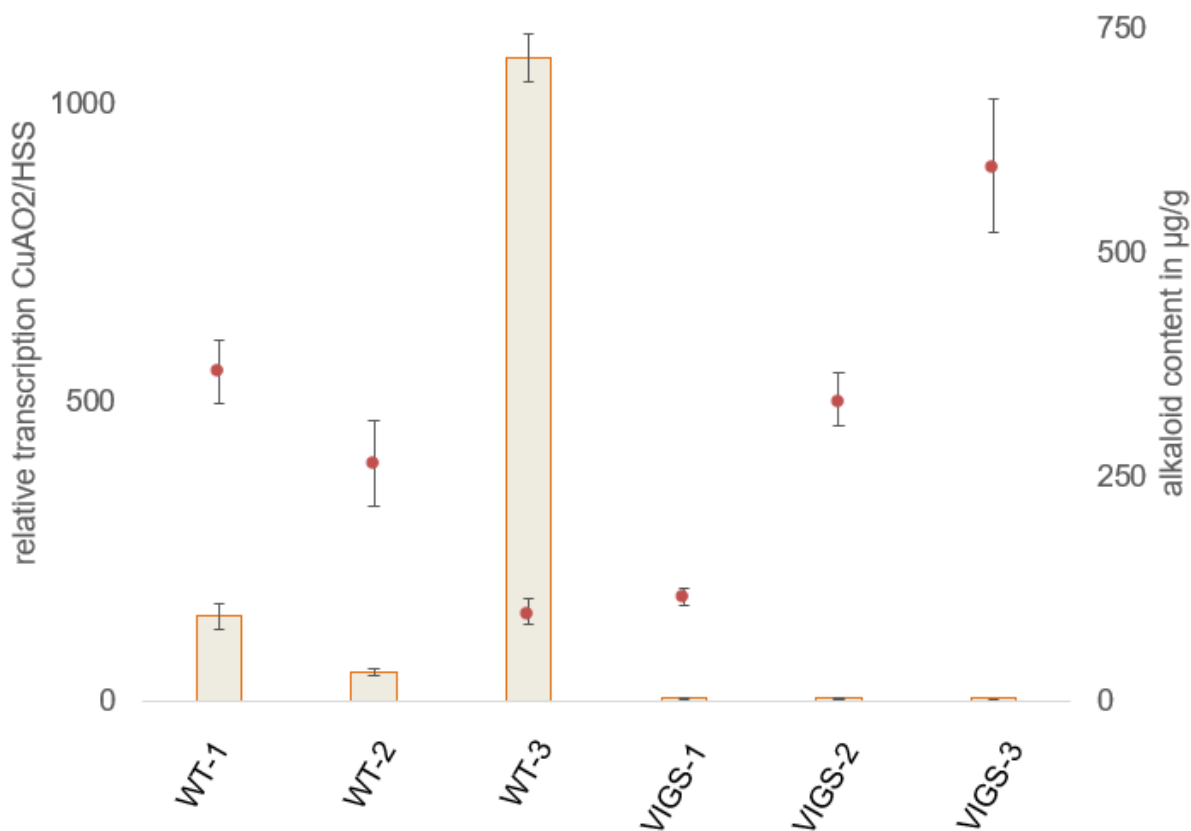


Figure 32: Virus-induced gene silencing analysis of CuAO2 in *H. indicum*. Plants infected with pTRV2-vector construct for CuAO2 have been analyzed in comparison to wild-type plants. Three leaves have been taken per individual and analyzed in triplicate. Each bar represents the mean \pm s.d. of 9 values (that is three technical replicates of three leaves per individual). To compensate for variation in the level of PA biosynthesis in these leaves, HSS transcript levels served as reference. The bars represent the ratio of CuAO2/HSS transcript levels. In addition, the alkaloid content in the analyzed tissue is given. Statistical analyses show that the relative transcript level of the CuAO2 knock-downs were significantly lower than those of the wild-type ($p=0.043$), while PA-levels do not show any significant change ($p=0.204$).

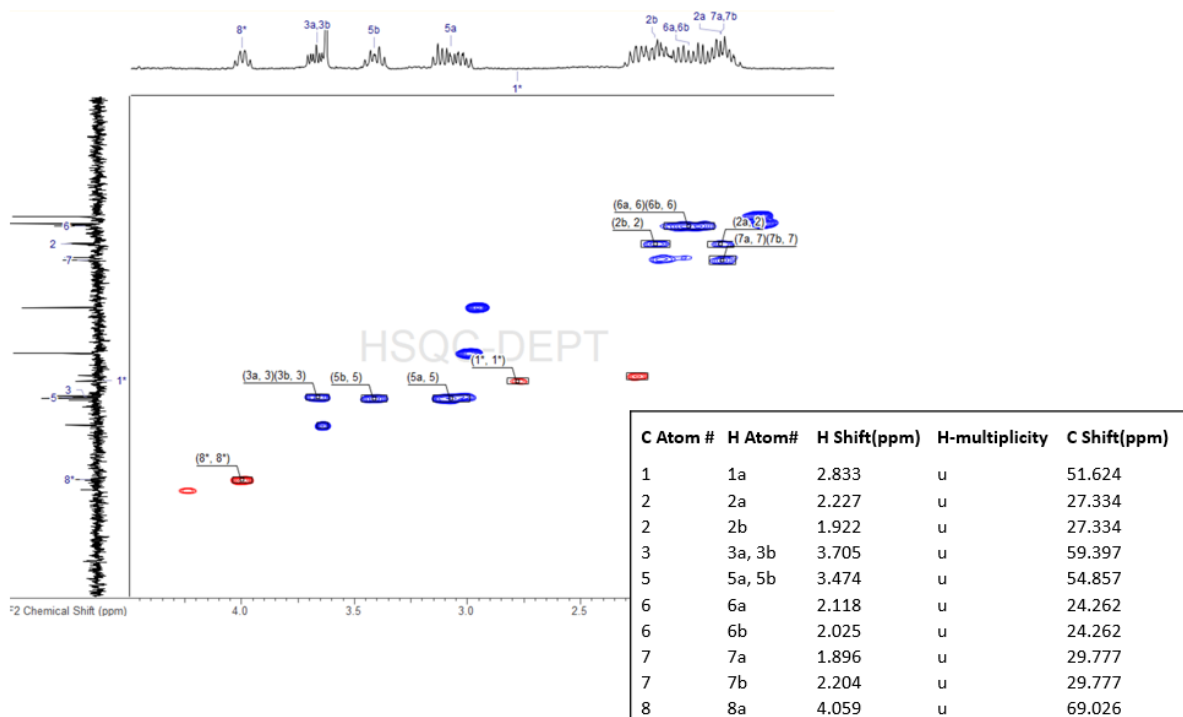


Figure 33 HSQC spectrum of the reaction product of HSO with homospermidine as substrate. The ^{13}C - ^1H correlations are given in detail.

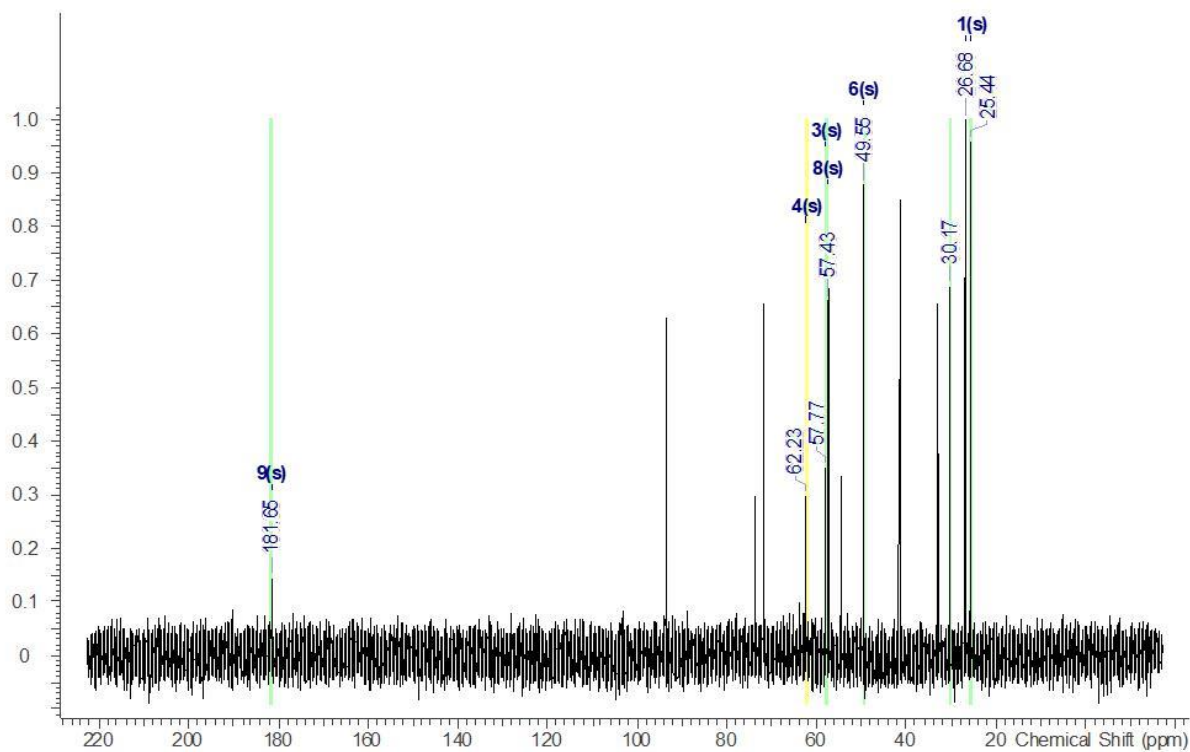


Figure 34: ^{13}C -DEPT spectra of the reaction product of HSO with homospermidine as substrate. The signal at 181.65 ppm indicates the presence of a carboxyl group.

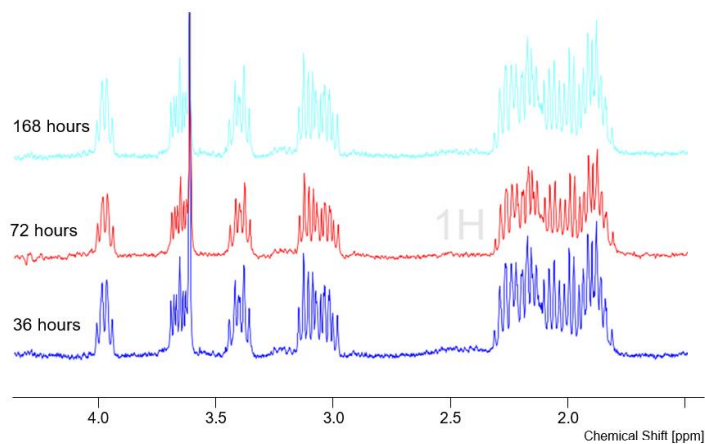


Figure 35: Stability test of 1-carboxypyrrolizidine as reaction product of HSO. 1D proton NMR spectra were recorded after 36, 72 and 168 h of storage at room temperature. No degradation was observed.

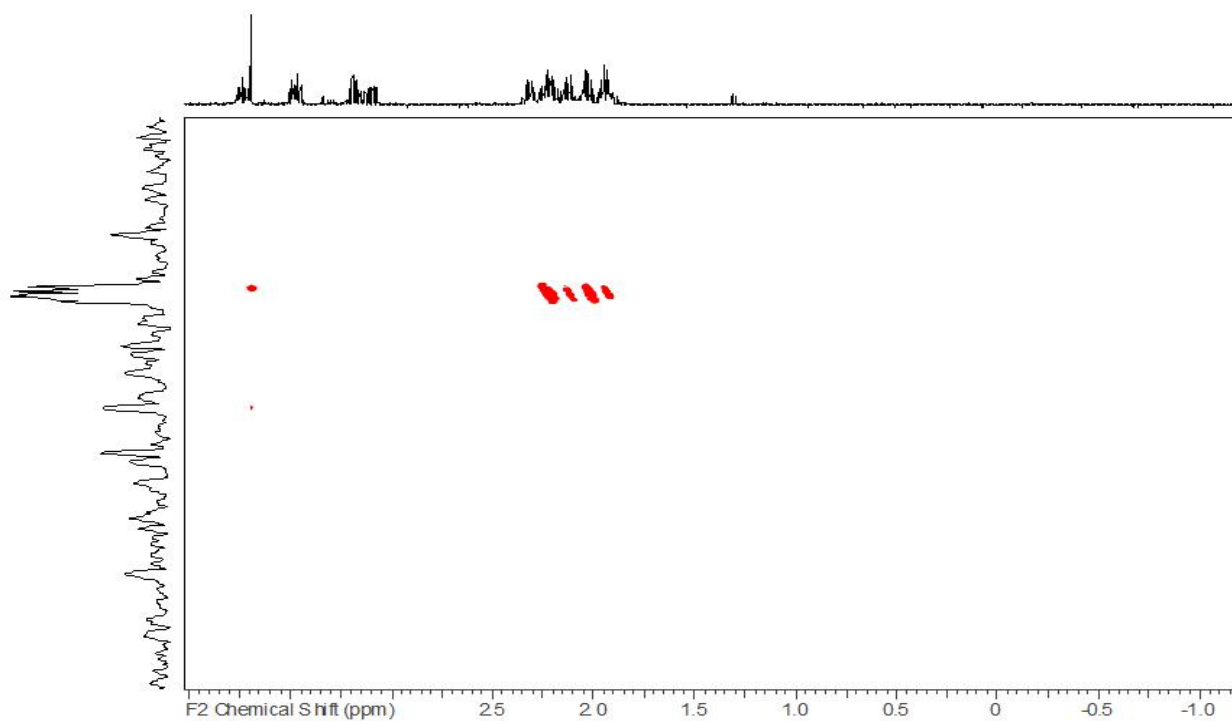


Figure 36: ^{15}N - ^1H HMBC of the reaction product of HSO with fully labelled [^{15}N]homospermidine as substrate confirming the presence of only one ^{15}N as part of the 1-carboxypyrrolizidine.

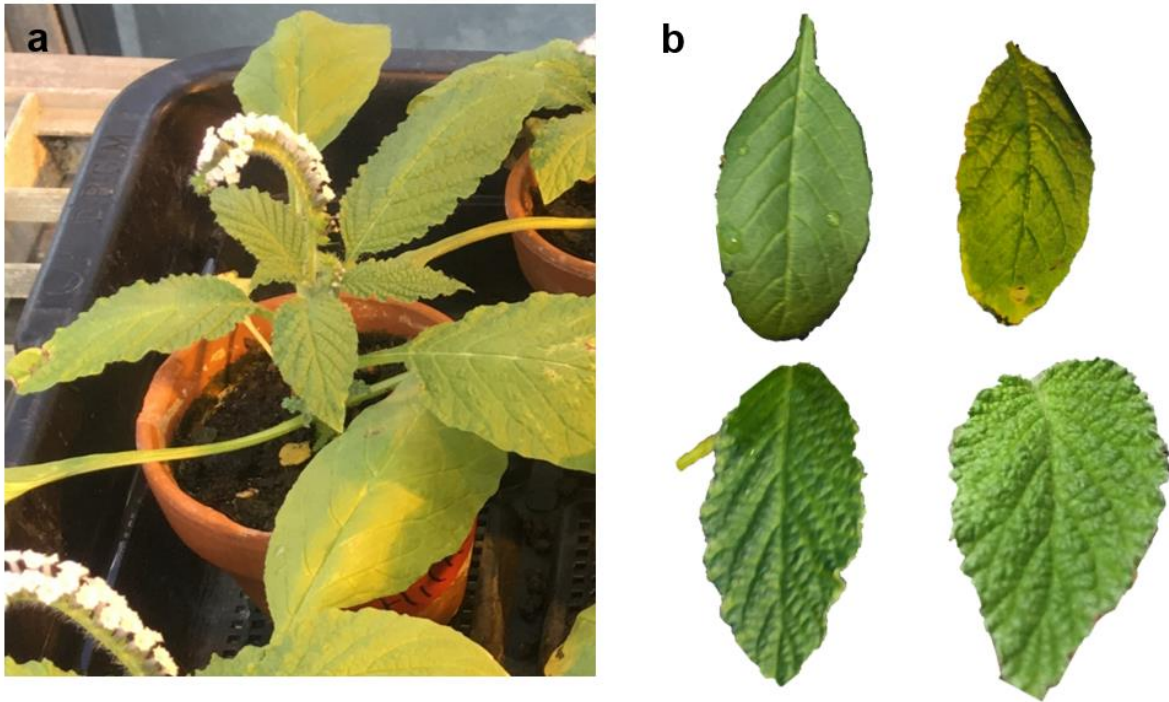


Figure 37: Different leaf morphology of *H. indicum*. The first 4 leaves of a young developing plant show usually an even, unwrinkled surface, while leaves developing later are characterized by a wrinkled surface structure. **a** An *H. indicum* plant cultivated in the greenhouse. **b** Two leaves with an even surface structure (top) and two leaves with the typical wrinkled structure of mature leaves (bottom).

7. Conclusions and General Perspective

The idea for the research project described in this thesis was to identify a further step in PA biosynthesis in a highly variable background of PA levels in species of the Boraginales. Therefore, PA variability with respect to levels of the alkaloids found in the individual plant tissues, the site and the time of synthesis, and a putative co-regulation of genes involved in PA-biosynthesis had to be evaluated.

The main results of this thesis are the following:

- 1.) A second site of PA biosynthesis was identified in common comfrey (*S. officinale*) in young leaves subtending a developing inflorescence.
- 2.) Analysis of flower parts and leaves of one individual revealed surprising intraindividual variability of PA levels. Also HSS transcript levels have been shown to be highly variable suggesting that PA biosynthesis is up- and down-regulated in the analyzed tissues.
- 3.) Referencing transcript levels of gene candidates of PA biosynthesis was suggested as a tool to test these candidates for coexpression with HSS even in a highly variable background.
- 4.) The involvement of a CuAO named homospermidine oxidase (HSO) in the PA biosynthesis was confirmed by coexpression, biochemical characterization, and *in planta* downregulation via VIGS.
- 5.) The reaction product of HSO was identified as 1-carboxypyrrolizidine resulting from double oxidation of homospermidine and providing the backbone structure for the necine base moiety.

7.1 HSO oxidation follows the blueprint of alkaloid biosynthesis

The oxidation of homospermidine by a CuAO is in good agreement with some general aspects of alkaloid biosynthesis (Fig. 3). These are the modification of a polyamine (*i.e.* putrescine/spermidine) and the further oxidation of this modified amine (*i.e.* homospermidine). Special in the case of the biosynthesis of PAs is the

requirement of two oxidations that allow the cyclization process, while almost all other alkaloids just undergo a single amine oxidation to create their core structure.

The elucidation of later steps in PA biosynthesis is challenging. A common pattern of alkaloid biosynthesis described in the introduction (Fig. 3) is best elucidated to the point when amine oxidation by CuAOs is followed by the cyclization that results in specific alkaloid backbones. Neither the pathways of tropane alkaloids, quinolizidine alkaloids, or pyrimidine alkaloids have been elucidated beyond the CuAO step. Here the different pathways may require specific enzymes to build up the complete alkaloid structure Robins (1989) took an educated guess based on the chemical properties and used an alcohol dehydrogenase to transform a putative necine-base precursor into the hydroxymethylpyrrolizidine. Even if this educated guess proves right, there are usually a lot of ADHs in plants. *Arabidopsis thaliana* has been shown to possess more than 9 different ADHs that are involved in secondary metabolism (Kim et al., 2004). Knockdown experiment of possible candidate genes further down the PA pathway could be designed since the VIGS method as described in **Chapter 3** or the RNAi method described recently for comfrey hairy-roots (Kruse et al., 2019) proved to be promising tools.

7.2 Biosynthesis of the necine base moiety

Figure 38 describes a detail of the hypothetical processes involved in homospermidine oxidation and the subsequent formation of the necine base moiety. This data nicely fits to previous work on PA biosynthesis. So the involvement of a CuAO for the oxidation of homospermidine is well in agreement with an experiment with a pea-seedling CuAO that was incubated with homospermidine in a biomimetic experiment over a time period of several days. In this experiment it was shown that a CuAO might be sufficient to yield the pyrrolizidine backbone (Robins, 1989). Even the pyrrolinium ion (Fig. 38, structure **3**) that was shown to be the product of the oxidation of only one of the two primary amino groups of homospermidine, was already confirmed as a possible precursor for PAs (Kelly & Robins, 1988). A possible intermediate of PA biosynthesis, named “metabolite x” was, even though it was not

isolated, described in earlier tracer-feeding experiments to have properties (e.g. high polarity, ionic state) (Frölich, 1996), that nicely match the chemical properties of the structure identified in this thesis as 1-carboxypyrrolizidine.

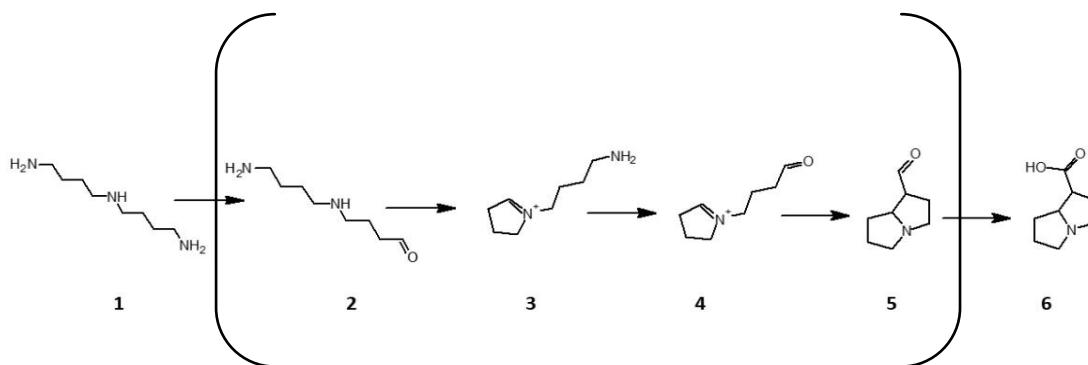


Figure 38: One route of necine backbone biosynthesis in detail (Fig 28 shows also alternative possibilities) - Proposed oxidation process of homospermidine (**1**) by HSO to the monoaldehyde (**2**). After a spontaneous cyclisation process the pyrrolinium ion (**3**) is formed that is further oxidized by the HSO (**4**). Afterwards another spontaneous cyclisation occurs that results in the formation of 1-formylpyrrolizidine (**5**) that is further oxidized to the 1-carboxypyrrolizidine (**6**).

7.3 Unique features of the double oxidation via HSO

Using the amine oxidase of bovine serum, also a CuAO, Houen et al. (2005) were able to show that incubation with homospermidine results in the formation of the pyrrolinium ion. Obviously, this animal-derived CuAO is not able to catalyze the oxidation of the second primary amino group of homospermidine, as it is done by HSO. This might also be one reason, why a necine-base-like structure is not described from animals, even though the occurrence of homospermidine in low levels is described in individual cases (Hamana & Matsuzaki, 1979). This suggests that the oxidation of both primary amino groups is a specific characteristic of HSO and a requirement for the formation of the necine backbone. The fact that a single enzyme is responsible for two successive steps in a biosynthetic route is not completely new

in the field of secondary metabolism. Such a case was already reported for polyketide biosynthesis in *Aspergillus terreus*. There it is reported that double oxidation of a cyclic nonaketide is catalyzed by a cytochrome P450-dependent monooxygenase, named LovA, yielding the monacolin J acid backbone (Barriuso et al., 2011).

7.4 Impact of this study for further research on PA biosynthesis

HSO was shown to be able to catalyze homospermidine at both primary amino groups. This suggests that after the first oxidation an intermediate will be released from the active site, cyclize spontaneously to a monocyclic structure that is then bound again with the other primary amino group by the active site of the HSO. To untangle these two steps of this biochemical conversion is challenging, but might also result in a better understanding about the rate limiting step. Structural analyses of the so-called substrate-channel of HSO in comparison to other HSO might give hints for the specific structural modifications that are responsible for the change in substrate specificity.

Assuming that the relevant intermediate is indeed the pyrrolinium-ion this could be tested as a substrate in comparison to homospermidine to allow a mathematical approach subtracting the conversion-rate of the pyrrolinium-ion from an assay with homospermidine. Such models are normally used for a sequence of coupled enzyme reactions (Easterby, 1981) and could also apply for the HSO-catalyzed reaction. Protocols for the chemical synthesis (Henry A. Kelly & Robins, 1988) and for the enzymatic formation of the pyrrolinium ion (Houen et al., 2005) are described in the literature.

For evolution of HSS it was shown in earlier works that it was recruited by several independent gene duplication events, suggesting that the evolution of PA biosynthesis is convergent in the individual PA-producing plant lineages (Kaltenegger et al., 2013; Reimann et al., 2004). The successful identification of HSO as the enzyme catalyzing the second specific step of PA biosynthesis provides the basis for further research of this pathway. One prominent question is, whether the HSO proves

also to be of polyphyletic origin. Another might be the question, if CuAOs involved in PA biosynthesis of other plant lineages also catalyze the oxidation of both primary amino groups, or whether there are cases, in which two successive amine oxidases might be responsible for this conversion. Also the characterization of the closest relatives of HSO involved in primary metabolism might provide insights about the necessary shifts in substrate specificity in this class of enzyme.

In the literature are some cases described in which plants possess a HSO, but are obviously unable to produce PAs. One such example is the non-PA producing species *Ipomoea alba* (Convolvulaceae) (Kaltenegger et al., 2013). For this species it was postulated that it branched off from other *Ipomoea* species before PA biosynthesis was completely established. Studies on this species could deliver insights into the evolution of the whole PA biosynthetic pathway, as *I. alba* might have not yet developed or lost a specialized HSO capable of oxidizing homospermidine and/or the pyrrolinium-ion.

The product of HSO, the 1-carboxypyrrolizidine, is structurally closely related to another compound found repeatedly in individual plant species, Chysin A, the methylester of 1-carboxypyrrolizidine (i.e. *Arnica montana*, Paßreiter, 1992). Chysin A has two stereocenters, but is always described to occur as one specific stereoisomer. In front of the observation that the *in vitro* reaction of HSO produces 1-carboxypyrrolizidine as a stereomeric mixture, it is not clear whether *in planta* additional factors might push the reaction to only one of the stereoisomers. These could be additional enzymes like isomerases. Chysin A that possesses exactly that stereochemistry that is later not found in the PAs might be interpreted as a detoxification product. Of note, Chysin A is not reported yet in all PA-producing plants, so this idea has to remain most speculative.

Another interesting observation is the occurrence of otonecine-type PAs in specific plant lineages like the Asteraceae and Orchidaceae (Hartmann & Witte, 1995). This type of PA is characterized by a methylated nitrogen within the necine base moiety

that results in a drastic change of the overall structure, i.e. the necine base is monocyclic (Fig. 39).

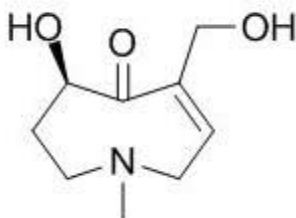


Figure 39: Otonecine, the necine base of otonecine-type pyrrolizidine alkaloids

A first idea that for these structures homospermidine cannot be a substrate and a HSO-like enzyme would not be involved. Examples for different precursors for the same class of alkaloids exist in the literature, e.g. for the biosynthesis of pyrimidine alkaloids like anabasine and nicotine (Watson et al., 1990) (Fig. 3). For PA biosynthesis this idea was discouraged by early tracer-feeding experiments showing retronecine and bicyclic necine bases can be incorporated into otonecine-type PAs (Kelly et al., 1989). For this case the identification and characterization of the enzymes responsible for breaking the bicyclic ring structure via a hydroxylation of the C-8 atom and methylation of the ring-bound nitrogen might characterize a highly developed trait in plant defense, as otonecine-type PAs cannot be detoxified by enzyme systems of insect that adapted to PAs by *N*-oxygenation (Naumann et al., 2002; Sehlmeier et al., 2010; Wang et al., 2012)

The observation that the HSO identified from *H. indicum* possesses an *N*-terminal targeting sequence for the vesicular pathway while HSS is described to be a cytosolic enzyme (Anke et al., 2004) requires further studies on the subcellular localization of PA-biosynthesis. That steps of PA biosynthesis might be localized within specific compartments was postulated earlier, as Böttcher et al. (1993) described PA-producing root cultures of *Senecio vulgaris* to accumulate homospermidine in the presence of the CuAO-inhibitor HEH. After release of this inhibition by transfer of the roots to fresh medium without inhibitor, the accumulated homospermidine was

incorporated exclusively into PAs. No degradation of the accumulated homospermidine was observed in contrast to homospermidine that was fed directly the roots. As similar observation was described by also by another group (Rana & Robins, 1983). If this subcellular localization will be confirmed, e.g. by reporter gene analyses of immunolabelling experiments, a transporter for the transport of homospermidine from the cytosol to the putative vesicles has to be postulated.

Contributions

The majority of the work of Chapter 2 was done by Thomas Stegemann and Lars H. Kruse. His contribution is already mentioned in his thesis, where this part was also published. Thomas Stegemann performed and setup the workflow of the analytical part of the radioactive tracer feeding, concerning sample preparation, HPLC methods and TLC-GC-MS methods.

This part is reflected in **3** where this setup was published in detail that Thomas Stegemann designed with. Thomas Stegemann wrote the manuscript and prepared the figures of Chapter 3 under the guidance of Dietrich Ober.

The presented work in **4** was designed by Thomas Stegemann with the help of Lars H. Kruse and Dietrich Ober. Thomas Stegemann did all experiments and analyses with the technical help of Karina Thoele and Maik Jahnsen. Moritz Brütt performed the microscopy. Lars H. Kruse helped preparing the figures. Data analysis and the interpretation of the results were done by Thomas Stegemann. Dietrich Ober and Thomas Stegemann wrote the manuscript in close cooperation.

The work of **5** was designed by Thomas Stegemann in close cooperation with Dietrich Ober. Thomas Stegemann performed all the experiments with the technical help of Maik Jansohn, the data analysis and the manuscript and figure preparations were done by me.

The research of **6** was designed by Thomas Stegemann, Mahmoud Mohamed and Dietrich Ober. Mahmoud Mohamed and Christian Sievert carried out gene cloning, Mahmoud Mohamed carried out *in planta* expression, enzyme assays, kinetics and site directed mutagenesis. Thomas Stegemann performed *in vivo* isotopic labeling, VIGS, and GC-MS-measurements. Mahmoud Mohamed and Thomas Stegemann performed qRT-PCR, Christian Sievert and Lars Hendrik Kruse conducted the bioinformatics analyses. Ulrich Giessler, Serhat Cicek and Thomas Stegemann did the NMR experiments and Manfred Nimtz carried out microsequencing. Dietrich Ober, Mahmoud Mohamed and Thomas Stegemann wrote the manuscript.

Acknowledgements

I want to deeply thank all my colleagues from the Ober working group for a fantastic time during my work. Nadine, Mahmoud, Britta, Franziska and Annika deserve a mention for creating an utmost friendly and delighting atmosphere. But I want to specially mention Lars H. Kruse as he was not only a coworker always challenging me, but also guiding me towards a successful completion of my thesis. Your help in developing deeper skills in molecular biology is greatly appreciated as well to this day. Dorothe Langel and Elisabeth Kaltenecker also deserve a special mentioning since they always provided an open mind for a scientific discussion and quick logic testing of upcoming theories and experimental designs. Arunraj and Moritz Brütt also are thanked for always showing interest in my work and expanding my horizons by discussion about your own projects. Brigitte and Margret are mentioned for their excellent technical support.

A special place is also reserved for my students. Karina, Felix, Silke, Anna-Lena, Daniel and Maik I can just hope that the experience for you working under my guidance was as exciting as it was for me guiding you through your challenging projects.

Also, many thanks to the Zidorn working group of the Kiel institute of pharmacy. The constant scientific discussion about my and their work made my days working in the lab a delight. Serhat, Frederike and Johanna it was a pleasure to work with you and I hope this will continue in the future. Prof. Dr. Christian Zidorn, thanks for the trust and working lunches during the last years that encouraged my scientific development. Dr. Ulrich Giresser is also mentioned for his help regarding NMR-experiments.

Of course, the biggest credit to my work deserves my advisor Prof. Dr. Ober as he not only gave me the opportunity to create this work, he also kept the perfect balance between freedom and control for me to develop my professional skills and scientific mind.

References

- Abd El-Mawla, A. M. A. (2010). Effect of certain elicitors on production of pyrrolizidine alkaloids in hairy root cultures of *Echium rauwolfii*. *Die Pharmazie-An International Journal of Pharmaceutical Sciences*, *65*(3), 224–226.
- Abdelhady, M. I. S., Beuerle, T., & Ober, D. (2009). Homospermidine in transgenic tobacco results in considerably reduced spermidine levels but is not converted to pyrrolizidine alkaloid precursors. *Plant Molecular Biology*, *71*(1–2), 145–155. <https://doi.org/10.1007/s11103-009-9514-x>
- Alcázar, R., Altabella, T., Marco, F., Bortolotti, C., Reymond, M., Koncz, C., Carrasco, P., & Tiburcio, A. F. (2010). Polyamines: Molecules with regulatory functions in plant abiotic stress tolerance. *Planta*, *231*(6), 1237–1249.
- Allain, C. C., Poon, L. S., Chan, C. S., Richmond, W., & Fu, P. C. (1974). Enzymatic determination of total serum cholesterol. *Clinical Chemistry*, *20*(4), 470–475.
- Allgaier, C., & Franz, S. (2015). Risk assessment on the use of herbal medicinal products containing pyrrolizidine alkaloids. *Regulatory Toxicology and Pharmacology*, *73*(2), 494–500.
- Almagro Armenteros, J. J., Tsirigos, K. D., Sønderby, C. K., Petersen, T. N., Winther, O., Brunak, S., von Heijne, G., & Nielsen, H. (2019). SignalP 5.0 improves signal peptide predictions using deep neural networks. *Nature Biotechnology*, *37*(4), 420–423. <https://doi.org/10.1038/s41587-019-0036-z>
- Angelini, R., Cona, A., Federico, R., Fincato, P., Tavladoraki, P., & Tisi, A. (2010). Plant amine oxidases “on the move”: An update. *Plant Physiology and Biochemistry*, *48*(7), 560–564. <https://doi.org/10.1016/j.plaphy.2010.02.001>
- Aniszewski, T. (2007). *Alkaloids - Secrets of Life: Alkaloid Chemistry, Biological Significance, Applications and Ecological Role*. Elsevier.

- Anke, S., Gondé, D., Kaltenecker, E., Hänsch, R., Theuring, C., & Ober, D. (2008). Pyrrolizidine alkaloid biosynthesis in *Phalaenopsis* orchids: Developmental expression of alkaloid-specific homospermidine synthase in root tips and young flower buds. *Plant Physiology*, *148*(2), 751–760.
- Anke, S., Niemüller, D., Moll, S., Hänsch, R., & Ober, D. (2004). Polyphyletic origin of pyrrolizidine alkaloids within the Asteraceae. Evidence from differential tissue expression of homospermidine synthase. *Plant Physiology*, *136*(4), 4037–4047.
- Ballas, S. K., Mohandas, N., Marton, L. J., & Shohet, S. B. (1983). Stabilization of erythrocyte membranes by polyamines. *Proceedings of the National Academy of Sciences*, *80*(7), 1942–1946.
- Barriuso, J., Nguyen, D. T., Li, J. W.-H., Roberts, J. N., MacNevin, G., Chaytor, J. L., Marcus, S. L., Vederas, J. C., & Ro, D.-K. (2011). Double oxidation of the cyclic nonaketide dihydromonacolin L to monacolin J by a single cytochrome P450 monooxygenase, LovA. *Journal of the American Chemical Society*, *133*(21), 8078–8081.
- Besford, R. T., Richardson, C. M., Campos, J. L., & Tiburcio, A. F. (1993). Effect of polyamines on stabilization of molecular complexes in thylakoid membranes of osmotically stressed oat leaves. *Planta*, *189*(2), 201–206.
- Betteridge, K., Cao, Y., & Colegate, S. M. (2005). Improved method for extraction and LC-MS analysis of pyrrolizidine alkaloids and their N-oxides in honey: Application to *Echium vulgare* honeys. *Journal of Agricultural and Food Chemistry*, *53*(6), 1894–1902.
- Bird, D. A., Franceschi, V. R., & Facchini, P. J. (2003). A tale of three cell types: Alkaloid biosynthesis is localized to sieve elements in opium poppy. *The Plant Cell*, *15*(11), 2626–2635.
- Boppré, M., Colegate, S. M., Edgar, J. A., & Fischer, O. W. (2008). Hepatotoxic pyrrolizidine alkaloids in pollen and drying-related implications for commercial processing of bee pollen. *Journal of Agricultural and Food Chemistry*, *56*(14), 5662–5672.
- Böttcher, F., Adolph, R.-D., & Hartmann, T. (1993). Homospermidine synthase, the first pathway-specific enzyme in pyrrolizidine alkaloid biosynthesis. *Phytochemistry*, *32*(3), 679–689.

- Böttcher, F., Ober, D., & Hartmann, T. (1994). Biosynthesis of pyrrolizidine alkaloids: Putrescine and spermidine are essential substrates of enzymatic homospermidine formation. *Canadian Journal of Chemistry*, *72*(1), 80–85.
- Boyce, S., Tipton, K. F., O'Sullivan, M. I., Davey, G. P., Gildea, M. M., McDonald, A. G., Olivieri, A., & O'Sullivan, J. (2009). Nomenclature and potential functions of copper amine oxidases. *Floris G, MondovìB (Eds) Copper Amine Oxidases. CRC Press, Boca Raton*, 5–17.
- Bradford, M. M. (1976). A rapid and sensitive method for the quantitation of microgram quantities of protein utilizing the principle of protein-dye binding. *Analytical Biochemistry*, *72*, 248–254. <https://doi.org/10.1006/abio.1976.9999>
- Brauchli, J., Lüthy, J., Zweifel, U., & Schlatter, C. (1982). Pyrrolizidine alkaloids from *Symphytum officinale* L. and their percutaneous absorption in rats. *Experientia*, *38*(9), 1085–1087.
- Broderick, S. R., & Jones, M. L. (2014). An Optimized Protocol to Increase Virus-Induced Gene Silencing Efficiency and Minimize Viral Symptoms in *Petunia*. *Plant Molecular Biology Reporter*, *32*, 219–233. <https://doi.org/10.1007/s11105-013-0647-3>
- Broghammer, A., Krusell, L., Blaise, M., Sauer, J., Sullivan, J. T., Maolanon, N., Vinther, M., Lorentzen, A., Madsen, E. B., Jensen, K. J., Roepstorff, P., Thirup, S., Ronson, C. W., Thygesen, M. B., & Stougaard, J. (2012). Legume receptors perceive the rhizobial lipochitin oligosaccharide signal molecules by direct binding. *Proceedings of the National Academy of Sciences of the United States of America*, *109*(34), 13859–13864. <https://doi.org/10.1073/pnas.1205171109>
- Bufler, U., Seufert, G., & Jüttner, F. (1990). Monoterpene patterns of different tissues and plant parts of Norway spruce (*Picea abies* L. Karst.). *Environmental Pollution*, *68*(3–4), 367–375.
- Burlat, V., Oudin, A., Courtois, M., Rideau, M., & St-Pierre, B. (2004). Co-expression of three MEP pathway genes and geraniol 10-hydroxylase in internal phloem parenchyma of *Catharanthus roseus* implicates multicellular translocation of intermediates during the biosynthesis of monoterpene indole alkaloids and isoprenoid-derived primary metabolites. *The Plant Journal*, *38*(1), 131–141.

- Castro, S., Silveira, P., & Navarro, L. (2008). Consequences of nectar robbing for the fitness of a threatened plant species. *Plant Ecology*, *199*(2), 201–208.
- Catalfamo, J. L., Martin, W. B., & Birecka, H. (1982). Accumulation of alkaloids and their necines in *Heliotropium curassavicum*, *H. spathulatum* and *H. indicum*. *Phytochemistry*, *21*(11), 2669–2675.
[https://doi.org/10.1016/0031-9422\(82\)83096-3](https://doi.org/10.1016/0031-9422(82)83096-3)
- Chang, C. M., Klema, V. J., Johnson, B. J., Mure, M., Klinman, J. P., & Wilmot, C. M. (2010). Kinetic and structural analysis of substrate specificity in two copper amine oxidases from *Hansenula polymorpha*. *Biochemistry*, *49*(11), 2540–2550.
- Chauhan, J. S., Rao, A., & Raghava, G. P. S. (2013). In silico platform for prediction of N-, O- and C-glycosites in eukaryotic protein sequences. *PLoS One*, *8*(6), e67008.
<https://doi.org/10.1371/journal.pone.0067008>
- Cheng, A.-X., Lou, Y.-G., Mao, Y.-B., Lu, S., Wang, L.-J., & Chen, X.-Y. (2007). Plant terpenoids: Biosynthesis and ecological functions. *Journal of Integrative Plant Biology*, *49*(2), 179–186.
- Colegate, S. M., Edgar, J. A., Knill, A. M., & Lee, S. T. (2005). Solid-phase extraction and HPLC-MS profiling of pyrrolizidine alkaloids and their N-oxides: A case study of *Echium plantagineum*. *Phytochemical Analysis: An International Journal of Plant Chemical and Biochemical Techniques*, *16*(2), 108–119.
- Cona, A., Rea, G., Angelini, R., Federico, R., & Tavladoraki, P. (2006). Functions of amine oxidases in plant development and defence. *Trends in Plant Science*, *11*(2), 80–88.
- Conant, G. C., & Wolfe, K. H. (2008). Turning a hobby into a job: How duplicated genes find new functions. *Nature Reviews. Genetics*, *9*(12), 938–950. <https://doi.org/10.1038/nrg2482>
- Cordell, G. A. (2013). Fifty years of alkaloid biosynthesis in Phytochemistry. *Phytochemistry*, *91*, 29–51.
- Couet, C. E., Crews, C., & Hanley, A. B. (1996). Analysis, separation, and bioassay of pyrrolizidine alkaloids from comfrey (*Symphytum officinale*). *Natural Toxins*, *4*(4), 163–167.

- Cramer, L., Schiebel, H.-M., Ernst, L., & Beuerle, T. (2013). Pyrrolizidine alkaloids in the food chain: Development, validation, and application of a new HPLC-ESI-MS/MS sum parameter method. *Journal of Agricultural and Food Chemistry*, *61*(47), 11382–11391.
- Denholm, A. A., Kelly, H. A., & Robins, D. J. (1991). Pyrrolizidine alkaloid biosynthesis. Synthesis of N-([4-¹⁴C]-4-aminobutyl)-1,2-didehydropyrrolidinium and its incorporation into different pyrrolizidine bases (necines). *Journal of the Chemical Society, Perkin Transactions 1*, *8*, 2003–2007. <https://doi.org/10.1039/P19910002003>
- Depristo, M. A. (2007). The subtle benefits of being promiscuous: Adaptive evolution potentiated by enzyme promiscuity. *HFSP Journal*, *1*(2), 94–98. <https://doi.org/10.2976/1.2754665>
- Dinesh-Kumar, S. P., Anandalakshmi, R., Marathe, R., Schiff, M., & Liu, Y. (2003). Virus-induced gene silencing. *Methods in Molecular Biology (Clifton, N.J.)*, *236*, 287–294. <https://doi.org/10.1385/1-59259-413-1:287>
- Easterby, J. S. (1981). A generalized theory of the transition time for sequential enzyme reactions. *Biochemical Journal*, *199*(1), 155–161. <https://doi.org/10.1042/bj1990155>
- Evans, P. T., & Malmberg, R. L. (1989). Do polyamines have roles in plant development? *Annual Review of Plant Biology*, *40*(1), 235–269.
- Facchini, P. J., & St-Pierre, B. (2005). Synthesis and trafficking of alkaloid biosynthetic enzymes. *Current Opinion in Plant Biology*, *8*(6), 657–666.
- Franc, V., Řehulka, P., Medda, R., Padiglia, A., Floris, G., & Šebela, M. (2013). Analysis of the glycosylation pattern of plant copper amine oxidases by MALDI-TOF/TOF MS coupled to a manual chromatographic separation of glycans and glycopeptides. *Electrophoresis*, *34*(16), 2357–2367. <https://doi.org/10.1002/elps.201200622>
- Fraudentali, I., Ghuge, S. A., Carucci, A., Tavladoraki, P., Angelini, R., Cona, A., & Rodrigues-Pousada, R. A. (2019). The Copper Amine Oxidase AtCuAO δ Participates in Abscisic Acid-Induced Stomatal Closure in Arabidopsis. *Plants*, *8*(6), 183.

- Frölich, C. (1996). *Vorkommen, Verteilung und Biosynthese von Pyrrolizidinalkaloiden in Boraginaceae und Orchidaceae*. Braunschweig, Techn. Univ., Diss.
- Frölich, C., Hartmann, T., & Ober, D. (2006). Tissue distribution and biosynthesis of 1, 2-saturated pyrrolizidine alkaloids in *Phalaenopsis* hybrids (Orchidaceae). *Phytochemistry*, *67*(14), 1493–1502.
- Frölich, C., Ober, D., & Hartmann, T. (2007). Tissue distribution, core biosynthesis and diversification of pyrrolizidine alkaloids of the lycopsamine type in three Boraginaceae species. *Phytochemistry*, *68*(7), 1026–1037.
- Fu, P. P., Xia, Q., Lin, G., & Chou, M. W. (2004). Pyrrolizidine Alkaloids—Genotoxicity, Metabolism Enzymes, Metabolic Activation, and Mechanisms. *Drug Metabolism Reviews*, *36*(1), 1–55.
<https://doi.org/10.1081/DMR-120028426>
- Fujita, H., Menezes, J. C. J. M. D. S., Santos, S. M., Yokota, S., Kamat, S. P., Cavaleiro, J. A. S., Motokawa, T., Kato, T., Mochizuki, M., Fujiwara, T., Fujii, Y., & Tanaka, Y. (2014). Inulavosin and its benzo-derivatives, melanogenesis inhibitors, target the copper loading mechanism to the active site of tyrosinase. *Pigment Cell & Melanoma Research*, *27*(3), 376–386.
<https://doi.org/10.1111/pcmr.12225>
- Geldner, N. (2013). The endodermis. *Annual Review of Plant Biology*, *64*, 531–558.
- Ge-Ling, Z., Riedl, H., & Kamelin, R. (n.d.). Boraginaceae. In *Flora of China: Gentianaceae through Boraginaceae* (Vol. 16, pp. 329–427).
- Gerdes, H. J., & Leistner, E. (1979). Stereochemistry of reactions catalysed by l-lysine decarboxylase and diamine oxidase. *Phytochemistry*, *18*(5), 771–775. [https://doi.org/10.1016/0031-9422\(79\)80011-4](https://doi.org/10.1016/0031-9422(79)80011-4)
- Gill, S. S., & Tuteja, N. (2010). Polyamines and abiotic stress tolerance in plants. *Plant Signaling & Behavior*, *5*(1), 26–33. <https://doi.org/10.4161/psb.5.1.10291>
- Gomez-Arroyo, J. G., Farkas, L., Alhussaini, A. A., Farkas, D., Kraskauskas, D., Voelkel, N. F., & Bogaard, H. J. (2011). The monocrotaline model of pulmonary hypertension in perspective.

- American Journal of Physiology-Lung Cellular and Molecular Physiology*, 302(4), L363–L369.
<https://doi.org/10.1152/ajplung.00212.2011>
- Gong, B., & Zhang, G. (2014). Interactions between plants and herbivores: A review of plant defense. *Acta Ecologica Sinica*, 34(6), 325–336. <https://doi.org/10.1016/j.chnaes.2013.07.010>
- Groß, F., Rudolf, E.-E., Thiele, B., Durner, J., & Astier, J. (2017). Copper amine oxidase 8 regulates arginine-dependent nitric oxide production in *Arabidopsis thaliana*. *Journal of Experimental Botany*, 68(9), 2149–2162.
- Grotewold, E. (2005). Plant metabolic diversity: A regulatory perspective. *Trends in Plant Science*, 10(2), 57–62. <https://doi.org/10.1016/j.tplants.2004.12.009>
- Grue-Sorensen, G., & Spenser, I. D. (1983). Deuterium nuclear magnetic resonance spectroscopy as a probe of the stereochemistry of biosynthetic reactions: The biosynthesis of retronecine. *Journal of the American Chemical Society*, 105(25), 7401–7404.
- Guss, J. M., Zanotti, G., & Salminen, T. A. (2009). Copper amine oxidase crystal structures. *Copper Amine Oxidases: Structures, Catalytic Mechanisms and Role in Pathophysiology*, 119–141.
- Habermehl, G., Hammann, P., Krebs, H. C., & Ternes, W. (2008). *Naturstoffchemie: Eine Einführung*. Springer-Verlag.
- Hamana, K., & Matsuzaki, S. (1979). Occurrence of sym-homosphermidine in the Japanese newt, *Cynops pyrrhogaster*. *FEBS Letters*, 99(2), 325–328.
- Hare, J. F., & Eisner, T. (1993). Pyrrolizidine alkaloid deters ant predators of *Utetheisa ornatrix* eggs: Effects of alkaloid concentration, oxidation state, and prior exposure of ants to alkaloid-laden prey. *Oecologia*, 96(1), 9–18. <https://doi.org/10.1007/BF00318024>
- Hartmann, T. (1999). Chemical ecology of pyrrolizidine alkaloids. In *Planta* (Vol. 207, pp. 483–495). Springer; JSTOR. <https://www.jstor.org/stable/23385595>
- Hartmann, T. (2007). From waste products to ecochemicals: Fifty years research of plant secondary metabolism. *Phytochemistry*, 68(22–24), 2831–2846.
<https://doi.org/10.1016/j.phytochem.2007.09.017>

- Hartmann, T. (2008). The lost origin of chemical ecology in the late 19th century. *Proceedings of the National Academy of Sciences*, *105*(12), 4541–4546. <https://doi.org/10.1073/pnas.0709231105>
- Hartmann, T., Ehmke, A., Eilert, U., von Borstel, K., & Theuring, C. (1989). Sites of synthesis, translocation and accumulation of pyrrolizidine alkaloid N-oxides in *Senecio vulgaris* L. *Planta*, *177*(1), 98–107. <https://doi.org/10.1007/BF00392159>
- Hartmann, T., & Ober, D. (2000). Biosynthesis and metabolism of pyrrolizidine alkaloids in plants and specialized insect herbivores. In *Biosynthesis* (pp. 207–243). Springer.
- Hartmann, T., & Ober, D. (2008). Defense by pyrrolizidine alkaloids: Developed by plants and recruited by insects. In *Induced plant resistance to herbivory* (pp. 213–231). Springer.
- Hartmann, T., & Witte, L. (1995). Chapter Four—Chemistry, Biology and Chemoecology of the Pyrrolizidine Alkaloids. In S. W. Pelletier (Ed.), *Alkaloids: Chemical and Biological Perspectives* (Vol. 9, pp. 155–233). Pergamon. <https://doi.org/10.1016/B978-0-08-042089-9.50011-5>
- Hartmann, T., & Zimmer, M. (1986). Organ-specific Distribution and Accumulation of Pyrrolizidine Alkaloids during the Life History of two Annual *Senecio* Species. *Journal of Plant Physiology*, *122*(1), 67–80. [https://doi.org/10.1016/S0176-1617\(86\)80085-2](https://doi.org/10.1016/S0176-1617(86)80085-2)
- Hashimoto, T., Mitani, A., & Yamada, Y. (1990). Diamine Oxidase from Cultured Roots of *Hyoscyamus niger*: Its Function in Tropane Alkaloid Biosynthesis. *Plant Physiology*, *93*(1), 216–221. <https://doi.org/10.1104/pp.93.1.216>
- Heim, W. G., Sykes, K. A., Hildreth, S. B., Sun, J., Lu, R.-H., & Jelesko, J. G. (2007). Cloning and characterization of a *Nicotiana tabacum* methylputrescine oxidase transcript. *Phytochemistry*, *68*(4), 454–463. <https://doi.org/10.1016/j.phytochem.2006.11.003>
- Holt, A., Smith, D. J., Cendron, L., Zanotti, G., Rigo, A., & Di Paolo, M. L. (2008). Multiple binding sites for substrates and modulators of semicarbazide-sensitive amine oxidases: Kinetic consequences. *Molecular Pharmacology*, *73*(2), 525–538. <https://doi.org/10.1124/mol.107.040964>

- Houen, G., Struve, C., Søndergaard, R., Friis, T., Anthoni, U., Nielsen, P. H., Christophersen, C., Petersen, B. O., & Duus, J. Ø. (2005). Substrate specificity of the bovine serum amine oxidase and in situ characterisation of aminoaldehydes by NMR spectroscopy. *Bioorganic & Medicinal Chemistry*, *13*(11), 3783–3796. <https://doi.org/10.1016/j.bmc.2005.03.020>
- Huxtable, R. J. (1990). Activation and pulmonary toxicity of pyrrolizidine alkaloids. *Pharmacology & Therapeutics*, *47*(3), 371–389. [https://doi.org/10.1016/0163-7258\(90\)90063-8](https://doi.org/10.1016/0163-7258(90)90063-8)
- Ignesti, G. (2003). Equations of substrate-inhibition kinetics applied to pig kidney diamine oxidase (DAO, E.C. 1.4.3.6). *Journal of Enzyme Inhibition and Medicinal Chemistry*, *18*(6), 463–473. <https://doi.org/10.1080/14756360310001605543>
- Irmer, S., Podzun, N., Langel, D., Heidemann, F., Kaltenecker, E., Schemmerling, B., Geilfus, C.-M., Zörb, C., & Ober, D. (2015). New aspect of plant–rhizobia interaction: Alkaloid biosynthesis in *Crotalaria* depends on nodulation. *Proceedings of the National Academy of Sciences*, *112*(13), 4164–4169. <https://doi.org/10.1073/pnas.1423457112>
- Irwin, R. E., & Maloof, J. E. (2002). Variation in nectar robbing over time, space, and species. *Oecologia*, *133*(4), 525–533. <https://doi.org/10.1007/s00442-002-1060-z>
- Iyengar, V. K., & Eisner, T. (1999). Female choice increases offspring fitness in an arctiid moth (*Utetheisa ornatrix*). *Proceedings of the National Academy of Sciences*, *96*(26), 15013–15016. <https://doi.org/10.1073/pnas.96.26.15013>
- Janes, S. M., Palcic, M. M., Scaman, C. H., Smith, A. J., Brown, D. E., Dooley, D. M., Mure, M., & Klinman, J. P. (1992). Identification of topaquinone and its consensus sequence in copper amine oxidases. *Biochemistry*, *31*(48), 12147–12154. <https://doi.org/10.1021/bi00163a025>
- Jenett-Siems, K., Kaloga, M., & Eich, E. (1993). Ipangulines, the first pyrrolizidine alkaloids from the convolvulaceae. *Phytochemistry*, *34*(2), 437–440. [https://doi.org/10.1016/0031-9422\(93\)80025-N](https://doi.org/10.1016/0031-9422(93)80025-N)
- Johnson, A. E., Molyneux, R. J., & Merrill, G. B. (1985). Chemistry of toxic range plants. Variation in pyrrolizidine alkaloid content of *Senecio*, *Amsinckia*, and *Crotalaria* species. *Journal of Agricultural and Food Chemistry*, *33*(1), 50–55. <https://doi.org/10.1021/jf00061a015>

- Johnson, B. J., Cohen, J., Welford, R. W., Pearson, A. R., Schulten, K., Klinman, J. P., & Wilmot, C. M. (2007). Exploring Molecular Oxygen Pathways in *Hansenula polymorpha* Copper-containing Amine Oxidase. *Journal of Biological Chemistry*, *282*(24), 17767–17776.
<https://doi.org/10.1074/jbc.M701308200>
- Kakar, F., Akbarian, Z., Leslie, T., Mustafa, M. L., Watson, J., van Egmond, H. P., Omar, M. F., & Mofleh, J. (2010). *An Outbreak of Hepatic Veno-Occlusive Disease in Western Afghanistan Associated with Exposure to Wheat Flour Contaminated with Pyrrolizidine Alkaloids* [Research Article]. *Journal of Toxicology; Hindawi*. <https://doi.org/10.1155/2010/313280>
- Kaltenegger, E., Eich, E., & Ober, D. (2013). Evolution of homospermidine synthase in the convulvulaceae: A story of gene duplication, gene loss, and periods of various selection pressures. *The Plant Cell*, *25*(4), 1213–1227. <https://doi.org/10.1105/tpc.113.109744>
- Kanagarajan, S., Muthusamy, S., Gliszczynska, A., Lundgren, A., & Brodelius, P. E. (2012). Functional expression and characterization of sesquiterpene synthases from *Artemisia annua* L. using transient expression system in *Nicotiana benthamiana*. *Plant Cell Reports*, *31*(7), 1309–1319.
<https://doi.org/10.1007/s00299-012-1250-z>
- Kanegae, T., Kajiya, H., Amano, Y., Hashimoto, T., & Yamada, Y. (1994). Species-Dependent Expression of the Hyoscyamine 6[beta]-Hydroxylase Gene in the Pericycle. *Plant Physiology*, *105*(2), 483–490. <https://doi.org/10.1104/pp.105.2.483>
- Karimi, M., Depicker, A., & Hilson, P. (2007). Recombinational Cloning with Plant Gateway Vectors. *Plant Physiology*, *145*(4), 1144–1154. <https://doi.org/10.1104/pp.107.106989>
- Katoh, A., Shoji, T., & Hashimoto, T. (2007). Molecular cloning of N-methylputrescine oxidase from tobacco. *Plant & Cell Physiology*, *48*(3), 550–554. <https://doi.org/10.1093/pcp/pcm018>
- Keller, M. A., Piedrafita, G., & Ralser, M. (2015). The widespread role of non-enzymatic reactions in cellular metabolism. *Current Opinion in Biotechnology*, *34*, 153–161.
<https://doi.org/10.1016/j.copbio.2014.12.020>

- Kelly, H. A., Kunec, E. K., Rodgers, M., & Robins, D. J. (1989). Biosynthesis of the seco-pyrrolizidine base otonecine. *Biosynthesis of the Seco-Pyrrolizidine Base Otonecine*, 11, 358–359.
- Kelly, Henry A., & Robins, D. J. (1988). Evidence for an immonium ion intermediate in pyrrolizidine alkaloid biosynthesis. *Journal of the Chemical Society, Chemical Communications*, 5, 329–330. <https://doi.org/10.1039/C39880000329>
- Kempf, M., Beuerle, T., Bühringer, M., Denner, M., Trost, D., Ohe, K. von der, Bhavanam, V. B. R., & Schreier, P. (2008). Pyrrolizidine alkaloids in honey: Risk analysis by gas chromatography-mass spectrometry. *Molecular Nutrition & Food Research*, 52(10), 1193–1200. <https://doi.org/10.1002/mnfr.200800051>
- Kempf, M., Reinhard, A., & Beuerle, T. (2010). Pyrrolizidine alkaloids (PAs) in honey and pollen-legal regulation of PA levels in food and animal feed required. *Molecular Nutrition & Food Research*, 54(1), 158–168. <https://doi.org/10.1002/mnfr.200900529>
- Khan, H. A., & Robins, D. J. (1985). Pyrrolizidine alkaloid biosynthesis. Synthesis of ¹⁴C-labelled homospermidines and their incorporation into retronecine. *Journal of the Chemical Society, Perkin Transactions 1*, 0, 819–824. <https://doi.org/10.1039/P19850000819>
- Kim, S.-J., Kim, M.-R., Bedgar, D. L., Moinuddin, S. G. A., Cardenas, C. L., Davin, L. B., Kang, C., & Lewis, N. G. (2004). Functional reclassification of the putative cinnamyl alcohol dehydrogenase multigene family in Arabidopsis. *Proceedings of the National Academy of Sciences*, 101(6), 1455–1460. <https://doi.org/10.1073/pnas.0307987100>
- Koncz, C., & Schell, J. (1986). The promoter of TL-DNA gene 5 controls the tissue-specific expression of chimaeric genes carried by a novel type of Agrobacterium binary vector. *Molecular and General Genetics MGG*, 204(3), 383–396. <https://doi.org/10.1007/BF00331014>
- Kotelnikova, K. V., Tretjakova, D. J., & Nuraliev, M. S. (2011). Shoot structure of *Symphytum officinale* L. (Boraginaceae) in relation to the nature of its axially shifted lateral branches. 18, 63–79.
- Koulman, A., Seeliger, C., Edwards, P. J. B., Fraser, K., Simpson, W., Johnson, L., Cao, M., Rasmussen, S., & Lane, G. A. (2008). E/Z-Thesinine-O-4'- α -rhamnoside, pyrrolizidine conjugates produced

- by grasses (Poaceae). *Phytochemistry*, 69(9), 1927–1932.
<https://doi.org/10.1016/j.phytochem.2008.03.017>
- Kováts, E. (1958). Gas-chromatographische Charakterisierung organischer Verbindungen. Teil 1: Retentionsindices aliphatischer Halogenide, Alkohole, Aldehyde und Ketone. *Helvetica Chimica Acta*, 41(7), 1915–1932. <https://doi.org/10.1002/hlca.19580410703>
- Kowalczyk, E., & Kwiatek, K. (2017). Determination of pyrrolizidine alkaloids in selected feed materials with gas chromatography-mass spectrometry. *Food Additives & Contaminants: Part A*, 34(5), 853–863. <https://doi.org/10.1080/19440049.2017.1302099>
- Kruse, L. H. (2017). *A multifaceted approach to identify unknown enzymes of pyrrolizidine alkaloid biosynthesis*. Christian-Albrechts Universität zu Kiel.
- Kruse, L. H., Stegemann, T., Jensen-Kroll, J., Engelhardt, A., Wesseling, A.-M., Lippert, A., Ludwig-Müller, J., & Ober, D. (2019). Reduction of Pyrrolizidine Alkaloid Levels in Comfrey (*Symphytum officinale*) Hairy Roots by RNAi Silencing of Homospermidine Synthase. *Planta Medica*, 85(14/15), 1177–1186.
- Kruse, L. H., Stegemann, T., Sievert, C., & Ober, D. (2017). Identification of a second site of pyrrolizidine alkaloid biosynthesis in comfrey to boost plant defense in floral stage. *Plant Physiology*, 174(1), 47–55.
- Kumar, V., Dooley, D. M., Freeman, H. C., Guss, J. M., Harvey, I., McGuirl, M. A., Wilce, M. C., & Zubak, V. M. (1996). Crystal structure of a eukaryotic (pea seedling) copper-containing amine oxidase at 2.2 Å resolution. *Structure (London, England: 1993)*, 4(8), 943–955.
[https://doi.org/10.1016/s0969-2126\(96\)00101-3](https://doi.org/10.1016/s0969-2126(96)00101-3)
- Kusano, T., Berberich, T., Tateda, C., & Takahashi, Y. (2008). Polyamines: Essential factors for growth and survival. *Planta*, 228(3), 367–381.
- Lang, null, Passreiter, null, Medinilla, null, Castillo, null, & Witte, null. (2001). Non-toxic pyrrolizidine alkaloids from *Eupatorium semialatum*. *Biochemical Systematics and Ecology*, 29(2), 143–147. [https://doi.org/10.1016/s0305-1978\(00\)00037-5](https://doi.org/10.1016/s0305-1978(00)00037-5)

- Langel, D., Ober, D., & Pelsler, P. B. (2011). The evolution of pyrrolizidine alkaloid biosynthesis and diversity in the Senecioneae. *Phytochemistry Reviews*, *10*(1), 3–74.
- Leegood, R. C. (2008). Roles of the bundle sheath cells in leaves of C3 plants. *Journal of Experimental Botany*, *59*(7), 1663–1673. <https://doi.org/10.1093/jxb/erm335>
- Li, R., Klinman, J. P., & Mathews, F. S. (1998). Copper amine oxidase from *Hansenula polymorpha*: The crystal structure determined at 2.4 Å resolution reveals the active conformation. *Structure (London, England: 1993)*, *6*(3), 293–307. [https://doi.org/10.1016/s0969-2126\(98\)00033-1](https://doi.org/10.1016/s0969-2126(98)00033-1)
- Liebisch, H. W., Radwan, A. S., & Schütte, H. R. (1969). [Biosynthesis of tropane alkaloids. X. On the formation of cuskygrine]. *Justus Liebigs Annalen Der Chemie*, *721*, 163–167. <https://doi.org/10.1002/jlac.19697210121>
- Lindigkeit, R., Biller, A., Buch, M., Schiebel, H.-M., Boppré, M., & Hartmann, T. (1997). The two Faces of Pyrrolizidine Alkaloids: The Role of the Tertiary Amine and its N-Oxide in Chemical Defense of Insects with Acquired Plant Alkaloids. *European Journal of Biochemistry*, *245*(3), 626–636. <https://doi.org/10.1111/j.1432-1033.1997.00626.x>
- Liscombe, D. K., & O'Connor, S. E. (2011). A virus-induced gene silencing approach to understanding alkaloid metabolism in *Catharanthus roseus*. *Phytochemistry*, *72*(16), 1969–1977. <https://doi.org/10.1016/j.phytochem.2011.07.001>
- Liu, J.-H., Wang, W., Wu, H., Gong, X., & Moriguchi, T. (2015). Polyamines function in stress tolerance: From synthesis to regulation. *Frontiers in Plant Science*, *6*, 827.
- Luebert, F., Cecchi, L., Frohlich, M. W., Gottschling, M., Guilliams, C. M., Hasenstab-Lehman, K. E., Hilger, H. H., Miller, J. S., Mittelbach, M., & Nazaire, M. (2016). Familial classification of the Boraginales. *Taxon*, *65*(3), 502–522.
- Lunelli, M., Di Paolo, M. L., Biadene, M., Calderone, V., Battistutta, R., Scarpa, M., Rigo, A., & Zanotti, G. (2005). Crystal structure of amine oxidase from bovine serum. *Journal of Molecular Biology*, *346*(4), 991–1004.

- Ma, X., & Gang, D. R. (2004). The Lycopodium alkaloids. *Natural Product Reports*, 21(6), 752–772.
<https://doi.org/10.1039/B409720N>
- Macht, D. I. (1915). THE HISTORY OF OPIUM AND SOME OF ITS PREPARATIONS AND ALKALOIDS. *Journal of the American Medical Association*, LXIV(6), 477–481.
<https://doi.org/10.1001/jama.1915.02570320001001>
- Mattocks, A. R. (1970). Role of the Acid Moieties in the Toxic Actions of Pyrrolizidine Alkaloids on Liver and Lung. *Nature*, 228(5267), 174–175. <https://doi.org/10.1038/228174a0>
- Mattocks, A. R. (1980). TOXIC PYRROLIZIDINE ALKALOIDS IN COMFREY. *The Lancet*, 316(8204), 1136–1137. [https://doi.org/10.1016/S0140-6736\(80\)92566-0](https://doi.org/10.1016/S0140-6736(80)92566-0)
- Mattocks, A. R., & White, I. N. H. (1971a). Pyrrolic Metabolites from Non-toxic Pyrrolizidine Alkaloids. *Nature New Biology*, 231(21), 114–115. <https://doi.org/10.1038/newbio231114a0>
- Mattocks, A. R., & White, I. N. H. (1971b). The conversion of pyrrolizidine alkaloids to N-oxides and to dihydropyrrolizine derivatives by rat-liver microsomes in vitro. *Chemico-Biological Interactions*, 3(5), 383–396. [https://doi.org/10.1016/0009-2797\(71\)90018-4](https://doi.org/10.1016/0009-2797(71)90018-4)
- McKey, D. (1979). The distribution of secondary compounds within plants. *Herbivores-Their Interaction with Secondary Plant Metabolites*, 55–134.
- Medda, R., Padiglia, A., & Floris, G. (1995). Plant copper-amine oxidases. *Phytochemistry*, 39(1), 1–9.
[https://doi.org/10.1016/0031-9422\(94\)00756-J](https://doi.org/10.1016/0031-9422(94)00756-J)
- Mestrom, L., Bracco, P., & Hanefeld, U. (2017). Amino Aldehydes Revisited. *European Journal of Organic Chemistry*, 2017(47), 7019–7025. <https://doi.org/10.1002/ejoc.201701213>
- Michael, A. J. (2016). Polyamines in eukaryotes, bacteria, and archaea. *Journal of Biological Chemistry*, 291(29), 14896–14903.
- Mizusaki, S., Tanabe, Y., Noguchi, M., & Tamaki, E. (1972). N-methylputrescine oxidase from tobacco roots. *Phytochemistry*, 11(9), 2757–2762. [https://doi.org/10.1016/S0031-9422\(00\)86509-7](https://doi.org/10.1016/S0031-9422(00)86509-7)
- Moll, S., Anke, S., Kahmann, U., Hänsch, R., Hartmann, T., & Ober, D. (2002). Cell-specific expression of homospermidine synthase, the entry enzyme of the pyrrolizidine alkaloid pathway in Senecio

- vernalis, in comparison with its ancestor, deoxyhypusine synthase. *Plant Physiology*, 130(1), 47–57.
- Morita, M., Shitan, N., Sawada, K., Montagu, M. C. E. V., Inzé, D., Rischer, H., Goossens, A., Oksman-Caldentey, K.-M., Moriyama, Y., & Yazaki, K. (2009). Vacuolar transport of nicotine is mediated by a multidrug and toxic compound extrusion (MATE) transporter in *Nicotiana tabacum*. *Proceedings of the National Academy of Sciences*, 106(7), 2447–2452. <https://doi.org/10.1073/pnas.0812512106>
- Mudge, E. M., Jones, A. M. P., & Brown, P. N. (2015). Quantification of pyrrolizidine alkaloids in North American plants and honey by LC-MS: Single laboratory validation. *Food Additives & Contaminants: Part A*, 32(12), 2068–2074. <https://doi.org/10.1080/19440049.2015.1099743>
- Mutterlein, R., & Arnold, C.-G. (1993). *Investigations concerning the content and the pattern of pyrrolizidine alkaloids in Symphytum officinale L. (comfrey)*. 138, 119–125.
- Naconsie, M., Kato, K., Shoji, T., & Hashimoto, T. (2014). Molecular evolution of N-methylputrescine oxidase in tobacco. *Plant & Cell Physiology*, 55(2), 436–444. <https://doi.org/10.1093/pcp/pct179>
- Nagakubo, T., Kumano, T., Ohta, T., Hashimoto, Y., & Kobayashi, M. (2019). Copper amine oxidases catalyze the oxidative deamination and hydrolysis of cyclic imines. *Nature Communications*, 10(1), 413. <https://doi.org/10.1038/s41467-018-08280-w>
- NAKAJIMA, K., OSHITA, Y., KAYA, M., YAMADA, Y., & HASHIMOTO, T. (1999). Structures and Expression Patterns of Two Tropinone Reductase Genes from *Hyoscyamus niger*. *Bioscience, Biotechnology, and Biochemistry*, 63(10), 1756–1764. <https://doi.org/10.1271/bbb.63.1756>
- Naumann, C., Hartmann, T., & Ober, D. (2002). Evolutionary recruitment of a flavin-dependent monooxygenase for the detoxification of host plant-acquired pyrrolizidine alkaloids in the alkaloid-defended arctiid moth *Tyria jacobaeae*. *Proceedings of the National Academy of Sciences*, 99(9), 6085–6090.
- Neumann, D. (1985). Storage of alkaloids. In *Biochem. Alkaloids* (pp. 49–55).

- Niemüller, D., Reimann, A., & Ober, D. (2012). Distinct Cell-Specific Expression of Homospermidine Synthase Involved in Pyrrolizidine Alkaloid Biosynthesis in Three Species of the Boraginales. *Plant Physiology*, *159*(3), 920–929. <https://doi.org/10.1104/pp.112.195024>
- Nurhayati, N., Gondé, D., & Ober, D. (2009). Evolution of pyrrolizidine alkaloids in Phalaenopsis orchids and other monocotyledons: Identification of deoxyhypusine synthase, homospermidine synthase and related pseudogenes. *Phytochemistry*, *70*(4), 508–516. <https://doi.org/10.1016/j.phytochem.2009.01.019>
- Ober, D., & Hartmann, T. (1999). Deoxyhypusine synthase from tobacco. CDNA isolation, characterization, and bacterial expression of an enzyme with extended substrate specificity. *The Journal of Biological Chemistry*, *274*(45), 32040.
- Ober, Dietrich. (2005). Seeing double: Gene duplication and diversification in plant secondary metabolism. *Trends in Plant Science*, *10*(9), 444–449.
- Ober, Dietrich, Gibas, L., Witte, L., & Hartmann, T. (2003). Evidence for general occurrence of homospermidine in plants and its supposed origin as by-product of deoxyhypusine synthase. *Phytochemistry*, *62*(3), 339–344.
- Ober, Dietrich, & Hartmann, T. (1999). Homospermidine synthase, the first pathway-specific enzyme of pyrrolizidine alkaloid biosynthesis, evolved from deoxyhypusine synthase. *Proceedings of the National Academy of Sciences*, *96*(26), 14777–14782.
- Padiglia, A., Medda, R., Pedersen, J. Z., Lorrapp, A., Peč, P., Frébort, I., & Floris, G. (1998). Inhibitors of plant copper amineoxidases. *Journal of Enzyme Inhibition*, *13*(5), 311–325.
- Paßreiter, C. M. (1992). Co-occurrence of 2-pyrrolidineacetic acid with the pyrrolizidines tussilaginic acid and isotussilaginic acid and their 1-epimers in Arnica species and Tussilago farfara. *Phytochemistry*, *31*(12), 4135–4137. [https://doi.org/10.1016/0031-9422\(92\)80428-H](https://doi.org/10.1016/0031-9422(92)80428-H)
- Peters, M., Oberrath, R., & Böhning-Gaese, K. (2003). Seed dispersal by ants: Are seed preferences influenced by foraging strategies or historical constraints? *Flora - Morphology, Distribution, Functional Ecology of Plants*, *198*(6), 413–420. <https://doi.org/10.1078/0367-2530-1210114>

- Pfister, J. A., Molyneux, R. J., & Baker, D. C. (1992). Pyrrolizidine Alkaloid Content of Houndstongue (*Cynoglossum officinale* L.). *Journal of Range Management*, *45*(3), 254–256. JSTOR.
<https://doi.org/10.2307/4002973>
- Pichersky, E., Noel, J. P., & Dudareva, N. (2006). Biosynthesis of Plant Volatiles: Nature's Diversity and Ingenuity. *Science*, *311*(5762), 808–811. <https://doi.org/10.1126/science.1118510>
- Planas-Portell, J., Gallart, M., Tiburcio, A. F., & Altabella, T. (2013). Copper-containing amine oxidases contribute to terminal polyamine oxidation in peroxisomes and apoplast of *Arabidopsis thaliana*. *BMC Plant Biology*, *13*, 109. <https://doi.org/10.1186/1471-2229-13-109>
- Rana, J., & Robins, D. J. (1983). Intact incorporation of [1,9-¹³C₂]-homospermidine into retronecine. *Journal of Chemical REsearch, Synopses*, 146–147.
- Reimann, A., Nurhayati, N., Backenköhler, A., & Ober, D. (2004). Repeated evolution of the pyrrolizidine alkaloid-mediated defense system in separate angiosperm lineages. *The Plant Cell*, *16*(10), 2772–2784.
- Robins, D. J. (1995). Pyrrolizidine alkaloids. *Natural Product Reports*, *12*(4), 413–418.
<https://doi.org/10.1039/NP9951200413>
- Robins, David J. (1989). Biosynthesis of pyrrolizidine alkaloids. *Chemical Society Reviews*, *18*(0), 375–408. <https://doi.org/10.1039/CS9891800375>
- Robins, David J. (1995). Chapter 1 Biosynthesis of Pyrrolizidine and Quinolizidine Alkaloids. In G. A. Cordell (Ed.), *The Alkaloids: Chemistry and Pharmacology* (Vol. 46, pp. 1–61). Academic Press.
[https://doi.org/10.1016/S0099-9598\(08\)60285-0](https://doi.org/10.1016/S0099-9598(08)60285-0)
- Sander, H., & Hartmann, T. (1989). Site of synthesis, metabolism and translocation of senecionine N-oxide in cultured roots of *Senecio erucifolius*. *Plant Cell, Tissue and Organ Culture*, *18*(1), 19–31. <https://doi.org/10.1007/BF00033462>
- Schmittgen, T. D., & Livak, K. J. (2008). Analyzing real-time PCR data by the comparative C_T method. *Nature Protocols*, *3*(6), 1101–1108. <https://doi.org/10.1038/nprot.2008.73>

- Sehlmeyer, S., Wang, L., Langel, D., Heckel, D. G., Mohagheghi, H., Petschenka, G., & Ober, D. (2010). Flavin-Dependent Monooxygenases as a Detoxification Mechanism in Insects: New Insights from the Arctiids (Lepidoptera). *PLoS ONE*, *5*(5). <https://doi.org/10.1371/journal.pone.0010435>
- Seiler, N., & Raul, F. (2005). Polyamines and apoptosis. *Journal of Cellular and Molecular Medicine*, *9*(3), 623–642.
- Serturmer, F. W. (1805). Darstellung der reinen Mohnsaure (Opiumsaeure) nebst einer chemischen Untersuchung des Opiums mit vorzuglicher Hinsicht auf einen darin neu entdeckten Stoff und die darin gehorigen Bemerkungen. *Trommsdorffs Journal Der Pharmazie*, *14*(1), 47–98.
- Shitan, N., Hayashida, M., & Yazaki, K. (2015). Translocation and accumulation of nicotine via distinct spatio-temporal regulation of nicotine transporters in *Nicotiana tabacum*. *Plant Signaling & Behavior*, *10*(7). <https://doi.org/10.1080/15592324.2015.1035852>
- Sievert, C., Beuerle, T., Hollmann, J., & Ober, D. (2015). Single cell subtractive transcriptomics for identification of cell-specifically expressed candidate genes of pyrrolizidine alkaloid biosynthesis. *Phytochemistry*, *117*, 17–24. <https://doi.org/10.1016/j.phytochem.2015.05.003>
- Singh, B., Sahu, P. M., Jain, S. C., & Singh, S. (2002). Antineoplastic and Antiviral Screening of Pyrrolizidine Alkaloids from *Heliotropium subulatum*. *Pharmaceutical Biology*, *40*(8), 581–586. <https://doi.org/10.1076/phbi.40.8.581.14659>
- Smith, L. W., & Culvenor, C. C. J. (1981). Plant Sources of Hepatotoxic Pyrrolizidine Alkaloids. *Journal of Natural Products*, *44*(2), 129–152. <https://doi.org/10.1021/np50014a001>
- Sobieszczuk-Nowicka, E., Paluch-Lubawa, E., Mattoo, A. K., Arasimowicz-Jelonek, M., Gregersen, P. L., & Pacak, A. (2019). Polyamines—a new metabolic switch: Crosstalk with networks involving senescence, crop improvement, and mammalian cancer therapy. *Frontiers in Plant Science*, *10*.
- Staiger, C. (2012). Comfrey: A Clinical Overview. *Phytotherapy Research*, *26*(10), 1441–1448. <https://doi.org/10.1002/ptr.4612>

- Stegemann, T., Kruse, L. H., Brütt, M., & Ober, D. (2019). Specific distribution of pyrrolizidine alkaloids in floral parts of comfrey (*Symphytum officinale*) and its implications for flower ecology. *Journal of Chemical Ecology*, *45*(2), 128–135.
- Stegemann, T., Kruse, L. H., & Ober, D. (2018). Radioactive Tracer Feeding Experiments and Product Analysis to Determine the Biosynthetic Capability of Comfrey (*Symphytum officinale*) Leaves for Pyrrolizidine Alkaloids. *Bio-Protocol*, *8*(3).
- Stedle, E., & Peterson, C. A. (1998). How does water get through roots? *Journal of Experimental Botany*, *49*(322), 775–788. <https://doi.org/10.1093/jxb/49.322.775>
- St-Pierre, B., Vazquez-Flota, F. A., & Luca, V. D. (1999). Multicellular Compartmentation of *Catharanthus roseus* Alkaloid Biosynthesis Predicts Intercellular Translocation of a Pathway Intermediate. *The Plant Cell*, *11*(5), 887–900. <https://doi.org/10.1105/tpc.11.5.887>
- Suzuki, K., Yamada, Y., & Hashimoto, T. (1999). Expression of *Atropa belladonna* Putrescine N-Methyltransferase Gene in Root Pericycle. *Plant and Cell Physiology*, *40*(3), 289–297. <https://doi.org/10.1093/oxfordjournals.pcp.a029540>
- Tavladoraki, P., Cona, A., & Angelini, R. (2016). Copper-Containing Amine Oxidases and FAD-Dependent Polyamine Oxidases Are Key Players in Plant Tissue Differentiation and Organ Development. *Frontiers in Plant Science*, *7*. <https://doi.org/10.3389/fpls.2016.00824>
- Tholl, D., Ober, D., Martin, W., Kellermann, J., & Hartmann, T. (1996). Purification, molecular cloning and expression in *Escherichia coli* of homospermidine synthase from *Rhodospseudomonas viridis*. *European Journal of Biochemistry*, *240*(2), 373–379.
- Tiburcio, A. F., Altabella, T., Bitrián, M., & Alcázar, R. (2014). The roles of polyamines during the lifespan of plants: From development to stress. *Planta*, *240*(1), 1–18. <https://doi.org/10.1007/s00425-014-2055-9>
- Tipping, A. J., & McPherson, M. J. (1995). Cloning and Molecular Analysis of the Pea Seedling Copper Amine Oxidase. *Journal of Biological Chemistry*, *270*(28), 16939–16946. <https://doi.org/10.1074/jbc.270.28.16939>

- Utelli, A.-B., & Roy, B. A. (2001). Causes and consequences of floral damage in *Aconitum lycoctonum* at high and low elevations in Switzerland. *Oecologia*, *127*(2), 266–273.
<https://doi.org/10.1007/s004420000580>
- van Dam, N. M., van der Meijden, E., & Verpoorte, R. (1993). Induced responses in three alkaloid-containing plant species. *Oecologia*, *95*(3), 425–430. <https://doi.org/10.1007/BF00320998>
- van Dam, N. M., Witte, L., Theuring, C., & Hartmann, T. (1995). Distribution, biosynthesis and turnover of pyrrolizidine alkaloids in *Cynoglossum officinale*. *Phytochemistry*, *39*(2), 287–292.
[https://doi.org/10.1016/0031-9422\(94\)00944-O](https://doi.org/10.1016/0031-9422(94)00944-O)
- Vojinović, V., Azevedo, A. M., Martins, V. C., Cabral, J. M. S., Gibson, T. D., & Fonseca, L. P. (2004). *Assay of H₂O₂ by HRP catalysed co-oxidation of phenol-4-sulphonic acid and 4-aminoantipyrine: Characterisation and optimisation*.
<https://doi.org/10.1016/j.molcatb.2004.02.003>
- Wang, L., Beuerle, T., Timbilla, J., & Ober, D. (2012). Independent Recruitment of a Flavin-Dependent Monooxygenase for Safe Accumulation of Sequestered Pyrrolizidine Alkaloids in Grasshoppers and Moths. *PLoS ONE*, *7*(2). <https://doi.org/10.1371/journal.pone.0031796>
- Watson, A. B., Brown, A. M., Colquhoun, I. J., Walton, N. J., & Robins, D. J. (1990). Biosynthesis of anabasine in transformed root cultures of *Nicotiana* species. *Journal of the Chemical Society, Perkin Transactions 1*, *9*, 2607–2610. <https://doi.org/10.1039/P19900002607>
- Weid, M., Ziegler, J., & Kutchan, T. M. (2004). The roles of latex and the vascular bundle in morphine biosynthesis in the opium poppy, *Papaver somniferum*. *Proceedings of the National Academy of Sciences*, *101*(38), 13957–13962. <https://doi.org/10.1073/pnas.0405704101>
- Weng, J.-K., Philippe, R. N., & Noel, J. P. (2012). The Rise of Chemodiversity in Plants. *Science*, *336*(6089), 1667–1670. <https://doi.org/10.1126/science.1217411>
- Wink, M., Schmeller, T., & Latz-Brüning, B. (1998). Modes of action of allelochemical alkaloids: Interaction with neuroreceptors, DNA, and other molecular targets. *Journal of Chemical Ecology*, *24*(11), 1881–1937.

- Wink, Michael. (2010). Introduction: Biochemistry, Physiology and Ecological Functions of Secondary Metabolites. In *Annual Plant Reviews Volume 40: Biochemistry of Plant Secondary Metabolism* (pp. 1–19). John Wiley & Sons, Ltd. <https://doi.org/10.1002/9781444320503.ch1>
- Wink, Michael, & Hartmann, T. (1979). Cadaverine-pyruvate transamination: The principal step of enzymatic quinolizidine alkaloid biosynthesis in *Lupinus polyphyllus* cell suspension cultures. *FEBS Letters*, *101*(2), 343–346. [https://doi.org/10.1016/0014-5793\(79\)81040-6](https://doi.org/10.1016/0014-5793(79)81040-6)
- Wisniewski, J.-P., Rathbun, E. A., Knox, J. P., & Brewin, N. J. (2000). Involvement of diamine oxidase and peroxidase in insolubilization of the extracellular matrix: Implications for pea nodule initiation by *Rhizobium leguminosarum*. *Molecular Plant-Microbe Interactions*, *13*(4), 413–420.
- Witte, L., Ehmke, A., & Hartmann, Th. (1990). Interspecific flow of pyrrolizidine alkaloids. *Naturwissenschaften*, *77*(11), 540–543. <https://doi.org/10.1007/BF01139268>
- Yang, T., Nagy, I., Mancinotti, D., Otterbach, S. L., Andersen, T. B., Motawia, M. S., Asp, T., & Geu-Flores, F. (2017). Transcript profiling of a bitter variety of narrow-leafed lupin to discover alkaloid biosynthetic genes. *Journal of Experimental Botany*, *68*(20), 5527–5537. <https://doi.org/10.1093/jxb/erx362>
- Ziegler, J., & Facchini, P. J. (2008). Alkaloid Biosynthesis: Metabolism and Trafficking. *Annual Review of Plant Biology*, *59*(1), 735–769. <https://doi.org/10.1146/annurev.arplant.59.032607.092730>
- Zorn, H., Peters, T., Nimtz, M., & Berger, R. G. (2005). The secretome of *Pleurotus sapidus*. *PROTEOMICS*, *5*(18), 4832–4838. <https://doi.org/10.1002/pmic.200500015>

THOMAS STEGEMANN

GEBURTSORT: ECKERNFÖRDE, GEBURTSTAG: 05.03.1987
STAATSANGEHÖRIGKEIT: DEUTSCH

Berufliche Laufbahn

August 2018 –
Applikationsspezialist GC, GC-MS/MS, **THERMOFISHER SCIENTIFIC GMBH, DREIEICH**

Juli 2015 – August 2018
Wissenschaftlicher Mitarbeiter, **BOTANISCHES INSTITUT CAU KIEL**

Januar 2015 – Juli 2015
Pharmazeut im Praktikum, **APOTHEKE AM RATHAUS, HEIKENDORF**

August 2012 – März 2014
Studentische Hilfskraft, **PHYSIOLOGISCHES INSTITUT CAU KIEL**

Bildungslaufbahn

Seit 2015
Promotion
Betreuer: Prof. Dr. Dietrich Ober, **Botanisches Institut CAU Kiel**

2010-2015
Approbation als Apotheker, **CAU KIEL**
Studium der Pharmazie

2007
Allgemeine Hochschulreife, **ISARNHOSCHULE GETTORF**

Further Publications not mentioned in this thesis

Scharenberg, F., Çiçek, S. S., **Stegemann, T.**, Piccolella, S., Pacifico, S., & Zidorn, C. (2019). Flavonol triglycosides from *Ornithopus compressus* L.(Fabaceae). *Industrial Crops and Products*, 137, 475-483.

Scharenberg, F., **Stegemann, T.**, Çiçek, S. S., & Zidorn, C. (2019). Sequestration of pyridine alkaloids anabasine and nicotine from *Nicotiana* (Solanaceae) by *Orobanche ramosa* (Orobanchaceae). *Biochemical Systematics and Ecology*, 86, 103908.

Kruse, L., **Stegemann, T.**, Jensen-Kroll, J., Engelhardt, A., Wesseling, A.-M., Lippert, A., Ludwig-Müller, J., Ober, D. (2019). Reduction of pyrrolizidine alkaloid levels in comfrey (*Symphytum officinale*) hairy roots by RNAi silencing of homospermidine synthase. *Planta Medica*

Erklärung

Die vorliegende Doktorarbeit ist – abgesehen von der Beratung durch meinen Betreuer Prof. Dr. Dietrich Ober – nach Inhalt und Form meine eigene Arbeit.

Kapitel 2 der Arbeit: „Identification of a second site of pyrrolizidine alkaloid biosynthesis in comfrey to boost plant defense in floral stage“ war ebenfalls Bestandteil des Promotionsverfahren von Lars Hendrik Kruse. Alle anderen Kapitel waren weder ganz noch zum Teil Bestandteil eines Prüfungsverfahrens an der CAU Kiel oder einer anderen Hochschule.

Die vorliegende Arbeit entstand unter Einhaltung der Regeln guter wissenschaftlicher Praxis der Deutschen Forschungsgemeinschaft.

Es wurde mir kein akademischer Grad entzogen.


Teilergebnisse aus dieser Arbeit wurden in folgende Beiträgen vorab veröffentlicht:

Kruse, L. H., Stegemann, T., Sievert, C., & Ober, D. (2017). Identification of a second site of pyrrolizidine alkaloid biosynthesis in comfrey to boost plant defense in floral stage.

Plant Physiology, 174(1), 47–55.

Stegemann, T., Kruse, L. H., Brütt, M., & Ober, D. (2019). Specific distribution of pyrrolizidine alkaloids in floral parts of comfrey (*Symphytum officinale*) and its implications for flower ecology. *Journal of Chemical Ecology*, 45(2), 128–135.

Stegemann, T., Kruse, L. H., & Ober, D. (2018). Radioactive Tracer Feeding Experiments and Product Analysis to Determine the Biosynthetic Capability of Comfrey (*Symphytum officinale*) Leaves for Pyrrolizidine Alkaloids. *Bio-Protocol*, 8(3).



Thomas Stegemann